ENVIRONMENTAL RADIOACTIVITY MONITORING VIA NEWLY DEVELOPED OPTICAL FIBER BASED THERMOLUMINESENCE DOSIMETER

SITI ROZAILA BINTI ZAHARIMAN

FACULTY OF SCIENCE
UNIVERSITY OF MALAYA
KUALA LUMPUR

2016

ENVIRONMENTAL RADIOACTIVITY MONITORING VIA NEWLY DEVELOPED OPTICAL FIBER BASED THERMOLUMINESENCE DOSIMETER

SITI ROZAILA BINTI ZAHARIMAN

DISSERTATION SUBMITTED IN FULFILMENT OF THE REQUIREMENTS FOR THE DEGREE OF MASTER OF SCIENCE

FACULTY OF SCIENCE
UNIVERSITY OF MALAYA
KUALA LUMPUR

2016

UNIVERSITI MALAYA

ORIGINAL LITERARY WORK DECLARATION

Name of Candidate: Siti Rozaila binti Zahariman ████████████

Registration/Matric No: SGR140090
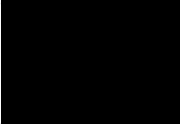
Name of Degree: Master of Science

Title of ~~Project Paper/Research Report~~/Dissertation/~~Thesis~~ ("this Work"):

Environmental Radioactivity Monitoring via Newly Developed Optical Fiber Based Thermoluminesence Dosimeter
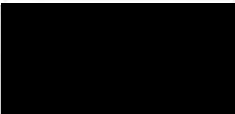
Field of Study: Experimental Physics

I do solemnly and sincerely declare that:

(1)   I am the sole author/writer of this Work;

(2)   This Work is original;

(3)   Any use of any work in which copyright exists was done by way of fair dealing and for permitted purposes and any excerpt or extract from, or reference to or reproduction of any copyright work has been disclosed expressly and sufficiently and the title of the Work and its authorship have been acknowledged in this Work;

(4)   I do not have any actual knowledge nor do I ought reasonably to know that the making of this work constitutes an infringement of any copyright work;

(5)   I hereby assign all and every rights in the copyright to this Work to the University of Malaya ("UM"), who henceforth shall be owner of the copyright in this Work and that any reproduction or use in any form or by any means whatsoever is prohibited without the written consent of UM having been first had and obtained;

(6)   I am fully aware that if in the course of making this Work I have infringed any copyright whether intentionally or otherwise, I may be subject to legal action or any other action as may be determined by UM.

Candidate's Signature: ████████   Date: 23 / 11 / 2016

Subscribed and solemnly declared before,

Witness's Signature: ████████   Date: 23 / 11 / 2016

Name: Assoc. Prof. Dr. Mayeen Uddin Khandaker

Designation: Associate Professor

Mayeen Uddin Khandaker
Associate Professor
Department of Physics
University of Malaya
50603 Kuala Lumpur, Malaysia

ii

ABSTRACT

Thermoluminesence dosimeters (TLD) are increasingly being used in a variety of fields, including in support of medical irradiations, environmental radioactivity monitoring, food sterilization, the radiation processing industry and in other such involvements. The conventional phosphor based TLDs suffer in performance, due in part to their manifestly hygroscopic nature and poor resolution. In their use as TLDs, the optical fibers do not suffer from these drawbacks and in addition are seen to offer a number of other potential advantages, including sensitivity, stability and reliability. These factors help to introduce the fibers as a potential alternative to the phosphor-based TLDs. Recent studies have highlighted the use of optical fibers in radiation dosimetry applications for a wide range of electron and photon beam irradiations. Nevertheless, they have yet to be investigated at the very much lower environmental doses, with practically no very low doses studies. Realizing the importance of low dose environmental radioactivity monitoring, highly sensitive optical fiber based TLD materials in the form of collapsed Photonic Crystal Fiber (PCFc) has been developed here. In this study, the newly developed collapsed PCFs (with different dopant concentrations of Ge and B) together with phosphor based TLDs (TLD-200 and TLD-100) have been buried in eight selected areas within Gebeng, Pahang (off-site of the Lynas Advanced Materials Plant) to obtain exposure records for two, four, six, and eight months. The TLD readout doses (via a TLD reader) are compared with the bulk radioactivity in the associated soils obtained via HPGe gamma-ray spectrometry. Parameters concerning thermoluminesence (TL) for the samples induced by x-ray and gamma-ray irradiation have been investigated, including the linearity of dose response, energy response, fading, effective atomic number and glow curve. Present study indicates that the developed PCFs could be advantageously utilized in very low dose radiation dosimetry applications.

ABSTRAK

Thermoluminesence (TLD) dosimetri semakin digunakan dalam pelbagai bidang seperti perubatan, pemantauan alam sekitar radioaktif, pensterilan dan radiasi pemprosesan makanan dalam industri dan lain-lain. Konvensional TLD berdasarkan fosfor mengalami kekurangan dalam prestasi disebabkan sifat hygroscopic (masalah berhadapan dengan kelembapan) dan kurang resolusi. Gentian optik yang menawarkan potensi kelebihan dari segi kepekaan, kestabilan dan kebolehpercayaan diperkenalkan sebagai alternatif yang berpotensi. Kajian baru-baru ini telah menekankan penggunaan gentian optik dalam aplikasi dosimetri sinaran seperti sinaran elektron dan foton. Walau bagaimanapun, mereka masih belum disiasat pada dos alam sekitar yang jauh lebih rendah. Menyedari kepentingan dos yang rendah dalam pemantauan radioaktif alam sekitar, gentian optic yang sangat sensitif iaitu collapsed Photonic Crystal Fiber (PCFc) telah diperkenalkan di sini. Oleh itu, dalam kajian ini, PCFs (dengan berbeza pendopan Ge dan B) yang baru diperkenalkan ini bersama-sama dengan TLD (TLD-200 dan TLD-100) yang berdasarkan fosfor telah ditanam di 8 kawasan terpilih di Gebeng, Pahang (di luar tapak daripada Lynas Advanced Materials Plant) untuk mendapatkan rekod pendedahan untuk dua, empat, enam, dan lapan bulan. Dos bacaan (melalui pembaca TLD) dibandingkan dengan radioaktif pukal dalam tanah yang berkaitan diperolehi melalui HPGe gamma-ray spektrometri. Parameter mengenai thermoluminesence (TL) bagi sampel yang diradiasi oleh x-ray dan gamma-ray telah disiasat, termasuk kelinearan tindak balas dos, tindak balas tenaga, pudar, dan keluk cahaya. Kajian ini menunjukkan bahawa PCFs yang baru diperkenalkan berpotensi digunakan dalam aplikasi dosimetri sinaran yang sangat rendah.

ACKNOWLEDGEMENTS

TABLE OF CONTENTS

LIST OF TABLES

LIST OF FIGURES

LIST OF ABBREVIATIONS

TL	Thermoluminescence
TLD	Thermoluminescence dosimeter
PCF	Photonic crystal fiber
PCFc	Collapsed photonic crystal fiber
FF	Flat Fiber
COF	Capillary optical fiber
Z_{eff}	Effective atomic number
HPGe	High purity Germanium
FSD	Focus to surface distance
PMT	Photomultiplier tube
TTP	Time temperature profile
NORM	Naturally occurring radioactive material
TENORM	Technologically enhanced NORM
GIE	Gebeng industrial estate
LAMP	Lynas advanced material plant
MCVD	Modified chemical vapour deposition
MOSTI	Ministry of Science and Technology Innovation
A	Activity concentration
Ra_{eq}	Radium equivalent
D_R	Absorbed dose
AEDE	Annual effective dose equivalent
H	Hazard index

CHAPTER 1 : INTRODUCTION

1.1 Overview

Our world is naturally radioactive and about 90% of human exposure arises from natural sources such as cosmic radiation, exposure to radon gas and terrestrial radionuclides (Lee et al., 2004). Every day, each of us is exposed to these naturally occurring radioactive materials (NORMs). In fact, radioactive nuclei can spontaneously decay at everywhere such as in the soil, air, earth crust, plant and even within our bodies (Abbasisiar et al., 2004). The natural radionuclides of concern are mainly Uranium, Thorium, Potassium and the radionuclides that are created via their radioactive decay chain (S. Hafezi and J. Amidi, 2005).

Basically, the sources of the radiation can be divided into two categories; the natural background radiation with naturally occurring radioactive material (NORM) and the man-made radiation from the artificial sources; medicine, military and industry. Most of these artificial facilities generate radioactive waste and some release an amount of radiation into the environment, disturbing and enhancing its NORM concentration (Wilson, 1994). This is called Technologically Enhanced Naturally Occurring Radioactive Material (TENORM) as a result of human activity such as manufacturing, minerals extraction, the hydrocarbons downstream industry, water processing, and other non-nuclear fuel industry related work (Kolo et al. 2015).

Being exposed to this radiation in a cumulative manner may eventually cause health problems. The ionizing radiation has sufficient energy to cause chemical changes in cells and damage them. Some cells may die or become abnormal, either temporarily or permanently. By damaging the genetic material (DNA) contained in the body's cells, radiation can cause cancer. The extent of the damage to the cells depends upon the amount and duration of exposure, as well as the organs exposed. A very large amount of

the radiation exposure can cause sickness or even death within hours or days (Hallenbeck, 1994). With low dose chronic exposures, it still remains very important to monitor the environmental radiation precisely, due to the statistical probability of ill health effects. Measurements based on the use of thermoluminescence dosimeter (TLD) systems have been the focus of present research. Thermoluminescence (TL) is the thermally stimulated emission of light from a material that has been subject to prior absorption of energy from an exciting source such as ultraviolet light, source of x-rays or other ionizing radiation. The amount of light emitted is proportional to the energy absorbed by the irradiated material (Furetta, 2003). Based on previous studies involving conventional phosphor based TLDs such as LiF and CaF_2, forming the commercial products TLD-100 and TLD-200 respectively, the advantages and disadvantages of such use are now well known, providing motivation in finding new materials that potentially improve upon existing detection capabilities. These well-established materials have several prominent disadvantages, including their cost, hygroscopic nature and relatively poor spatial resolution of a few mm size (Izewska, J. and Rajan, 2005).

As a result of prior studies of the phosphor-based media, in recent years there has been increasing interest in the study of the advantageous features of optical fiber luminescent techniques. Commercially available optical fibers (with outer diameter typically ~100 μm) have actually been seen to offer the basis of highly sensitive high spatial resolution dosimeters, the silica medium overcoming hygroscopic problems (Hashim et al., 2009). By using modified chemical vapour deposition (MCVD) techniques, these silica-based optical fibers exhibit a number of advantageous physico-chemical characteristics, including being mechanically robust, chemically inert, biocompatible and re-usable, also being easily sterilisable via heating etc.

A remaining challenge has been that of improving the TL yield of the fibers, a matter attracting the attention of several researchers, including (Mahdiraji et al., 2015), with present work forming part of evaluation of this particular part. The work (shown in Figure 1.1) started with (a) capillary optical fibres (COF), subsequently moving on to the collapsing down of pure silica hollow capillary fibres into (b) flat fibres (FF), and then further still by stacking a group of pure SiO_2 capillaries (hexagonal shaped array of small capillaries) into the outer of glass tube to form what is known as a (c) Photonic Crystal Fibre (PCF). Next, by collapsing down the PCF assembly, to be subsequently referred to as (d) collapsed PCF (PCFc) (Dermosesian et al., 2015). It has been shown that considerable enhancement in TL yield can be obtained, the fused inner walls generating defects beyond that existing in the unstrained media. In irradiation by 6 MeV electrons, the mass-normalised TL yield of the pure FF and pure uncollapsed PCF have been shown to be improved by ~ 12 × and ~ 17.5 × compared to that of pure COF (Bradley et al., 2015). Further, in making use of 20 MeV electron beam irradiation, the TL yield of pure collapsed PCF (PCFc) has been shown to be ~ 7.5 × of that of pure uncollapsed PCF (Dermosesian et al., 2015).
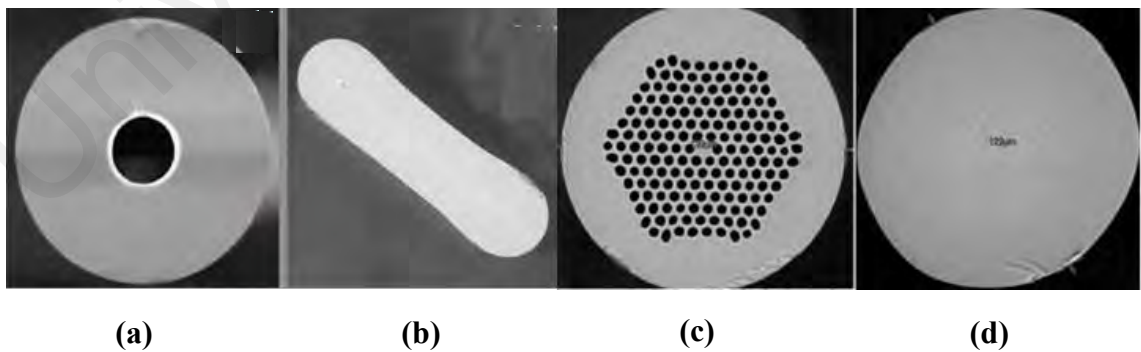
Figure 1.1: (a) Capillary Optical Fibre (COF) **(b)** Flat Fibre (FF) **(c)** Photonic Crystal Fibre (PCF) **(d)** Collapsed Photonic Crystal Fibre (PCFc).

The outcome of such studies can be linked with the results of previous investigations in which the focus has been on extrinsically doped tailor-made silica fibres, doped with atomic species of Ge, Al (Yaakob et al., 2011), Ba and Li, zirconium dioxide (ZrO2) (Villa-Sanchez et al., 2007), manganese doped calcium tetraborate (CaB4O7:Mn) nanocrystal (Tabatabaei et al., 2006), Cd and Zn (Tiwari et al., 2014). Compared to pure COF, the TL yield has been shown to be increased by a factor $\sim 3 \times$ when doped by Ge (Mahdiraji et al., 2015) and by $\sim 6 \times$ for Ge-doped COF collapsed into FF (Bradley et al., 2015). Most notably, when Ge and B co-dopants have been introduced into a preform of COF, to subsequently be collapsed down into FF, its TL response has been observed to increase by a factor of 31 (Mahdiraji et al., 2015).

Among of all of these studies, the PCFc resulted in the greatest TL yield producing the most sensitive fiber TLD, the fused inner walls generating greater numbers of defects than that existing in the unstrained media during the drawing-down process. Given that the dopant of Ge and B increased the previous TL yield of COF and FF, present study focused on the characteristics of PCFc with different dopant concentrations of Ge and B. Herein, conventional phosphor TLD-100 and TLD-200 are used as a comparator.

1.2   Problem statements

Conventional phosphor based TLDs such as the LiF and CaF$_2$ based products TLD-100 and TLD-200 have several prominent disadvantages, including their cost, hygroscopic nature and relatively poor spatial resolution of a few mm size (Izewska, J. and Rajan, 2005). By using the MCVD process, optical fibers made for telecommunications purposes (with outer diameter typically ~100 μm) have been modified and actually been seen to offer the basis of highly sensitive high spatial

4

resolution dosimeters, the silica overcoming the hygroscopic problem (Hashim et al., 2009). Based on the previous studies, dopants and additional defects induced during the drawing-down process help to increase the TL yield of the fibers. However, there is little information on the effect of PCFc, the most sensitive fiber TLD, as a result of different dopant concentrations of Ge and B.

Although the PCFc is very sensitive, with TL yields greater than TLD-100, it has yet to be investigated at the very low doses typical of environmental levels, even though it has been suggested to be sufficient for the purpose. In present study, environmental radiation levels have been monitored at selected areas within Gebeng Industrial Estate (GIE) in Pahang, Malaysia, adjacent to the Lynas Advance Material Plant (LAMP) where it has been suggested that TENORM concentrations may constitute a risk due to public exposures.

1.3 Motivation and goals

The specific aims of this study include:

- Laboratory study:
    i. To study the characteristics of fiber based TLDs (Collapsed Photonic Crystal Fiber (PCFc) with Ge and B dopant) and phosphor based TLDs (TLD-100 and TLD-200) irradiated to photons at ionizing energies.

- Environmental study:
    i. To compare the response of both fiber and phosphor based TLDs for various environmental dose levels in selected areas within Gebeng Industrial Estate (GIE), in Pahang.

ii.   To compare the correlation between the doses obtained via TLDs (fiber and phosphor based) with the radiation doses of the adjacent soils of the selected areas obtained via the HPGe gamma-ray spectrometry.

1.4 Thesis structure

This thesis is organized into five chapters.

Chapter 1 includes the introduction, problem statements, motivation and goals that will lead to the work contained in this thesis.

In Chapter 2, basic concepts of radioactive decay are discussed. Review of environmental radioactivity including NORM and TENORM and also information concerning the TL dosimetry are explained. Detailed overviews of the optical properties of silica-based material also are discussed.

Chapter 3 is divided into two main parts. The first part concerns sample preparation for characterisation studies (in the laboratory) while the second part provides a detailed description of the sample preparation for the at-site environmental study. Details of the fabrication process, annealing, irradiation of the optical fiber and phosphor based TLD materials and the instrumentation methods that have been used in the experiments are explained. Sampling locations for this study are also described briefly. The calculations and conversions used to obtain the main objective are also explained in this chapter, to compare both radiation dose by TLDs and gamma spectroscopy of adjacent soils.

In Chapter 4, all the results obtained in this research are presented and is also divided into two main parts, with results of the characterization study (i.e. screening, annealing, energy response, dose response, TL glow curve, effective atomic number and

fading), followed by presentation of results of the environmental study (i.e. TL readout of samples and gamma spectroscopy from the soils). Finally, comparison results of both radiation dose by TLDs and gamma spectroscopy of adjacent soils are discussed.

Finally, chapter 6 summarizes the main findings achieved from this research and suggests several directions for future studies.

CHAPTER 2 : LITERATURE REVIEW

2.1 Radioactivity

Radioactivity or radioactive decay refers to the emission of radiation from unstable nuclei of atoms (each source type being referred to as a radionuclide). Some occur naturally in the environment while others are man-made, as by-products of nuclear reactions. Generally, whether an atom can exist as stable or unstable depends on the number of protons and number of neutrons in the nucleus (Wilson, 1994). During the decay process, the radionuclide become less radioactive over time, eventually becoming stable. The time it takes for the radionuclide to decay to half of its starting activity is called the radiological half-life, denoted as $t_{1/2}$. Each radionuclide has a unique half-life, and it can range from a fraction of a second to billions of years. For example, iodine-131 has an eight-day half-life, whereas plutonium-239 has a half-life of 24,000 years. A radionuclide with a short half-life is more radioactive than one with a longer half-life, emitting more radiation during a given time period (Jha, 2004).

2.2 Types of radioactive decay and emitted radiation

The emitted radiation following radioactive decay can be considered as three types that are alpha, beta and gamma radiation. These radiations are the ionizing radiations that capable of knock out the electrons from the interacting atom, upsetting the electron/proton balance and giving the atom a positive charge.

2.2.1 Alpha radiation decay (α)

Alpha radiation consists of alpha particles (helium nuclei) that are made up of two protons and two neutrons each and thus carrying a double positive charge as in Figure

2.1. Due to their relatively large mass and charge, they have an extremely limited ability to penetrate matter. Alpha radiation can be stopped by a thin piece of paper (of some several tens of microns thick) or the dead outer layer of the skin, as shown in Figure 2.4. Consequently, alpha radiation from nuclear sources outside of the body does not present a radiation hazard. However, when alpha-radiation-emitting nuclear substances are taken into the body (for example, by breathing them in or by ingestion), the energy of the alpha radiation is completely absorbed into body tissues. For this reason, alpha radiation is only an internal hazard (Hallenbeck, 1994). An example of a nuclear substance that undergoes alpha decay is Plutonium-240, which decays to Uranium-236.
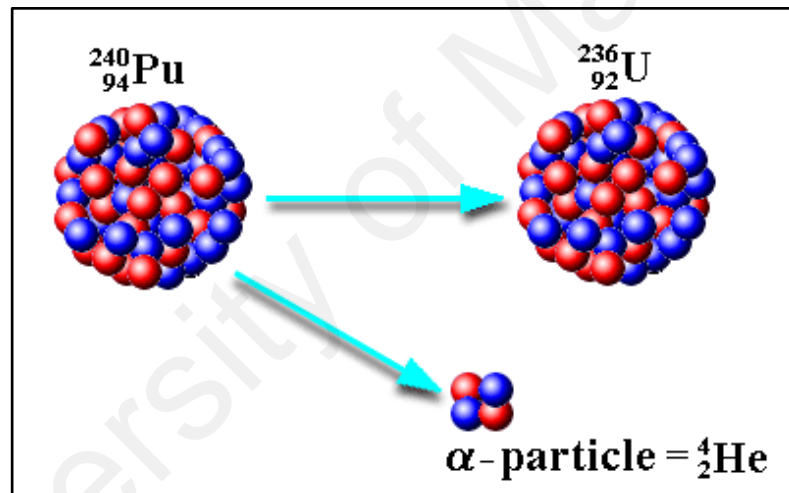
Figure 2.1: Alpha radiation decay.

2.2.2 Beta radiation decay (β)

As shown in Figure 2.2 (a), during beta-minus decay, a neutron in the nucleus of an atom turns into a proton, an electron (β^-) and an antineutrino (v^-). The electron and antineutrino ejected from the nucleus, which now has one more proton than it started with. Since an atom gains a proton during beta-minus decay, it changes from one element to another. For example, after undergoing beta-minus decay, an atom of

radium (with 88 protons) becomes an atom of actinium (with 89 protons). During beta-plus decay as in Figure 2.2 (b), a proton in an atom's nucleus turns into a neutron, a positron and a neutrino. The positron (β^+) and neutrino (v^+) ejected from the nucleus, which now has one less proton than it started with. Since an atom loses a proton during beta-plus decay, it changes from one element to another. For example, after undergoing beta-plus decay, an atom of protactinium (with 91 protons) becomes an atom of thorium (with 90 protons). Although the number of protons and neutrons in an atom's nucleus change during beta decay, the total number of particles (protons + neutrons) remains the same. Beta particles generally are very small and can penetrate more deeply than alpha particles. However, most beta radiation can be stopped by small amounts of shielding, such as sheets of plastic, glass or metal as shown in Figure 2.4. When the source of radiation is outside the body, beta radiation with sufficient energy can penetrate the body's dead outer layer of skin and deposit its energy within active skin cells (Hallenbeck, 1994). However, beta radiation is very limited in its ability to penetrate to deeper tissues and organs in the body. Beta-radiation-emitting nuclear substances can also be hazardous if taken into the body.
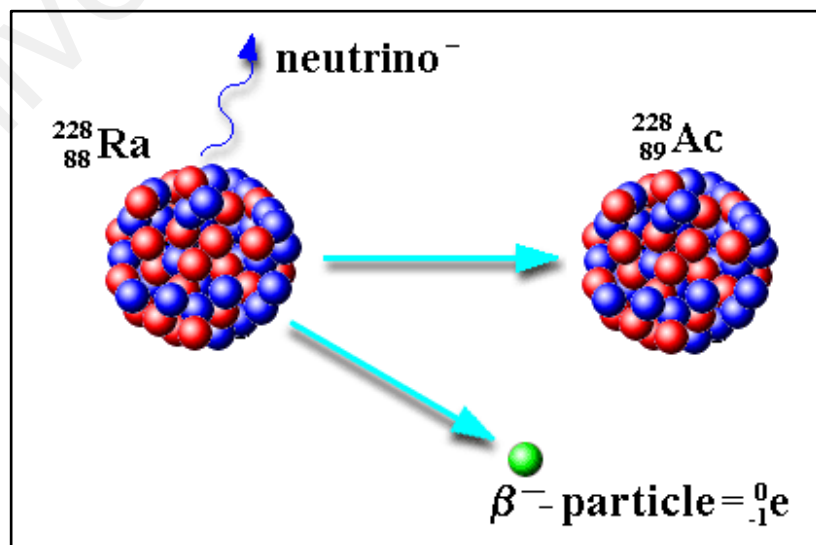
(a)
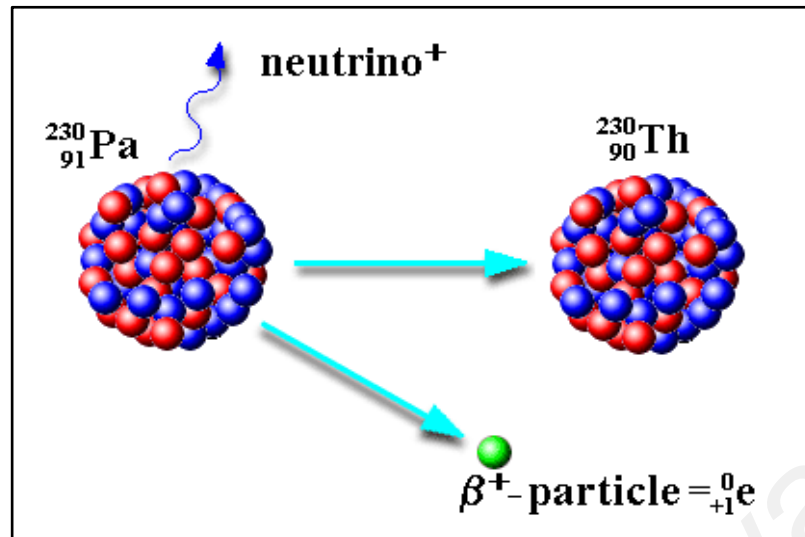
(b)

Figure 2.2: Beta **(a)** minus; electron and **(b)** plus; positron radiation decay.

2.2.3   Photon radiation; gamma (γ) and x-ray decay

Photon radiation is electromagnetic radiation. There are two types of photon radiation; gamma (γ) and x-ray, the first resulting from nucleon de-excitation, with rearrangements predicted within a shell model description, while the second results from electron rearrangements as predicted within an atomic shell model description. Gamma radiation consists of photons that originate from within the nucleus, and x-ray radiation consists of photons that originate from outside the nucleus, and are thus typically lower in energy than gamma radiation. Photon radiation can penetrate very deeply, significantly reduced in intensity by materials that are quite dense and of medium to high atomic number, as for instance steel and lead, as shown in Figure 2.4. In general, it can travel much greater distances than alpha or beta radiation, and it can penetrate bodily tissues and organs when the radiation source is outside the body. This radiation can also be hazardous if photon-emitting nuclear substances are taken into the body (Gofman, 1981). An example of a nuclear substance that undergoes photon emission is Plutonium-240 as shown in Figure 2.3.

11
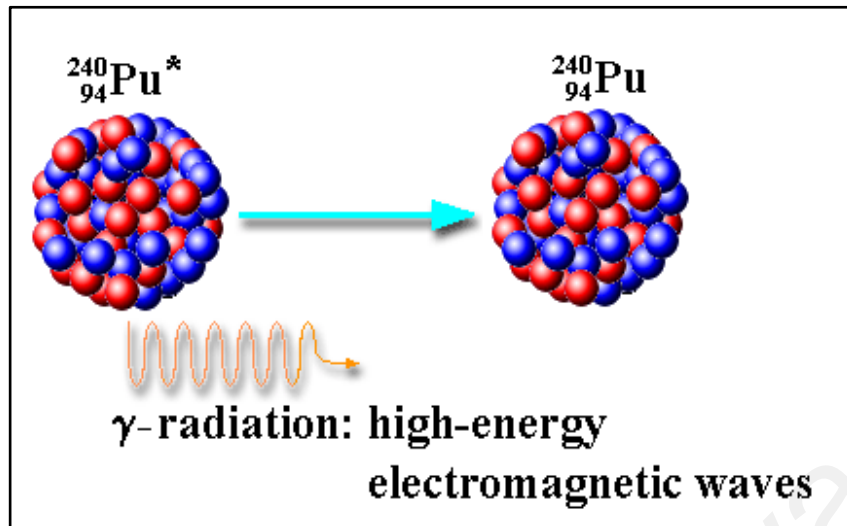
Figure 2.3: Gamma radiation decay.
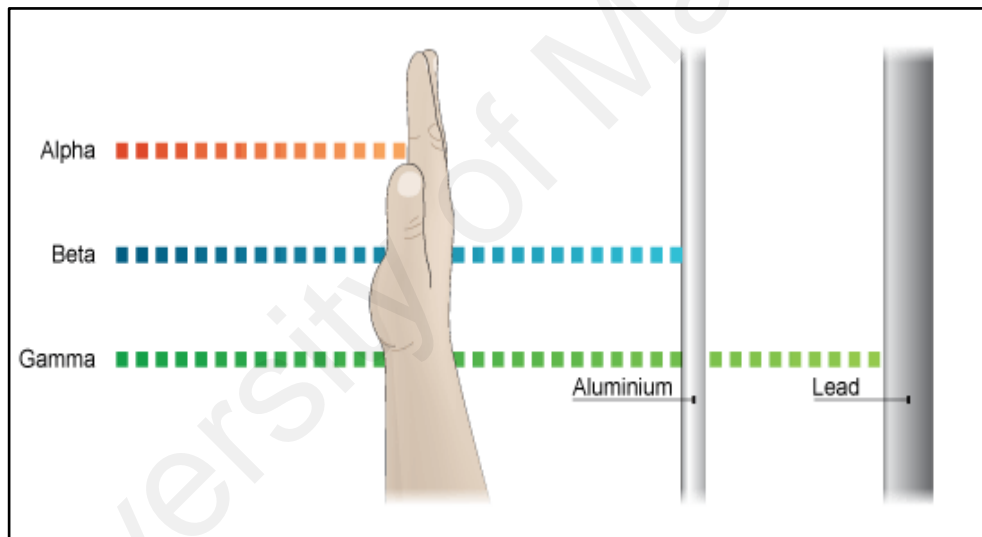
Figure 2.4: Penetration ability of alpha, beta and gamma radiation.

2.3 NORM and TENORM

Naturally Occurring Radioactive Materials (NORMs) is the material found in the earth's environment that contains radioactive elements of natural origin. NORM exists in water, soils, plants, coal, petroleum, humans and animals. If the NORM is concentrated, then the emissions can be damaging to humans, both on a short-term and a long term basis

(Zielinski et al., 1999). These elements are naturally decaying and are considered primary contributors to the yearly background radiation dose of an individual.

The sources of NORM can be classified into those materials which come from the earth's crust, referred to as terrestrial sources and representing the largest contribution to the annual dose of an individual, and cosmic ray interactions with the atmospheric gases, referred to as cosmogenic sources. Different parts of the world have different radioactive dose levels from the terrestrial sources, depending upon the geological makeup. Primary NORM radionuclides have long half-life, such as uranium, thorium, potassium and a number of their decay products such as radium. Radon isotopes which will end up in ground, water, air and biological systems have moderate half-lives from seconds to hours (Amin et al., 2013). In different parts of the world, locations with higher soil concentrations of uranium and thorium generally produce higher dose rates. Potassium-40, one of the major sources of terrestrial NORM, is also contained in the skeletal component of the human body. With a long half-life of about 1.25 billion years, it still exists in measurable quantities today (UNSCEAR, 2000). Generally, in foodstuffs such as banana there are appreciable levels of potassium and indeed these fill a vital dietary requirement especially for the bones in our body; with the presence of stable potassium there is also a measurable level of potassium-40.

As mentioned, cosmogenic NORM occurs as a result of interactions between certain gases in the Earths' atmosphere and cosmic rays. The amount of dose of cosmic radiation that one will receive will depend on differences in elevation, atmospheric conditions, and the Earths' magnetic field. At higher altitudes greater levels of cosmic radiation are received i.e. mountain dwellers and frequent flyers are typically exposed to greater doses than others. The intensity of cosmic radiation is very much greater outside of the Earths' atmosphere and magnetic field (UNSCEAR, 2000).

TENORM or technologically enhanced NORM is the term used for terrestrial sources that are incremented over the existing natural radionuclide material (NORM) concentrations found in undisturbed environments. In industries related to the extractive industries, including manufacturing, mineral extraction, water processing, and others (Kolo et al., 2015) the radioactive waste that is generated will release some amount of radiation into the environment, disturbing and enhancing NORM concentration (Shale, 2011). The waste from extraction and processing of rare earth elements and from fossil fuel power plants is TENORM and if not handled effectively this can become a channel to public exposure. Thorium dust, which is a known cancer-inducing agent, can easily be blown by wind and carried by water over long distances, thereby creating radiation hazards over large spans of area (Kolo et al., 2015).

Oil and gas industries waste also contribute to technologically enhanced NORM concentration in the marine environment (Zielinski et al., 1999). As mentioned by (Alam and Mohamed 2011)), most of this TENORM is in the form of a complex of barium, radium and sulphates and this is insoluble in sea water, such that it will commonly end up in the water. As a result, the marine environment will be at risk of enhanced exposure. Human lives can also be at risk since marine products, not least fish and shellfish, can accumulate TENORM, subsequently being transferred to the human body through the food chain. Exposure to radioactivity increases one's risk of various cancers (Wilson, 1993).

2.4 Natural decay series of primordial radioactive

The natural decay series occur when particularly long-lived unstable nuclides decay into other nuclides, moving towards a stable state. Most nuclides do not decay directly to a stable state but rather they undergo a series of decays until eventually a stable nuclide is reached. This natural decay series, related with primordial radionuclides, start with uranium-238, uranium-235, and thorium-232, as shown in Figure 2.5, Figure 2.6, and Figure 2.7 respectively. All of these are approximately in a state of secular equilibrium in nature, in which the activities of all radionuclides within each series are effectively the same as that of the parent radionuclide. There are two conditions to achieve this state. First, the parent radionuclide must have a longer half-life compared to the other radionuclides in the series. Second, a sufficiently long period of time must elapse to allow for ingrowth of the decay products.

As in the figures previously shown, by emitting subatomic particles like alpha and beta particles, unstable radionuclides will decay to more stable radionuclides. The emission of alpha will release two protons and two neutrons (helium nuclei) while the emission of betas will release one electron in the process. Gamma emission is also typically involved in this series as newly formed nuclides (after alpha or beta decay) will appear in excited states with a surplus energy that is dissipated through the gamma emission process. Therefore excited nuclides have a tendency to release the excess of energy by emission of gamma rays (photons) to return to a more stable state (Argonne National Laboratory, 2005).
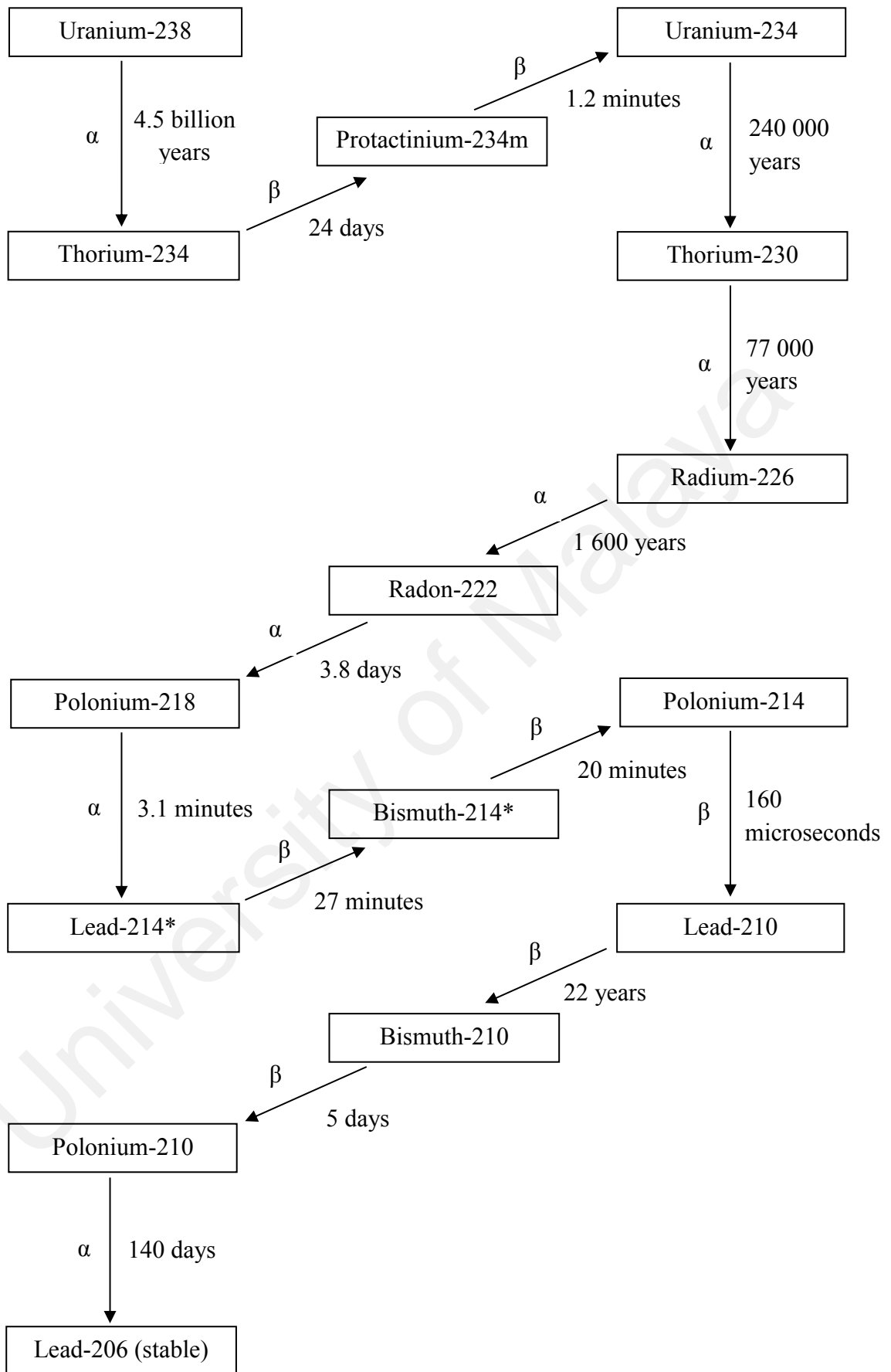
Figure 2.5: Uranium-238 decay series.
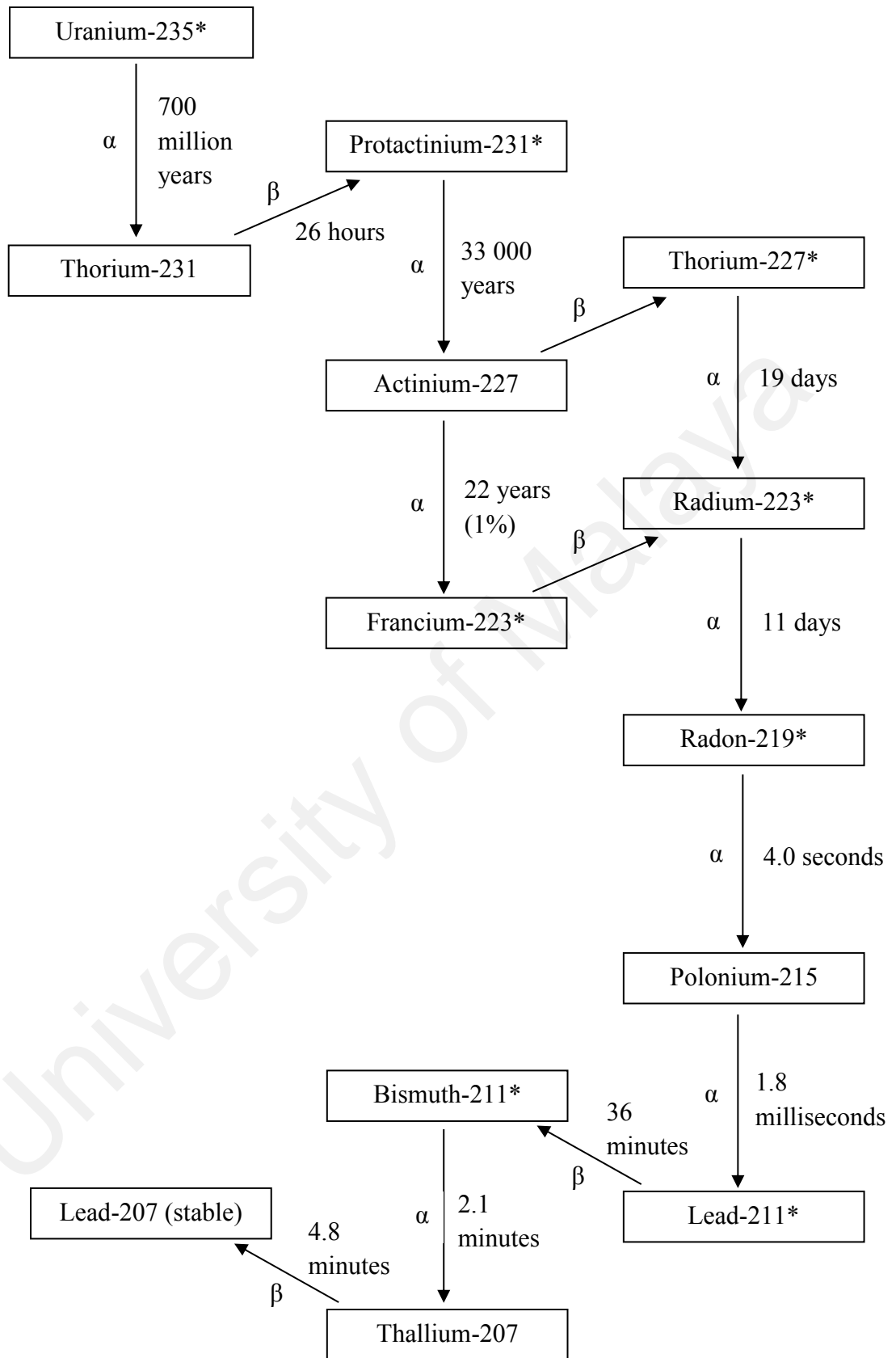
Figure 2.6: Uranium-235 decay series.
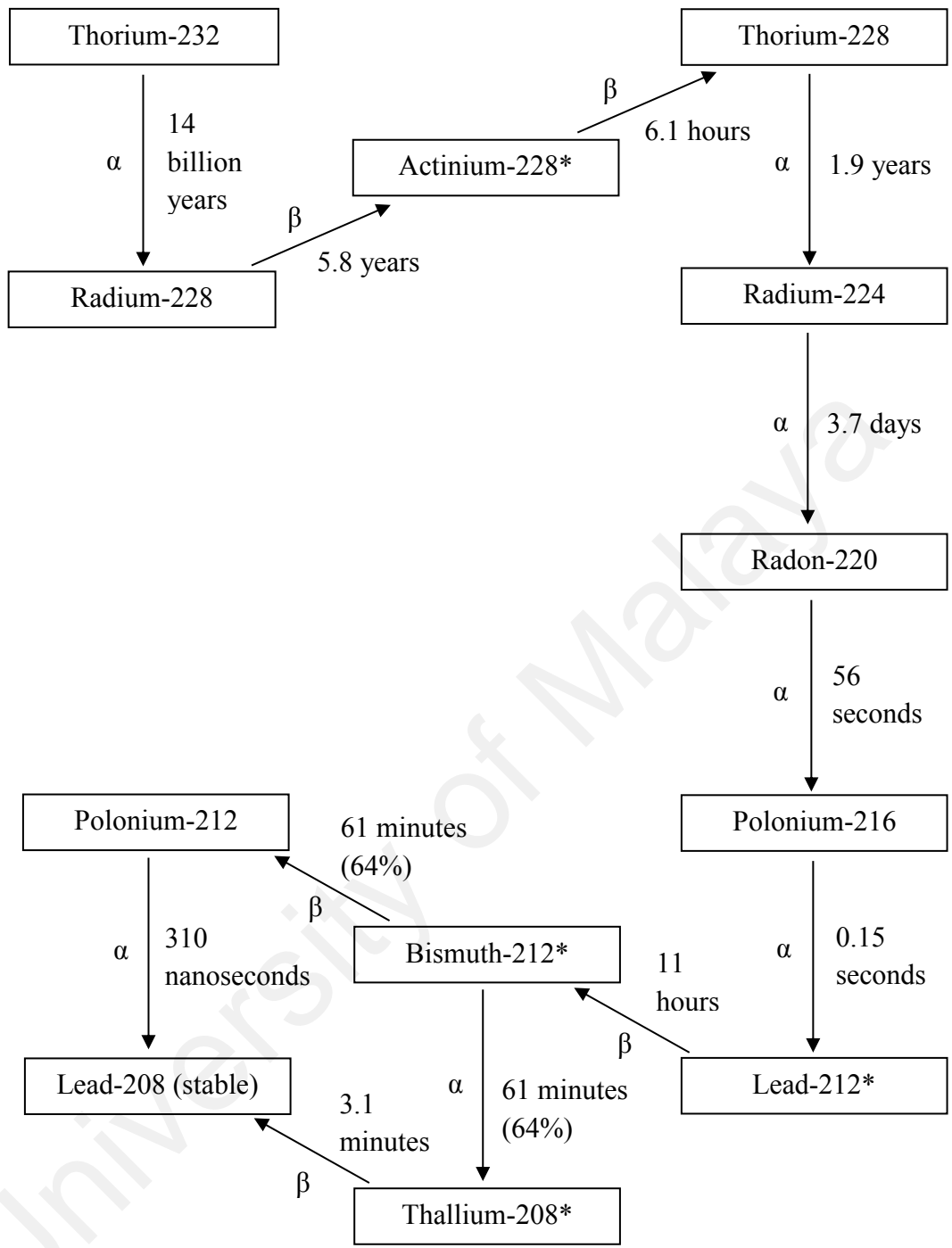
Figure 2.7: Thorium-232 decay series.

NOTES:

The symbols α and β indicate alpha and beta decay, and the times shown are half-lives.

The intrinsic (*) indicates that the isotope is also a significant gamma emitter.

2.5   Thermoluminesence dosimeter (TLD)

Thermoluminescence (TL) or more definitively Thermally Stimulated Luminescence is a phenomenon in which a selected medium emits light under application of heat (Furetta, 2003). TL dosimeter (TLD) is a device that can measure the absorbed dose, or other relevant quantities like KERMA (kinetic energy released in the medium), exposure or equivalent dose, which is produced due to the interaction of the ionizing radiation with a material (Attix, 2008). The TLD is based on electron-hole trapping levels like in insulators or semiconductors material that exist prior to irradiation, the trapped electrons and holes being promoted into the trapping levels through irradiation. Subsequently they are released as a light by the use of thermal relaxation (the application of heat), including from deep traps. To provide for greater sensitivity to irradiation, it is desirable to have higher TL yield through the existence of a greater population of trapped electrons or holes, the filling and de-trapping then corresponding to the radiation absorbed dose. This technique of trap level acts as a 'memory cell' of the ionizing radiation dose.

2.5.1   Phosphor-based TLD

In TL dosimetry applications, phosphor based TLDs are commonly used as radiation dosimeters to measure radiation dose from sources to which the phosphor has been exposed. It was first proposed by Farrington Daniels and his research group at the University of Wisconsin, USA that the TL phenomenon could be used as a radiation dosimeter, an irradiated material containing stored energy which could be thermally released (Daniels et al., 1952). For present study, TLD-100 (LiF:Mg,Ti) and TLD-200 (CaF_2:Dy) are the phosphor based TLDs that will be used. As one of the main parameters in environmental dose-rate, the chosen TL phosphors should be of high

sensitivity and have low fading characteristics. Hence, TLD-200 is often chosen for this as this TL phosphor has all of these characteristics. TLD-100 is used as the standard reference medium with an assigned relative sensitivity of 1.00 (McKeever et al., 1995).

Lithium fluoride (LiF) TL phosphor was one of the first phosphors suggested for TLD. The TL of LiF is sufficient to detect relatively low exposures (diagnostic x-ray levels in particular) and it has a low energy dependence. The most widely used and also extensively studied version consists of LiF doped with approximately 170-ppm Mg^{2+} ions and approximately 7 ppm Ti^{4+} ions, known as TLD-100 (Bos et al., 1990). Its effective atomic number is 8.14 which is sufficiently close to that of biological tissue (7.4) so as to provide a response which varies only slightly with photon energy. Thus it can be considered as tissue equivalent (Furetta, 2003). TLD-100 comes in a variety of forms such as powder, rod, chips or cards; the chips form is the most widely used for dosimetric purpose, as in present study, as shown in Figure 2.8, with $3.2 \times 3.2 \times 0.89$ mm^3 size. The general characteristics of TLD-100 are shown in Table 2.1.
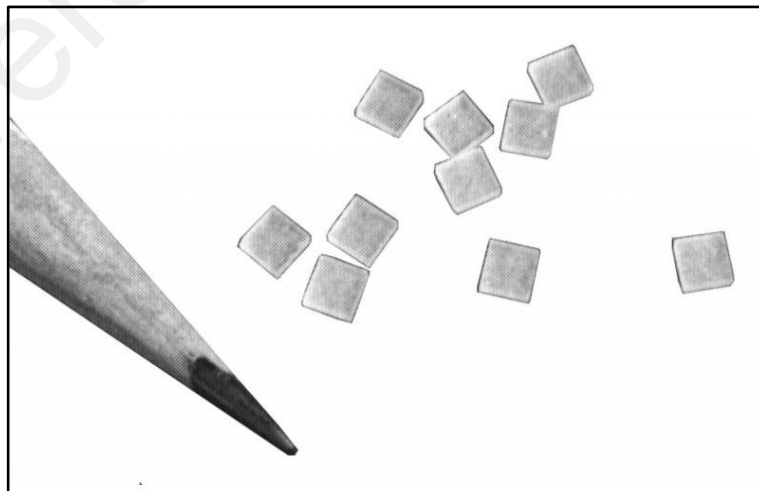
Figure 2.8: Phosphor TLD-100 in chips form.

Table 2.1: General characteristics of phosphor TLD-100 ((Savva, 2010).

Characteristics	
Useful dose range	50 µGy – 10^3 Gy
Dosimetric peak temperature (°C)	195
Effective atomic number	8.2
Density (gm/cc)	2.64
Energy response (30 keV relative to ^{60}Co)	1.3
Relative gamma ray sensitivity	1
Light (UV) sensitivity	Very low
TL fading	5% per year at 20 °C (with anneal)

CaF$_2$:Dy (dysprosium doped calcium fluoride) has been commercialized by Harshaw under the name TLD-200. As with TLD-100, TLD-200 also comes in a variety of forms such as rods, powder, chips and cards. In this study, we used phosphor TLD-200 in chips forms as shown in Figure 2.9 with the size of $3.2 \times 3.2 \times 0.89$ mm^3. TLD-200 presents a complicated glow curve consisting of six peaks, while the TL response is linear up to 1 kGy (Furetta, 2003). The general characteristics of TLD-200 are shown in Table 2.2.

Figure 2.9: Phosphor TLD-200 in chips form.

Table 2.2: General characteristics of phosphor TLD-200 (Mahesh et al., 1989).

Characteristics	
Useful dose range	$\mu Gy - 10^3$ Gy
Dosimetric peak temperature (°C)	200
Effective atomic number	16.3
Density (gm/cc)	3.18
Energy response (30 keV relative to ^{60}Co)	15.6
Relative gamma ray sensitivity	16
Light (UV) sensitivity	High
TL fading	12% per month

2.5.2 Fiber-based TLD

Figure 2.10 shows the basic structure of an optical fibre which consists of fiber cladding (outer layer) and the core (inner layer), with different indices of refraction. The fiber cladding is most often fabricated from very pure silica (SiO_2), in the form of Suprasil F300, a product of Heraeus (Hanau, Germany). TL properties of SiO_2 optical fiber depends on the trapping process that is caused by the occurrence of structural defects in the material. Types and concentration of the impurities in the material also affects its TL response (Begum et al., 2014). The potential of the commercial SiO_2 doped optical fiber has been investigated by a number of researchers for several radiation types including photons (Youssef. A. et al., 2001), electrons (Hashim et al., 2009), alphas (Ahmad Termizi Ramli et al., 2009), synchrotron radiation (A.T. Abdul Rahman et al., 2010). The properties of fiber such as water and corrosion resistance, good spatial resolution (~ 100 μm), and an ability to be re-used numbers of times following thermal annealing, make it possible to be used as TLD (D.A. Bradley et al., 2012).
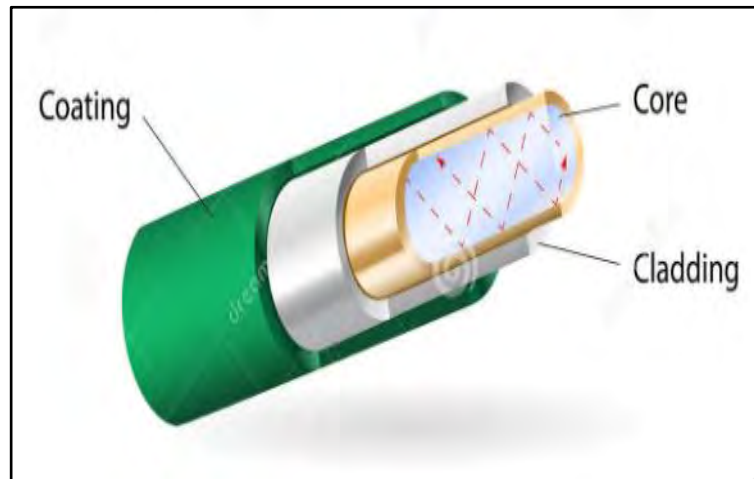
Figure 2.10: Basic structure of commercial single-mode (SM) optical fiber produced for telecommunication purpose, consisting of three main parts: coating, cladding and a core.

2.6 Thermoluminescence (TL) mechanism

In a perfect crystal structure, there exists a bandgap between the valence band and conduction band, where the electron or hole states are forbidden. However, when it is disturbed by the presence of defects, one or more additional energy levels can be introduced into the forbidden gap. As shown in Figure 2.11 (a), the additional levels are localized at the crystal defect, with electrons (e^-) found in the valence band. When the material is irradiated, e^- from the valence band can be excited to the conduction band, where they move freely. The holes (h) which remain in the valence band (and can be thought of as an absence of electrons) also move freely inside the crystal until they are trapped in hole traps or recombined with electrons. The presence of defects in the crystal cause the e^- and hole to be trapped at the forbidden band as in Figure 2.11 (b). If these traps are deep, the charges carriers will not have enough energy to escape. By heating the crystal, they may acquire enough energy to escape. Subsequently, the released e^- may leave the traps and recombine with holes at recombination centres with the emission of light (shown in Figure 2.11 (c))
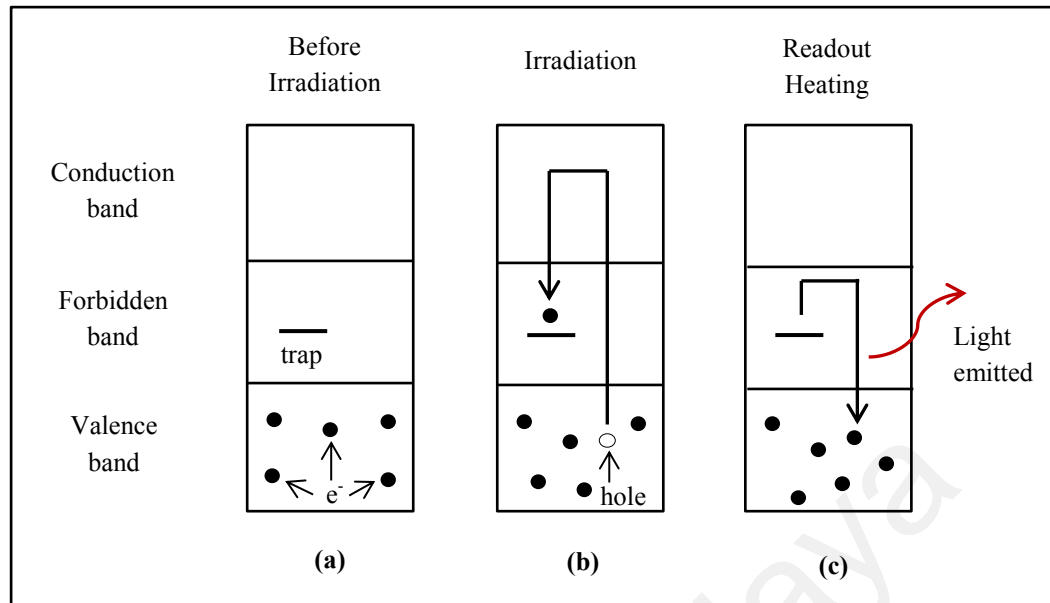
Figure 2.11: Mechanism of TL

2.7 Characteristics of TLD

The most important characteristics of TL material allow them to be used for instance as dosimeters in radiation monitoring, i.e. personal, environmental and clinical dosimetry. These characteristics are as follows:

- High sensitivity; high concentration of electron or hole traps and a high efficiency of light emission associated with recombination.

- Have a linear TL response over wide range of doses especially for low doses of irradiation.

- Good storage stability of trapped charges over time to avoid undesirable fading even during extended storage at room temperature or slightly higher temperature

- Good resistance against disturbing environmental factors such as light (optical fading), humidity, organic solvents, gases and moisture.

- Have a low photon energy dependence of response.

- High precision and high accuracy are required for any kind of applications.

(Furetta, 2003).

CHAPTER 3 : EXPERIMENTAL METHODS

3.1 Introduction

In this chapter, details of the experimental methods will be discussed, the text being divided into two main parts. The first part involves the preparation and work carried out at the laboratory, with the focus on sample characterisation studies, while the second part involves the preparation and work carried out at the field measurements site (at selected areas within Gebeng, Pahang) for the environmental study.

3.2 Laboratory work: Sample preparation for characteristics study

By using the modified chemical vapour deposition (MCVD) process in Multimedia University, extrinsically doped optical fibre has been produced by prefabricating a single glass rod known as preform. As shown in Figure 3.1, as a starting process a mixture of oxygen, silicon tetrachloride ($SiCl_4$) and $GeCl_4$ (for Ge doped) and additionally BCl_3 (for Ge and boron doping) is passed into a rotating silica glass tube, being treated together with the supply of heat from the outside at a temperature of 2100 °C (Siti Shafiqah et al., 2015).
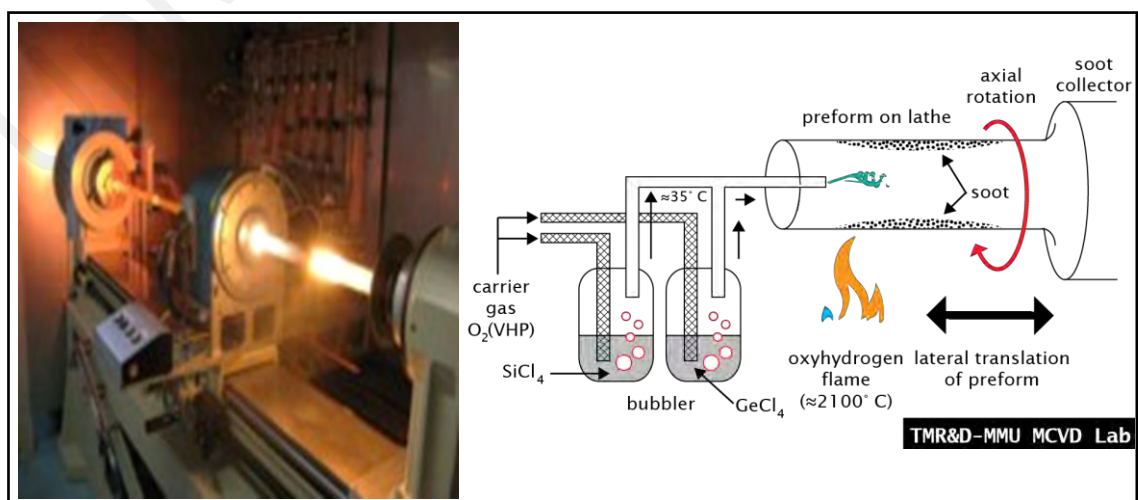
Figure 3.1: Fabrication of preform via MCVD process at Multimedia University.

These silica glass tubes (the preform) are later drawn into single fibre through use of a pulling tower located at the Department of Electrical Engineering, University of Malaya, as shown in Figure 3.2.
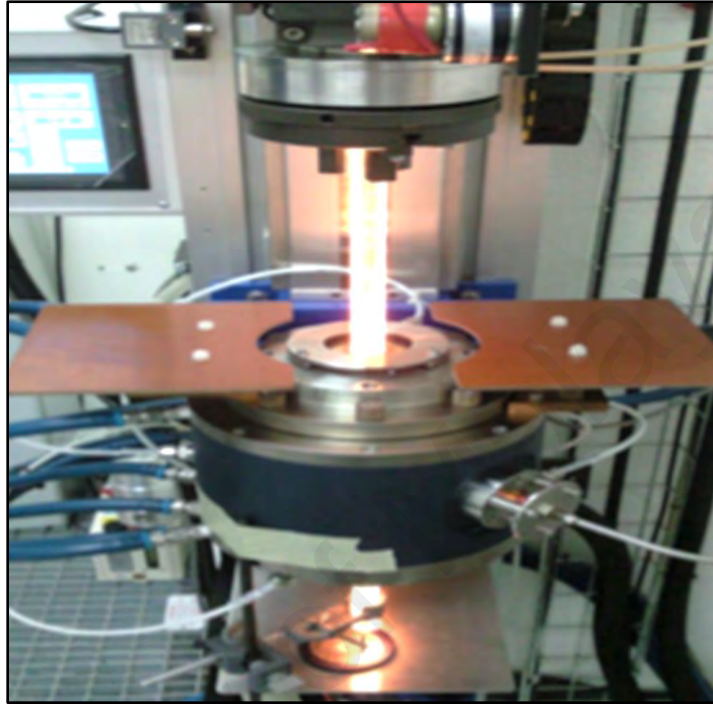
Figure 3.2: Fibre pulling tower at Department of Electrical Engineering, University of Malaya shows heated preform and ready to be pulled by addition of tension.

For present study we have investigated the performance of the most sensitive fibres that we currently have (Mahdiraji et al., 2015), namely the collapsed Photonic Crystal Fibres (PCFc) doped with Ge or Ge-B as shown in Figure 3.3 (a). The preform is then re-pulled into a cross-sectional diameter of 125 μm for PCFc-Ge and 140 μm for PCFc-Ge-B fibre (matching with typical values for the commercially available optical fibres that have been investigated as TLDs in the past) as shown in Table 3.1. Lengths of 0.5 ± 0.1 cm of collapsed PCFs rod have then been cut using a diamond-cutter and weighed using an electronic balance.

Table 3.1: Respective types, diameter and mass of fibres used.

Sample	Diameter (± 10 µm)	Mass (± 0.1 mg)
PCFc-Ge	125	0.1
PCFc-Ge-B	140	0.1

(a)   **(b)**
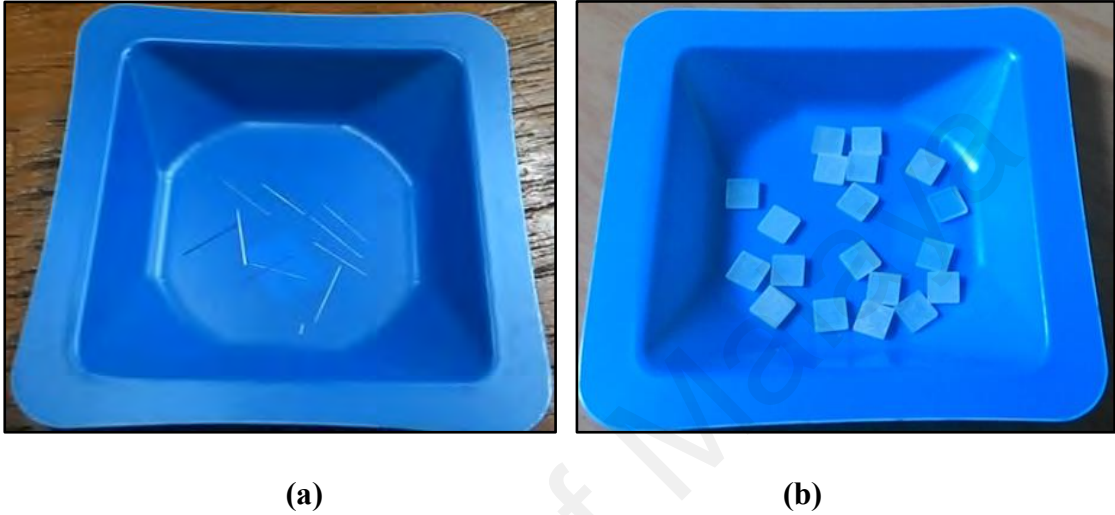
Figure 3.3: (a) Collapsed Photonic Crystal Fiber (PCFc) cut into 0.5 ± 0.1 cm length; **(b)** Phosphor TLDs sample.

The response of the collapsed PCFs (Figure 3.3 (a)) have been compared with the phosphor TLDs (Figure 3.3 (b)); TLD-100 (mean mass of 23.4 mg) and TLD-200 (mean mass of 28.5 mg) chips (Thermo Fisher Scientific Inc, Waltham, MA, USA), the latter being of dimension $3.2 \times 3.2 \times 0.89$ mm^3.

3.2.1 Annealing process

With use of a Harshaw furnace (shown in Figure 3.4), annealing has been performed of the collapsed PCFs and TLD-100 held at 400 °C while for TLD-200 these are held at 500 °C. All the samples were annealed for a period of 1 hour, removing any previously stored triboluminescence and irradiation history, also stabilising the trap structure (Furetta, 2003). In this process, the samples were wrapped with aluminium foil to

minimize the possibility of loss of samples and contamination from the multi-user furnace and were put on a ceramic plate. As a control measure after 1 hour of annealing, with the samples remaining in the furnace, additional thermal stress has been avoided by allowing the samples to cool down naturally over a period of 24 h (Hashim et al., 2014). In order to minimize exposure to ambient light levels the samples were then retained in individual small plastic bags and placed in a light-tight box, ready for irradiation.

Figure 3.4: Harshaw furnace for sample annealing.

3.2.2 Sample irradiation

Irradiations were made using X-ray and gamma beams, from an ERESCO 200 MF4 (Figure 3.5 (a)) and a conventional Gammacell-220 ^{60}Co (Figure 3.7) respectively, both located at the Department of Physics, University of Malaya. The sample characteristics studies, including TL dose and energy response, glow curve, fading, and other such factors, were investigated by irradiating the samples to these sources.

3.2.2.1 ERESCO 200 MF4 X-ray
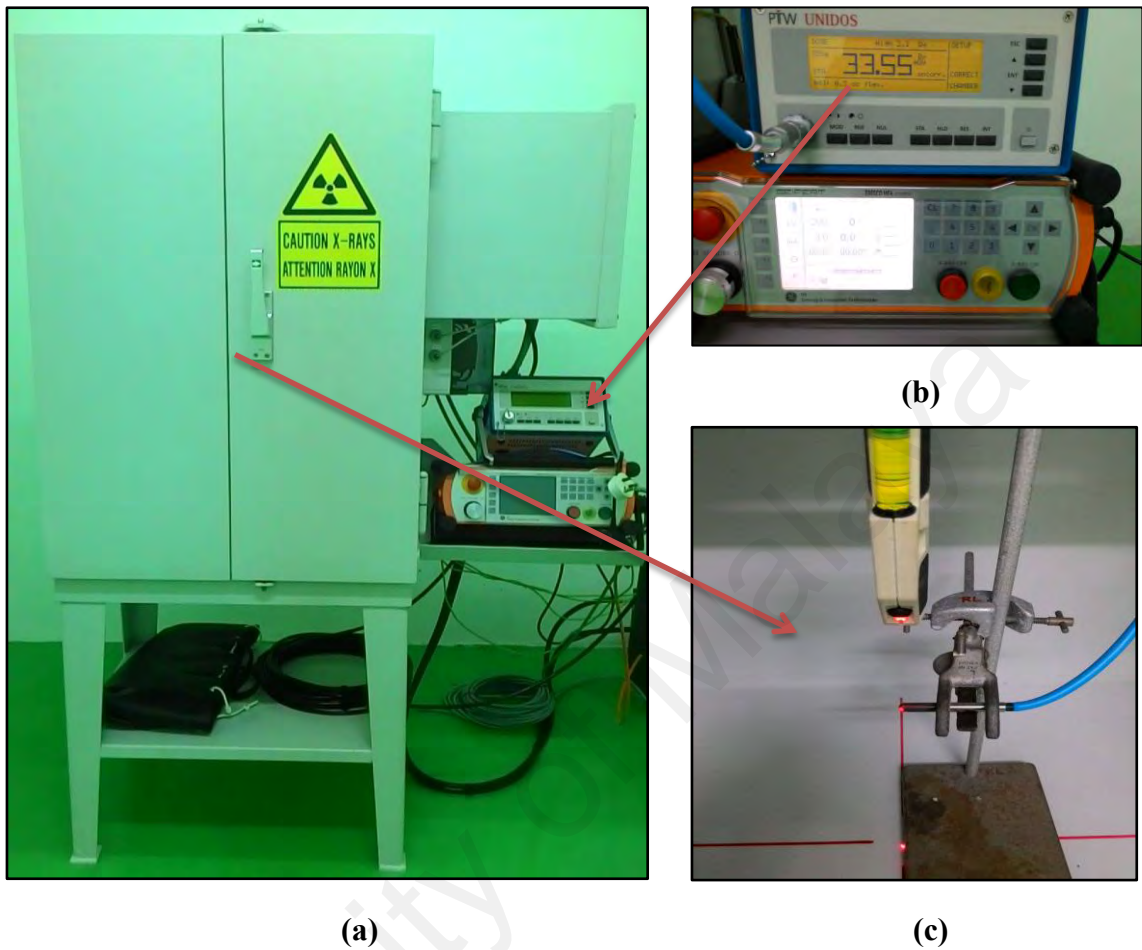
Figure 3.5: (a) ERESCO 200 MF4 X-ray source **(b)** UNIDOS display
(c) For dose calibration the PTW UNIDOS ionization chamber is placed on the central
axis of X-ray source, exactly at the same point that the samples will be placed at later.

As shown in Figure 3.5 (a), this particular x-ray machine has an extended operating
range of peak accelerating potential from 10 to 200 kV, nominally equivalent to the
supply of an energy range from 5 to 100 keV, the x-ray tube beams being estimated to
have an effective energy of the order of one-third to one-half of the maximal values
(Ramli et al., 2015). It also has a tube current range from 0.5 to 10 mA, inherent
filtration of 0.8 mm ± 0.1 mm Be and has a large 40° × 60° emergent beam. By using
this machine, we can control the tube potential value and time for the x-ray exposure.
However, in order to deliver the particular x-ray irradiation doses at clearly defined

energy, the machine have to be calibrated, conducted herein using a PTW UNIDOS ionization chamber as shown in Figure 3.5 (b) and (c). For irradiations, the samples are placed on the central axis of the x-ray source at a focus to surface distance (FSD) of 38 cm.

The x-ray machine working principle can be explained by referring to the x-ray tube schematic in Figure 3.6. This evacuated tube is where the x-rays are produced. As a result of the current being supplied to the filament at the cathode, the cathode heats up producing emission of electrons. Due to the large potential difference applied between the anode and cathode, these electrons immediately travel with high speed towards the anode. The beam of electrons strikes the tungsten anode and knocks out electrons in the lower atomic orbitals. Higher orbital electron move to replace those empty positions while releasing its energy in the form of photon called x-ray photons. The electrons also slow down as a result of coulombic interactions and produce bremsstrahlung x-ray radiation.
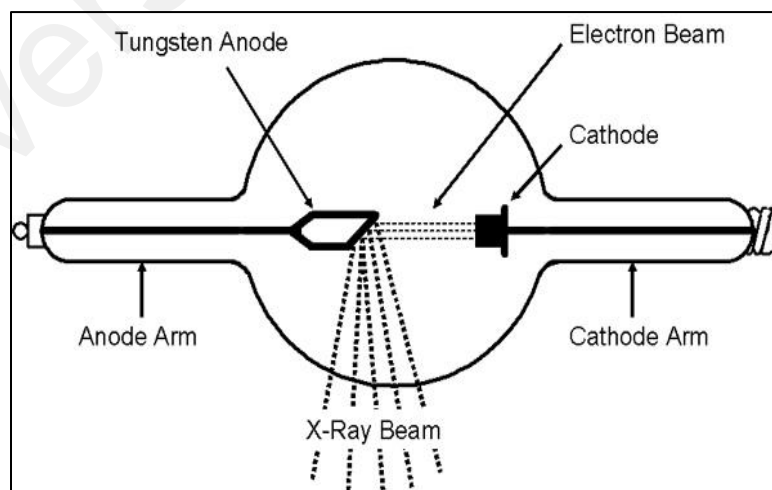
Figure 3.6: Illustration of x-ray tube.

3.2.2.2   Gammacell 220 ^{60}Co

This Gammacell 220 ^{60}Co gamma irradiator is a source that is capable of delivering high doses of gamma radiation. As shown in Figure 3.7, this unit basically consists of an annular source permanently enclosed within a lead shield, a cylindrical drawer, and a drive mechanism to move the drawer up or down along the source centre-line. The drawer has a chamber to carry the samples to be irradiated from outside of the shield to the source. The diameter and the length of the irradiation chamber are about 6 inches (approx 15 cm) and 8 inches (approx 20 cm) respectively. The ^{60}Co radionuclide contained in this Gammacell emits two photon energies, 1.1732 MeV and 1.3325 MeV.

To irradiate samples to a known dose using this Gamma cell, we need to know the dose-rate in order to control the exposure time. For this we use the dose rate formula:

$$D_t = D_o e^{-\lambda t} \tag{3.1}$$

with D_t the dose rate in Gy/s, D_o the initial dose rate at November 1995 of the Gammacell 220 ($D_o = 0.525$ Gy/s), λ the decay constant ($\lambda = 4.1681 \times 10^{-9}$ s^{-1}) and t the time difference from November 1995 to present day (in seconds).

By considering the time difference from the November 1995 to present day, we get the D_t value at present day, to allow time control for a required dose (for example 1 Gy). This is calculated using equation (2);

$$D_t = {D}/{t}$$
$$t = {D}/{D_t} \tag{3.2}$$

where t is the time control in seconds and D is the required dose in Gy.

Figure 3.7: A conventional Gammacell-220 ^{60}Co, located at Department of Physics, University of Malaya.

3.2.3 Sample readout

As shown in Figure 3.8, the sample TL measurements have been carried out using a Harshaw 3500 TLD reader (USA) supported by WinREMS software. The facility is located at the Department of Physics, University of Malaya.

Figure 3.8: A Harshaw 3500 TLD reader, supported by WinREMS software, the vacuum tweezers being used for sample handling.

A schematic diagram of a TLD reader is shown in Figure 3.8. The sample is placed within a metallic support (tray otherwise referred to as a planchette) inside the chamber. There, the heating coil is in good thermal contact with the samples held in the tray. The thermocouple is also used to measure the temperature of the heating cycle in the chamber. The readout chamber should be continuously supplied with a slow flow of nitrogen gas in order to reduce sample oxidation and other spurious phenomena thus decrease the background. (Van Dam and Marinello, 2006). The thermoluminescence which is emitted passes through a set of optical filters and enters the photomultiplier tube (PMT) where a photocathode inside it converts the light emission to current (electrical signal). That current is amplified inside the PMT to give an output that can easily be measured. The output current from the PMT is proportional to the number of photons which are generated, and is typically proportional to the absorbed dose when the output is integrated. The glow curves are displayed during dose measurements so as to provide a maximum amount of information.
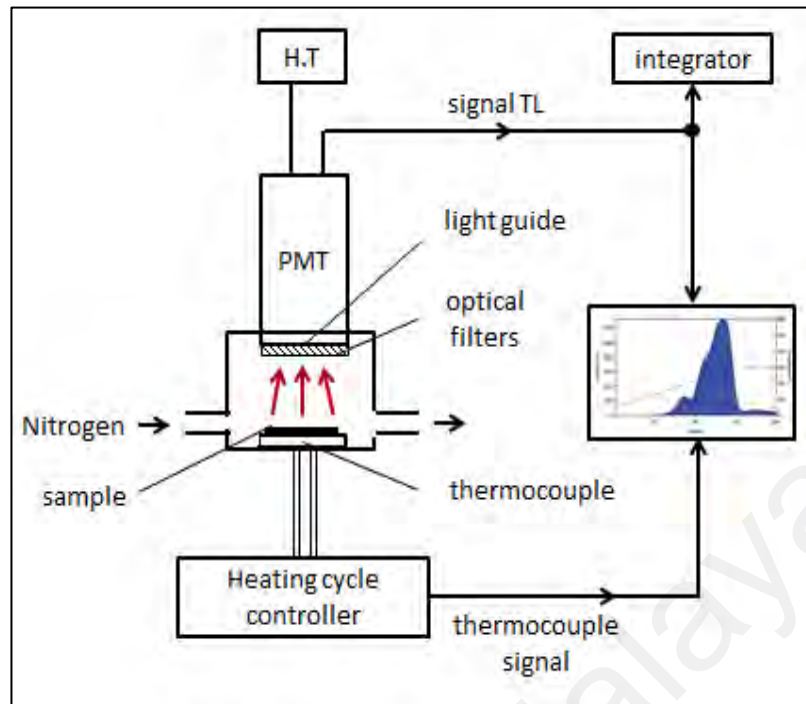
Figure 3.9: Schematic diagram for TLD reader.

In present study, the readout system of the TLD reader was set up with the following parameters: preheat temperature of 50 $^{\circ}$C, heating rate of 10 $^{\circ}$C.s^{-1} and maximum temperature for data acquisition of 400 $^{\circ}$C. This time-temperature profile (TTP) has been set to obtain the complete capture of TL glow curve under optimum conditions. Following the readout process, the TL readings for the samples are normalized to its unit mass, obtaining results in nC/g.

3.3 On site work: Sample preparation for environmental study

For the environmental study, both collapsed PCFs and phosphor TLDs have been buried at eight selected locations within Gebeng, Pahang. After several selected exposure durations, those samples have been collected and the absorbed radiation dose has been readout using the TLD reader. At the same locations, soil samples have also been collected and their radioactivity has been measured using a High Purity Germanium

(HPGe) gamma-ray spectrometry. The absorbed radiation doses measured by the TLDs have then been compared against the radiation dose ascertained from the HPGe soils analysis released.

3.3.1 Sampling locations

Shown in Figure 3.10 and Table 3.2 are details of the eight selected areas within Gebeng Industrial Estate (GIE), in Pahang, all being at various distances off-site of the Lynas Advanced Material Plant (LAMP) chosen in this study. These locations have potential for TENORM contributions from site emissions, albeit to a very subtle extent based on a-priori data from others. The sampling locations comprise an undisturbed area, a recreation lake, a swamp area, a construction area, and a beach area, with various distances of 1, 5, 10, and 20 km from LAMP.

Figure 3.10: Sampling locations within Gebeng Industrial Estate (GIE), Pahang which is off-site of LAMP.

Table 3.2: Sampling location coordinates off-site of LAMP, Gebeng, Pahang.

Sampling ID	Location	Coordinates		Distance from LAMP site (km)
		Latitude, N	Longitude, E	
L1	LAMP gate	3° 59' 52.4"	103° 22' 26.3"	1
L2	Opposite LAMP	3° 59' 50.1"	103° 22' 25.6"	1
L3	Bridge to rail	3° 59' 35.4"	103° 21' 35.6"	5
L4	Construction area	3° 58' 12.4"	103° 24' 32.2"	5
L5	Swamp area	3° 54' 39.7"	103° 21' 52.6"	10
L6	Nondisturbed areas	4° 06' 46.7"	103° 22' 44.5"	10
L7	Recreation lake	3° 50' 12.4"	103° 17' 47.2"	20
L8	Beach area	4° 10' 47.3"	103° 25' 26.4"	20

At each area (shown in Figure 3.11 to 3.18), four holes about 20 cm depth were prepared for four different exposure durations. Tagging were done purposely to identify the buried samples area as shown in Figure 3.19. All of the samples were buried on May 2015, with subsequent sample collections starting in July 2015 (two months of sample burial), and then later in September 2015 (four months of sample burial), November 2015 (six months of sample burial) and finally on January 2016 (eight months of sample burial).

Table 3.3: Duration of burial of TLDs sample.

Month	May 2015	July 2015	Sept. 2015	Nov. 2015	Jan. 2016
Activity	Burial of all samples	First sc (after two months of sample burial)	Second sc (after four months of sample burial)	Third sc (after six months of sample burial)	Fourth sc (after eight months of sample burial)

*sc: sample collection

Figure 3.11: L1 sampling location.

Figure 3.12: L2 sampling location.

Figure 3.13: L3 sampling location.

Figure 3.14: L4 sampling location.

Figure 3.15: L5 sampling location.

Figure 3.16: L6 sampling location.

Figure 3.17: L7 sampling location.

Figure 3.18: L8 sampling location.

(a)   **(b)**

Figure 3.19: Tagging for each sampling location.

3.3.2   Preparation of TLD samples

From the screening process, the selected samples of collapsed PCFs (Ge and Ge-B doped) and phosphor TLDs (TLD-100 and TLD-200) which ranged in the ± 5% of the mean TL yield were retained in a different bottle as shown Figure 3.20. The bottles were labelled with different colour; yellow label for PCFc-Ge and TLD-100 (in the same bottle), while blue label for PCFc-Ge-B and TLD-200 (in the same bottle). This is purposely for easier identification of samples after sample collection. For every sample collection, three bottles were prepared for each sample to obtain an average data later.
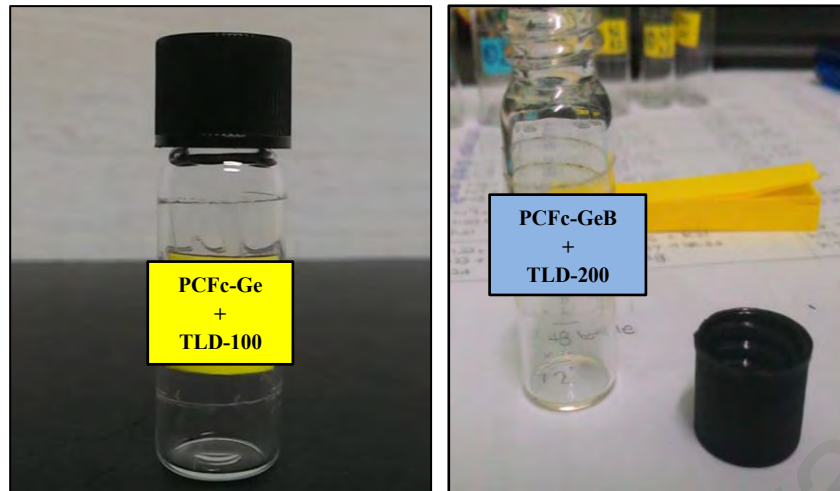
Figure 3.20: Labelled bottles retaining samples. Each bottle contained 5 PCF samples and 1 chip of phosphor TLD. Later, after collection and measurement, the TL responses of each sample have been normalized to its mass (g).

For each sample collection, the samples were kept in the black box shown in Figure 3.21 and maintained at room temperature in order to minimize effects from exposure to direct sunlight and laboratory light. The box was also kept away from any source of radiation that might influence the absorbed radiation dose of the TLDs. All these kinds of exposure (light, heat and radiation) may cause dissipation of electrons present within the crystal structure of the samples and reduce the TL signal by measurable amounts. It was noted on collection that there was moisture inside a number of the bottles. All the PCFs and phosphor TLDs were taken out from the bottles (Figure 3.22) and then left to dry for a few hours (Figure 3.23) to allow subsequent TL measurements to proceed.

Figure 3.21: Black box used to retain the samples after sample collection, subsequently stored at room temperature.
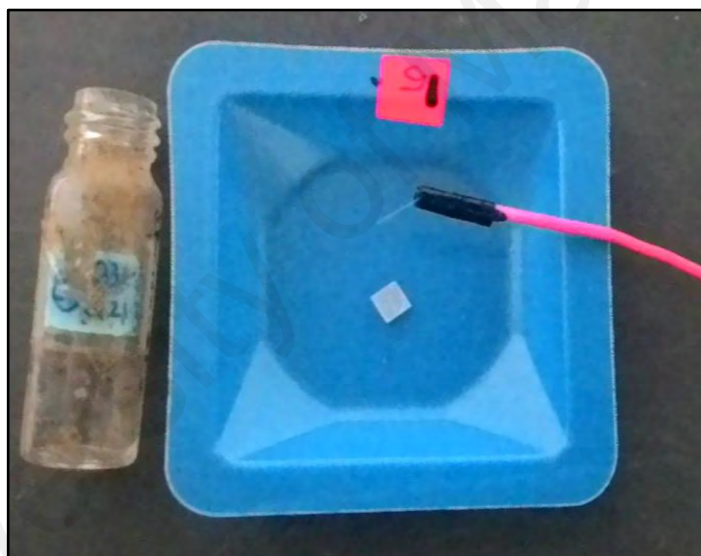
Figure 3.22: Samples were taken out from the bottle; it was noted that the surrounding light was ensured to be dim, to avoid factors that might influence the TL results.
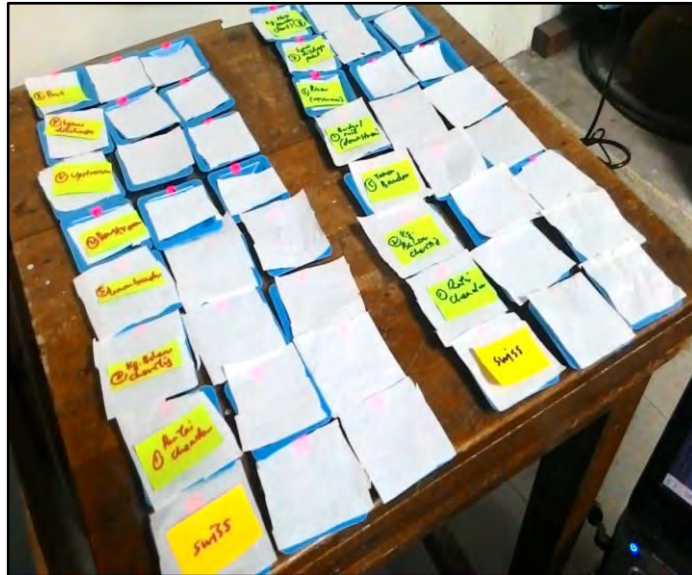
Figure 3.23: Samples left for a few hours for drying process.

3.3.3 Soil samples collection

At each sampling location, soils of nominal mass 1 kg per sample (approximate dry weights) were collected using a shovel and then packed into clearly-labelled and well-secured polyethylene bags as shown in Figure 3.24, seeking to prevent sample contamination. The samples were finally transported to the Physics Radiation Laboratory, University of Malaya for analysis.

Figure 3.24: Packed and labelled polyethylene contained collected soil samples from selected sampling locations.

At the laboratory, stones, organic material and foreign media (i.e. waste material) were firstly removed from the soil samples. The samples were then left in the open to dry (shown in Figure 3.25) at room temperature for about 2 days. Later, they were further dried in an oven at 100 °C for about 24 hours to ensure a complete drying process, important in minimizing errors in the spectral analysis (Kolo et al., 2015).

Figure 3.25: Soil samples left to open-dry for about 2 days.

Figure 3.26: Samples placed in an oven at 100°C for 24 hours for the complete drying process.

The dried samples were then screened and homogenized using the sieve as shown in Figure 3.27. Finally, the homogenized soil samples were packed into clearly-labelled Marinelli beakers, tightly sealed (shown in Figure 3.28) and stored for about 5 weeks to allow daughter radionuclides to attain radioactive secular equilibrium with the respective long-loved parents. Later, the soils were sent to Nuclear Malaysia for radiometric analysis.

Figure 3.27: Screened soil samples using sieve to ensure homogeneity.

Figure 3.28: Labelled and sealed Marinelli beaker.

3.3.4   High Purity Germanium (HPGe) Gamma-ray Spectrometric Measurement

The assessment of concentration of ^{226}Ra (^{238}U), ^{228}Ra (^{232}Th) and ^{40}K in all samples was carried out using a high-purity germanium (HPGe) gamma-ray spectrometer connected with a multichannel analyzer (16,384 channel) at Nuclear Malaysia Laboratory. The detector was a coaxial 3 inch diameter closed end-cap type, operated at 2,500 V HV bias supply. To reduce the background radioactivity the detector was shielded in a chamber made of lead, cadmium and copper (total thickness 11 cm). This p-type detector was designed to provide 25% relative efficiency with FWHM resolution of 0.82 keV at the 122 keV gamma-ray line of ^{57}Co and 1.85 keV at the 1332 keV gamma-ray line of ^{60}Co. Before measurement, the detector was calibrated for energy and efficiency using a customize multinuclides gamma-ray standard solution comprising of ^{210}Pb, ^{241}Am, ^{109}Cd, ^{57}Co, ^{123m}Te, ^{51}Cr, ^{113}Sn, ^{85}Sr, ^{137}Cs, ^{88}Y and ^{60}Co in the same counting geometry as that used for the samples. The source was purchased from Isotope Products Laboratories, USA (source no. 1290-84 and 1755).

Figure 3.29: High-purity germanium (HPGe) gamma-ray spectrometry machine located at Nuclear Malaysia.

3.3.4.1 Activity concentration (A)

Each sample was counted for 43,200 s (12 hours) a sufficiently long enough period to appreciably minimize counting errors. The specific activity concentration of ^{226}Ra, ^{232}Th and ^{40}K in all investigated samples were calculated by following expression (M U Khandaker et al., 2012):

$$A\left(\frac{Bq}{kg}\right) = \frac{CPS \times 1000}{\varepsilon_\gamma \times I_\gamma \times W} \tag{3.3}$$

where, A is the specific concentration of the sample in Bq/kg, CPS is the net counts per second for each sample, ε_γ is the efficiency of the detector for the respective gamma-ray peak, I_γ is the corresponding gamma-ray intensity and W is the sample weight in gram.

3.3.4.2 Radium equivalent activity (Ra_{eq})

The naturally occurring radionuclides ^{226}Ra, ^{232}Th and ^{40}K are not homogenously distributed in soil, with for example the inhomogeneity between ^{226}Ra and its decay products being due to disequilibrium. For uniformity in exposure estimates, the radionuclide concentrations have been defined in terms of radium equivalent activity (Ra_{eq}) in Bq/kg according to (Miah et al., 2012). It is quantitatively expressed as follows (UNSCEAR, 2000):

$$Ra_{eq} = A_{Ra} + 1.43A_{Th} + 0.077A_K \tag{3.4}$$

where Ra_{eq} is the radium equivalent activity in Bq/kg and A_{Ra}, A_{Th}, A_K are the specific activty of ^{226}Ra, ^{232}Th and ^{40}K in Bq/kg, respectively.

3.3.4.3 Absorbed dose rates (D_R)

The absorbed dose rates (D_R) due to gamma radiations in air, 1 m above the ground, are estimated with the assumption that ^{226}Ra, ^{232}Th and ^{40}K are uniformly distributed and other radionuclides outside these contributed insignificantly to the total environmental background dose (Kolo et al., 2015). D_R can be calculated as follows (UNSCEAR, 2000):

$$D_R \left(\frac{nGy}{h}\right) = (0.461\, A_{Ra} + 0.623\, A_{Th} + 0.0414\, A_K) \tag{3.5}$$

where D_R is the absorbed dose in nanogray per hour and A_{Ra}, A_{Th}, A_K are the specific activity measured in Bq/kg for ^{226}Ra, ^{232}Th and ^{40}K.

3.3.4.4 Annual effective dose rates *(AEDE)*

The absorbed dose rate was converted into annual effective dose equivalent by using a conversion factor of 0.7 Sv/Gy as recommended by (UNSCEAR, 2000) and 0.2 for the outdoor occupancy factor by considering that the people on average spend ~20% of their time outdoors. The effective dose due to natural activity in the soil was calculated by:

$$AEDE \left(\frac{mSv}{year}\right) = D_R \left(\frac{nGy}{h}\right) \times 8760 \left(\frac{h}{year}\right) \times 0.7 \left(\frac{Sv}{Gy}\right) \times 0.2 \times 10^{-6} \left(\frac{mSv}{year}\right)$$

$$= D_R \times 1.21 \times 10^{-3} \left(\frac{mSv}{year}\right) \tag{3.6}$$

3.3.4.5   External hazard index (H)

The radiation hazard incurred due to external exposure to gamma rays from the studied soil samples has been quantified in terms of the external hazard index (H_{ex}) that can be calculated by (UNSCEAR, 2000):

$$H_{ex} = \frac{A_{Ra}}{370} + \frac{A_{Th}}{259} + \frac{A_{K}}{4810} \qquad (3.7)$$

The radiation exposure from radon and its short-lived daughter radionuclides represents caused a risk to respiratory organs. The internal radiation exposure is quantified by the internal hazard index (H_{in}) and is calculated as follows (UNSCEAR, 2000):

$$H_{in} = \frac{A_{Ra}}{185} + \frac{A_{Th}}{259} + \frac{A_{K}}{4810} \qquad (3.8)$$

3.4   Radiation absorbed dose of buried TLDs and collected soils

For the buried TLDs samples, the TL values were readout using the mentioned TLD reader, obtaining results in nC/g (representing the area of the glow curve due to de trapped electrons, later normalized to unit mass of each detector). From the dose response curve for TLD samples subjected to a mean X-ray energy of 40 keV, to be discussed in section 4.2.4.1, for low dose irradiations from 0.5- to 10 mGy (the expected range of environmental doses), the value of the gradients or so called calibration factor has been used to evaluate the radiation absorbed dose by the TLD samples.
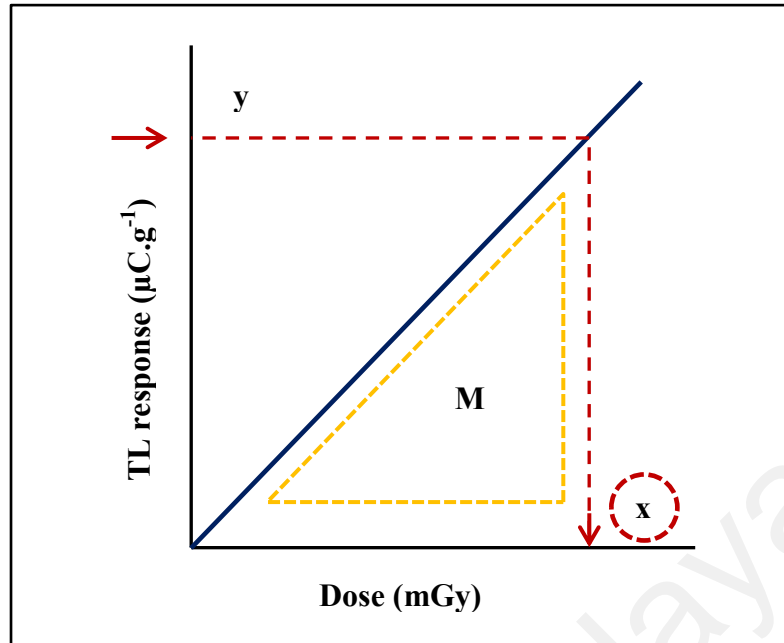
Figure 3.30: Illustrated dose response curve from the TLD samples. y was the readout TL response from the TLD samples measured by TLD reader and x was the absorbed dose by the TLD samples.

From the graph illustrated in Figure 3.30;

$$\text{Gradient}, M = \frac{y}{x} = \frac{TL\ response\ (\mu C.g^{-1})}{Dose\ (mGy)} \tag{3.9}$$

Hence, using equation (3.9), we can determine the value of absorbed dose of the TLD samples (x). For comparison with the radioactivity of soils, we first understood that the majority of the absorbed dose resulted indirectly from gamma (γ-rays) compared to x-ray emissions. In turn, this draws attention to the energy response curve (to be discussed in section 4.2.3), as illustrated in Figure 3.31, and the ratio of $TL_{x\text{-ray}}$ to $TL_{\gamma\text{-ray}}$. Noting also that the TL measurements were made for periods of two, four, six, and eight months of sample burial, hence, all the calculated TL absorbed dose of TLD samples were then scaled to a one year period. Finally, the calibration factors used for each of the TLD samples were different based on the gradient of the dose response curve for the several types of TLD.
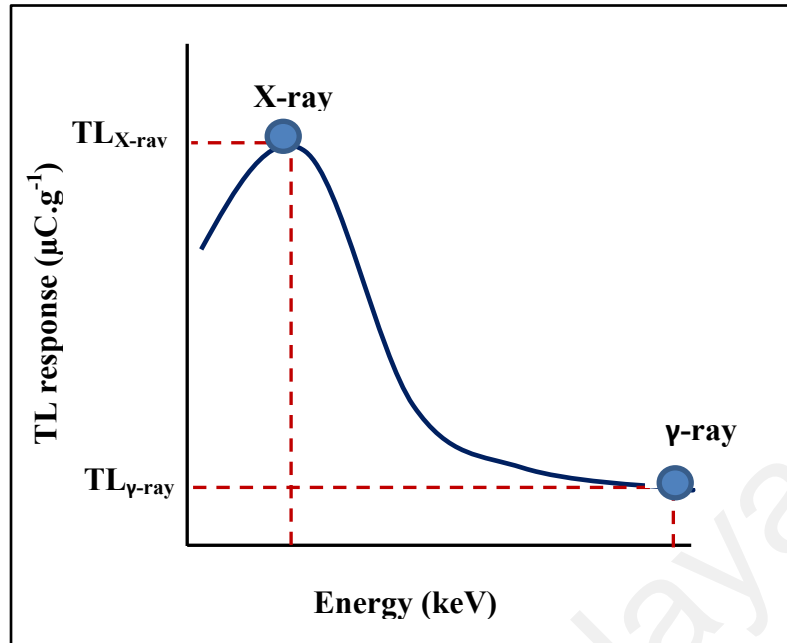
Figure 3.31: Illustrated energy response curve from the TLD samples subjected to x-ray and gamma-ray at fixed dose.

For the collected soils, the absorbed dose rate was calculated by using equation 5 as discussed in section 3.3.4.3 which results in values quoted in nGy/h. Hence, to obtain the results in units of dose per year;

$$D_R = \left(\frac{nGy}{h}\right) \times 8760 \left(\frac{h}{year}\right) \tag{3.10}$$

$$= \left(\frac{nGy}{year}\right)$$

CHAPTER 4 : RESULT AND DISCUSSIONS

4.1 Introduction

The results of this research have been divided into two parts, specifically laboratory characterization studies and at site environmental studies (as discussed in Chapter 3).

4.2 Laboratory work: Characterization study

These characterization studies are importance in checking the various influencing factors, including the sensitivity of the samples before being applied in evaluating the environmental doses. The characteristics study include screening for sensitivity and the effects of the annealing process, energy response, dose response, TL glow curve, effective atomic number and fading.

4.2.1 Screening Process

The purpose of this process is to select the samples that give response to within ± 5 % of the mean TL response. It is recognized that the concentration of dopant is not homogenous along the length of the optical fibre, varying from point to point (Abdul Rahman et al. 2014). Hence, it is important to select those samples that have approximately the same response to the radiation. In the screening process, the samples were irradiated to a dose of 2 Gy at 100 keV of x-ray mean photon energy. Initially, the TL response of ~ 600 PCFc-Ge-B samples per unit mass were obtained as shown in Figure 4.1 (a) and again ~ 550 cuts of PCFc-Ge in Figure 4.2 (a). The responses of these samples were measured and calculated. After the screening process, only 430 samples were selected as shown in Figure 4.1 (b) and Figure 4.2 (b). Then, for the phosphor TLDs, based on Figure 4.3 (b), some 110 TLD-100 samples were selected from the

previous 120 samples as shown in Figure 4.3 (a) and about 115 of TLD-200 samples (shown in Figure 4.4 (b)) were selected from the previous 120 samples as shown in Figure 4.4 (a).The selected samples were then used for the present set of experiments, studying their characteristics in the laboratory and also for the environmental part.
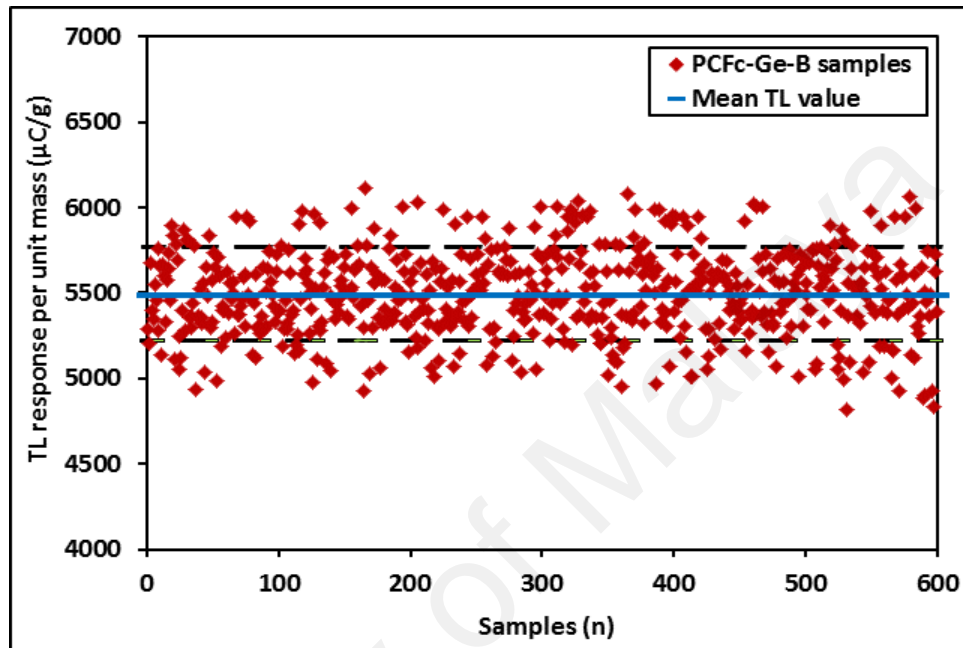
(a)
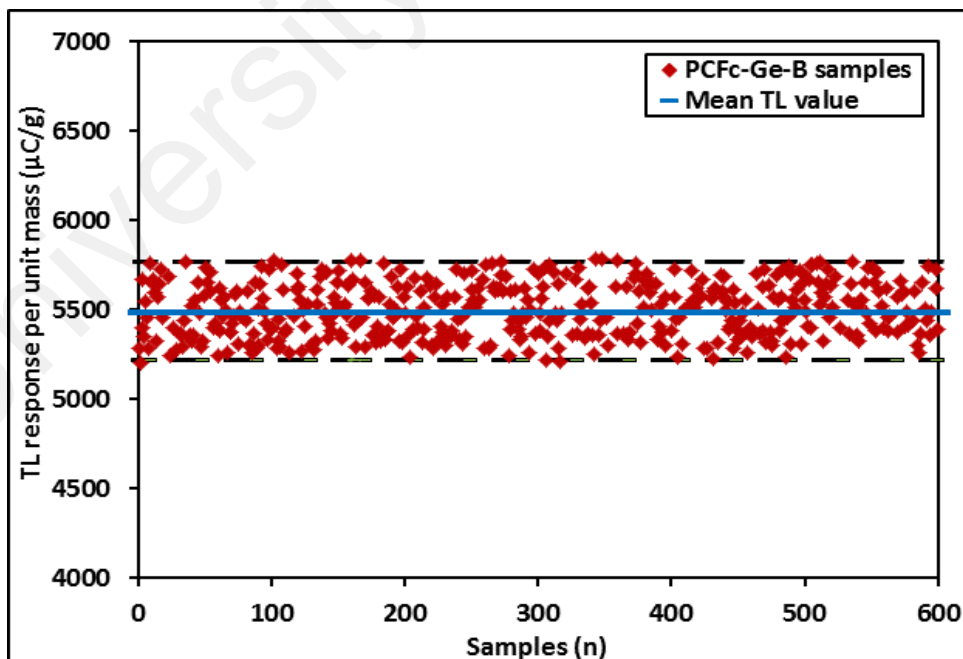
(b)

Figure 4.1: (a) TL response of PCFc-Ge-B samples before the screening process. **(b)** The actual number of PCFc-Ge-B samples falling within the selection criteria (± 5% of the mean TL value).
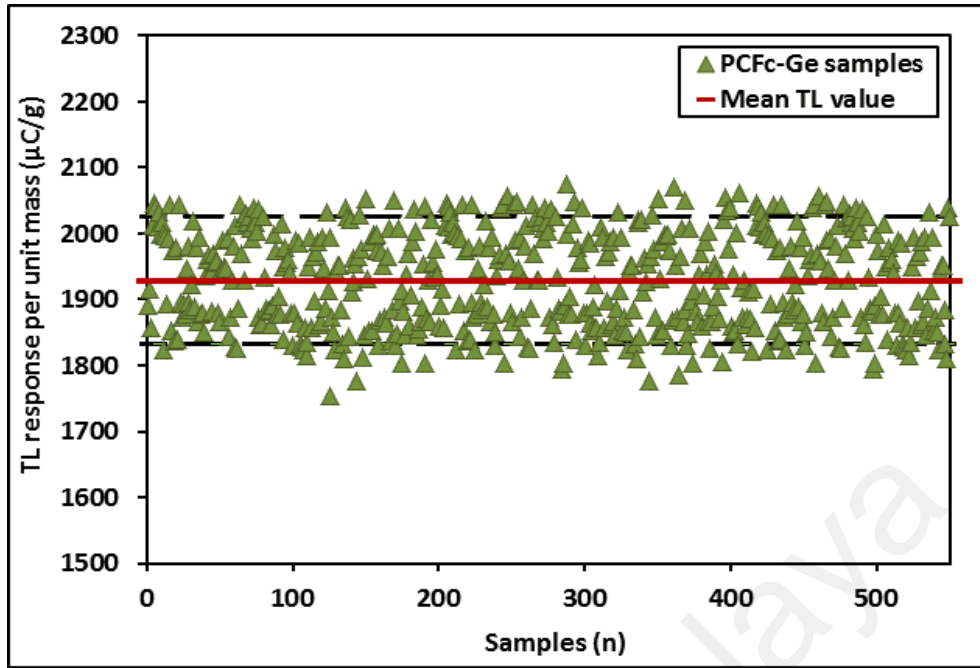
(a)
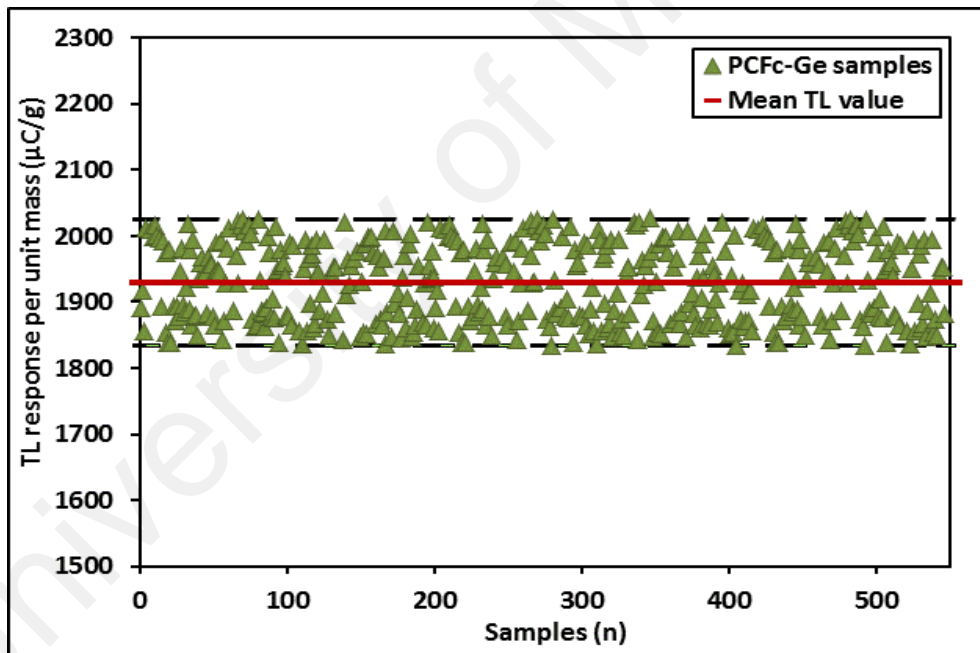
(b)

Figure 4.2: (a) TL response of PCFc-Ge samples before the screening process.
(b) The actual number of PCFc-Ge samples falling within the selection criteria (± 5 %
of the mean TL value).
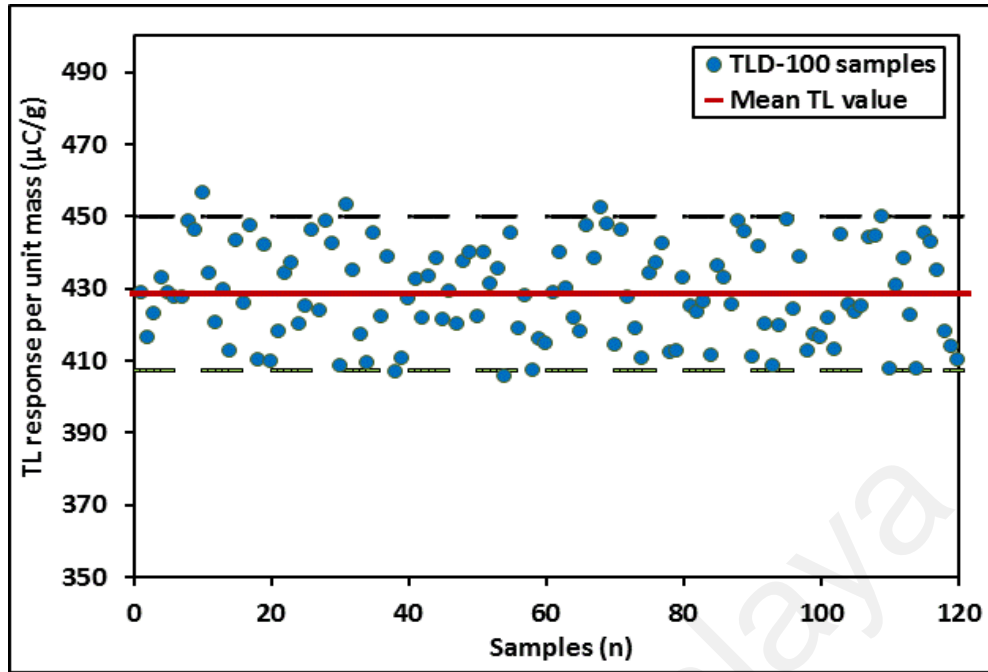
(a)
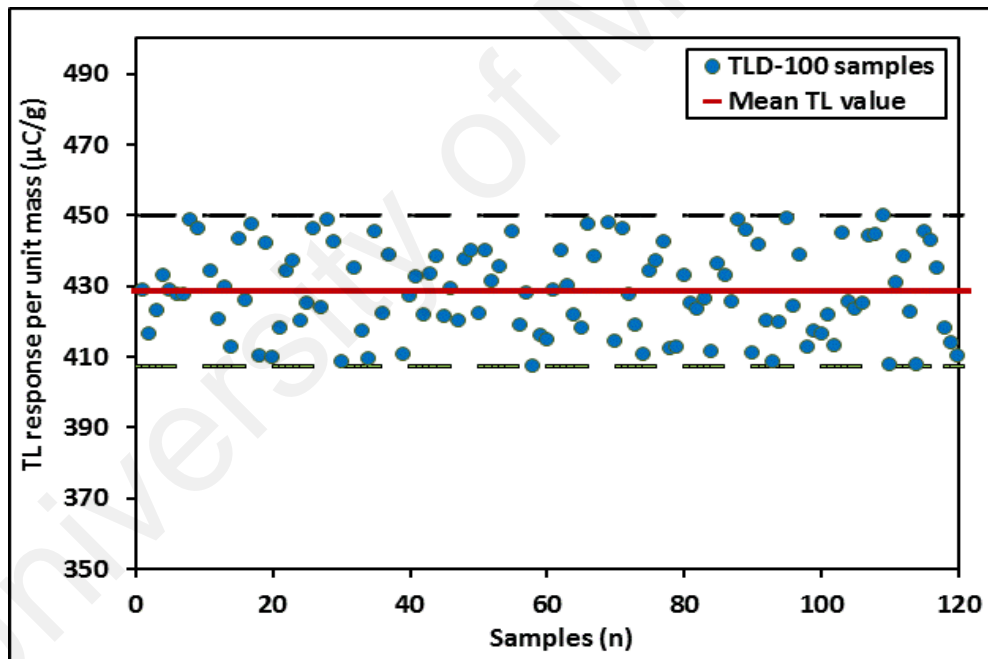
(b)

Figure 4.3: (a) TL response of TLD-100 samples before the screening process.

(b) The actual number of TLD-100 samples falling within the selection criteria (± 5 % of the mean TL value).
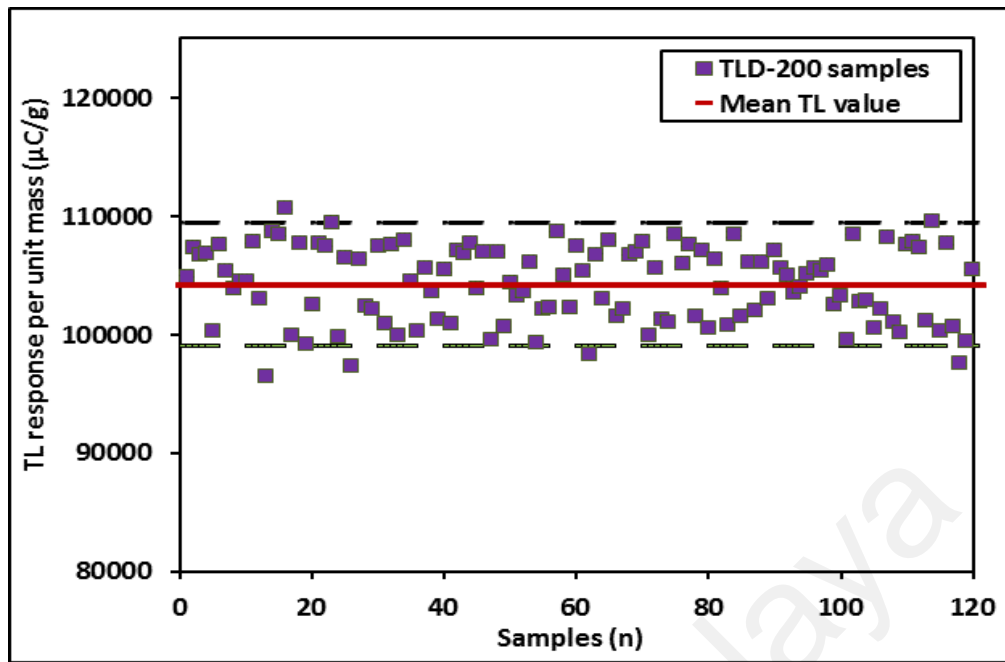
(a)
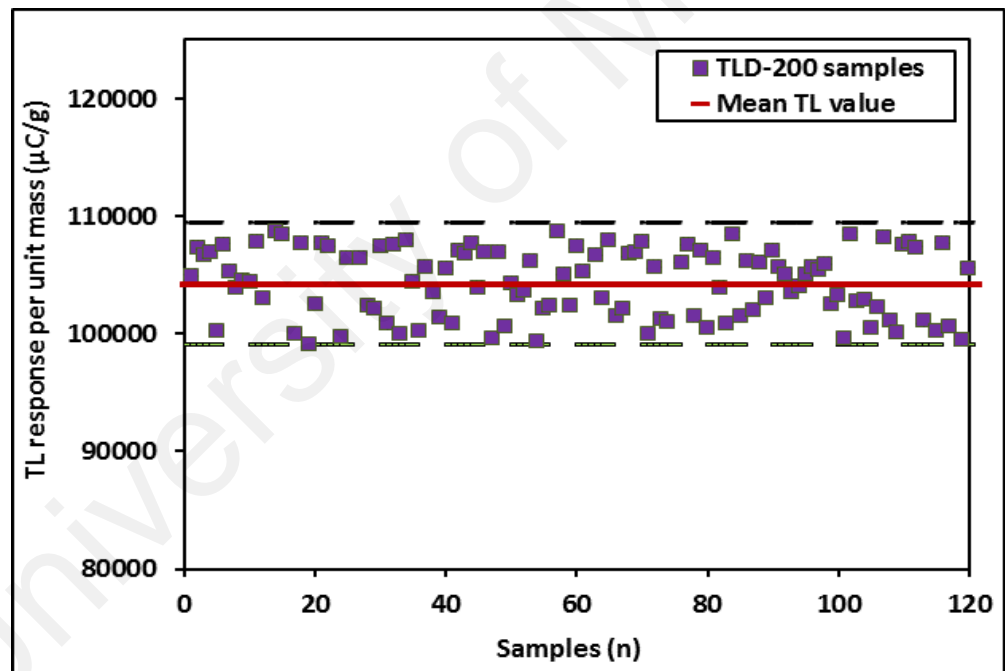
(b)

Figure 4.4: (a) TL response of TLD-200 samples before the screening process.
(b) The actual number of TLD-200 samples falling within the selection criteria (± 5 % of the mean TL value).

4.2.2 Annealing study

Annealing is the thermal treatment needed to erase any irradiation memory from the dosimetric material, being important in restoring the material to initial conditions prior to first irradiation, further to stabilize the trap structure (Furetta, 2003). In present study, we investigated the best combination of annealing temperature and time (threshold temperature and time) to erase any effect of previous irradiation of PCF samples. The most favourable choice is the one in which the TL residual signal is practically the same as background. For both studies, the samples were initially irradiated to a dose of 2 Gy at 100 keV of x-ray mean photon energy. This annealing study obtained from the PCFc-Ge-B and other PCF samples the representation of all those measured PCF samples that met the ± 5% of mean criterion.

4.2.2.1 Effect of annealing temperature

After the samples were irradiated, they were then annealed over temperatures from 100 °C to 500 °C, in increments of 100 °C for a constant annealing time of one hour. The measurements were recorded by averaging three repeated sample readings using the Harshaw 3500 TLD reader. Based on Figure 4.5, it was observed that the residual TL response decreased with the temperature, and at 400 °C, the value of residual TL response started to be constant, also approaching the background value. Hence, 400 °C was chosen as the threshold temperature, Tc and considered the best temperature to erase all previous irradiation memory.
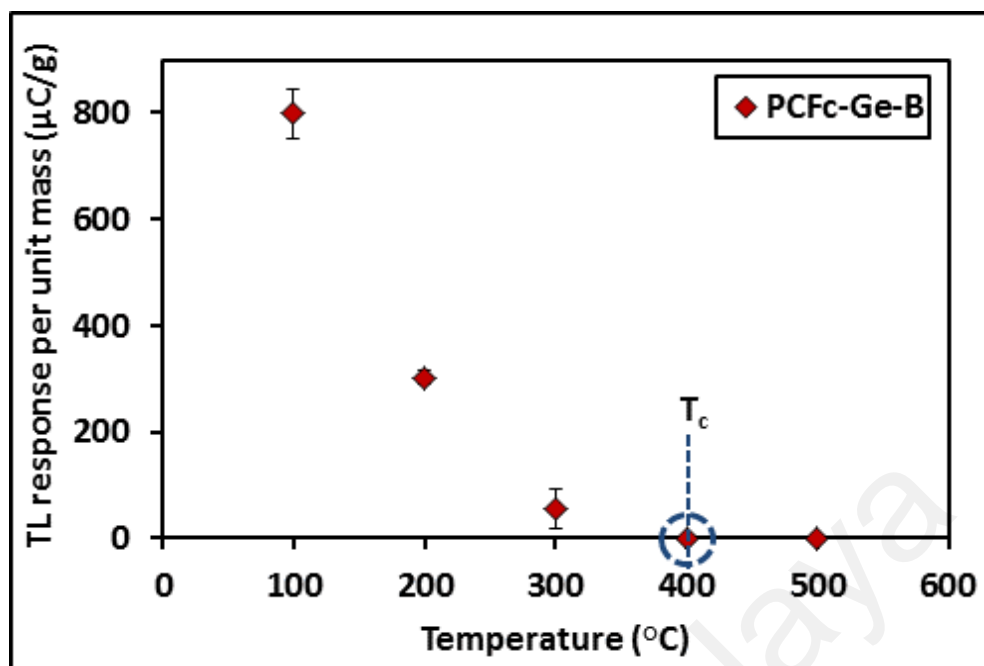
Figure 4.5: Residual TL response of PCFc-Ge-B from 100 °C to 500 °C. T_c is the threshold value where the temperature starts to constant.

4.2.2.2 Effect of annealing time

Based on the threshold temperature, T_c (400 °C) obtained from previous study; the same procedures were repeated using different annealing time, starting from 20 minutes to 100 minutes, in increments of 20 minutes. Based on Figure 4.6, it was observed that at 60 minutes, the residual TL response started to approach the background value. By analysing both results in Figure 4.5 and Figure 4.6, we can conclude that the optimal annealing temperature-time regime for the PCF samples was at 400 °C for 1 hour. It is noted that this annealing procedure is very important in maintaining the performance of the samples.
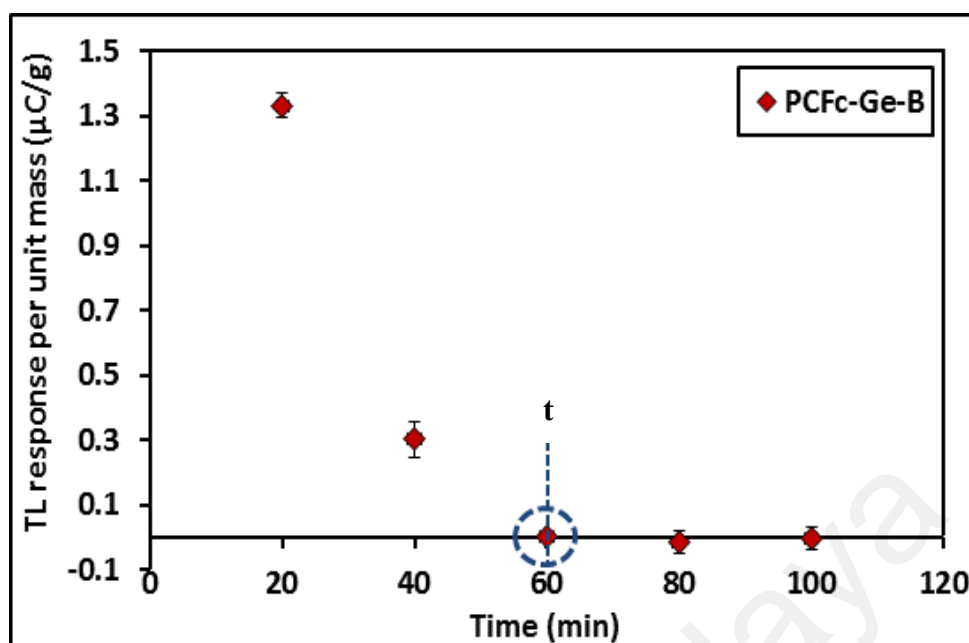
Figure 4.6: Residual TL response of PCFc-Ge-B annealed at 400 °C at different time from 20 min to 100 min.

4.2.3 Energy response

Energy dependence is the variation of the detected TL output as a function of the energy of the absorbed radiation at a constant dose (Furetta, 2003). As seen in Figure 4.7, the TL response per unit mass was depicted for x-ray mean photon energies from 10 keV to 100 keV (taken to be one-half of the kVp) and ^{60}Co mean gamma energy of 1250 keV (from equally probable emissions at 1170 keV and 1330 keV). Both collapsed forms of PCFs, TLD-100, and TLD-200 show a similar pattern of variation, albeit differing markedly in magnitude as a direct consequence of the effective atomic number of those types of media, together with the associated dependencies of the photoelectric effect and Compton scattering and the complexities of attenuation in the differing dimensions of the three TL types. From the results, it was apparent that TLD-200 showed superior response compared to other samples. The response of the PCFc-Ge-B approximates double that of the PCFc-Ge, while TLD-100 shows a very low response

compared to the PCFs, of the order of one-tenth of that of the PCFc-Ge-B. In this regard, the outcome has been appreciably influenced by the effective atomic number of the TLD-200 and PCFs, both being significantly greater than that of the TLD-100 (see Table 4.2 and associated discussions in 4.2.6). The greatest TL responses were observed to occur at an effective energy of 60 keV for TLD-200, 40 keV for PCFc-Ge-B and TLD-100 and at 30 keV for PCFc-Ge, noting that it was particularly at the lower photon energies ranging from 10 keV to 50 keV that the dominant effect of the photoelectric effect was seen to be most pronounced. Overall, the greatest TL response of the samples was observed between photon energies of 30 keV to 60 keV.
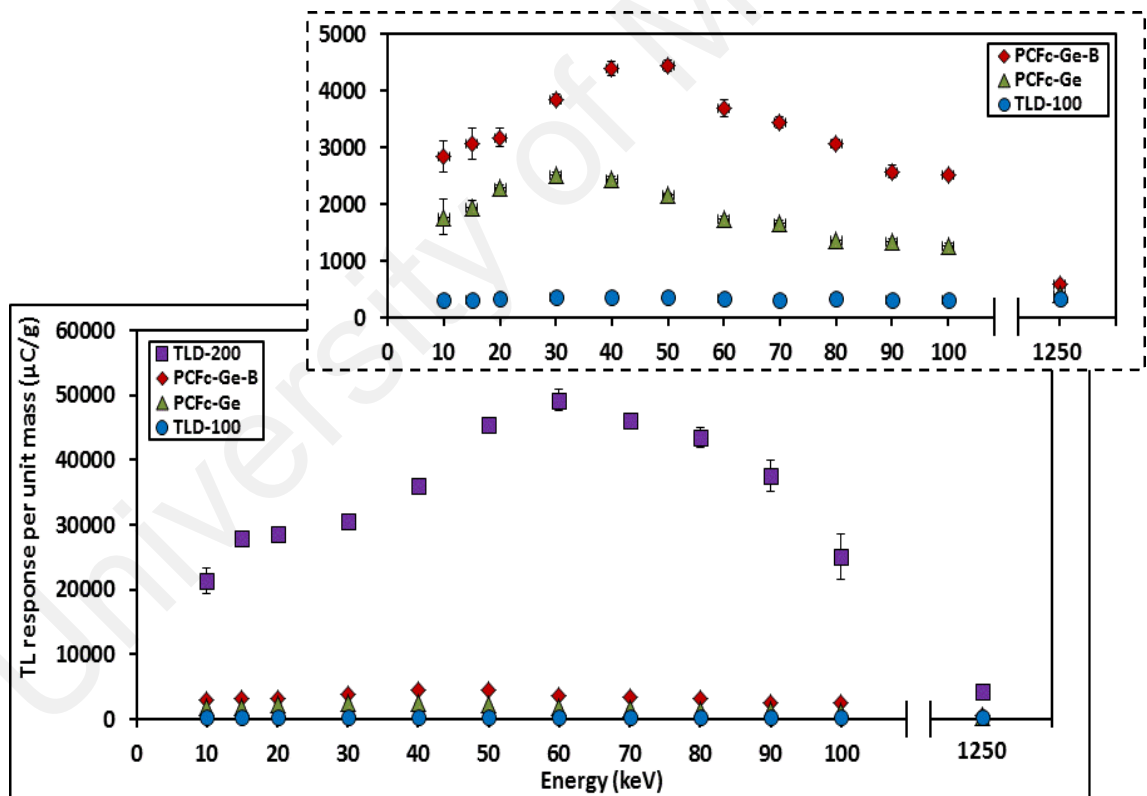
Figure 4.7: Energy dependence of collapsed PCFs and phosphor TLDs irradiated to a dose of 1 Gy using x-rays producing effective energies of 10 keV to 100 keV (taken to be one-half of the kVp) and ^{60}Co irradiation at a mean energy of 1250 keV. The inset provides an expanded view of the PCFs and TLD-100.

4.2.4 Dose response

Dose response is defined as the functional dependence of the intensity of the measured TL signal upon the absorbed dose (Furetta, 2003). The linearity of the TL response over a wide range or dose is one of the important characteristics for the ideal dosimeter. Prior to practical application for the environmental study, laboratory tests have been conducted (to check the feasibility of the samples to low dose irradiation). The samples were irradiated to low doses obtained using 40 keV x-rays and 1.25 MeV Co-60 gamma-rays.

4.2.4.1 Irradiation to x-ray source

Figure 4.8 shows the dose response of the collapsed PCFs and phosphor TLDs subjected to a range from 0.5 mGy to 10 mGy of 40 keV of mean X-ray source. Each point represents the mean of three repeated measurements, normalized to sample mass, with error bars of one standard deviation. Clearly shown is the superior response of TLD-200 compared to PCFs and TLD-100. The TL response per unit absorbed dose of TLD-200, PCFc-Ge-B, PCFc-Ge and TLD-100 were 20.81 µC/g.mGy, 2.0 µC/g.mGy, 1.493 µC/g.mGy and 0.221 µC/g.mGy respectively. Specifically, the TL yield of the TLD-200, PCFc-Ge-B and PCFc-Ge have been found to be respectively $\sim 90 \times$, $\sim 9 \times$ and $\sim 7 \times$ that of TLD-100.
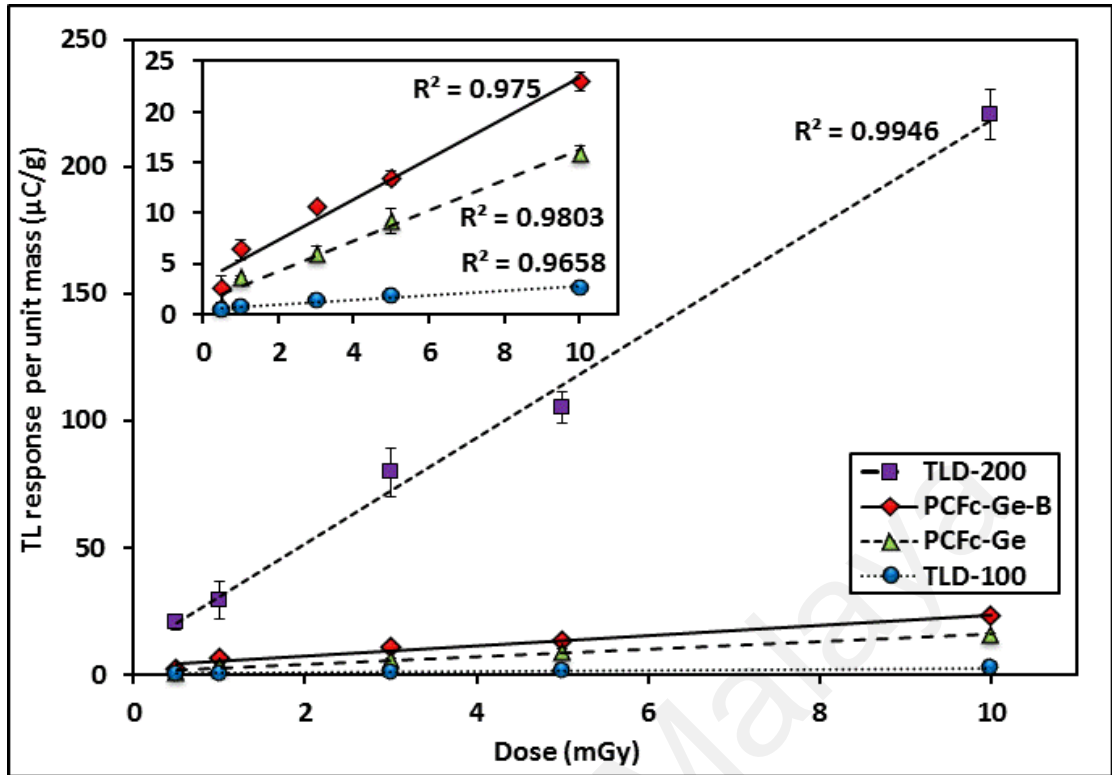
Figure 4.8: TL response of the collapsed PCFs and phosphor TLDs subjected a range from 0.5 mGy to 10 mGy of 40 keV of mean x-ray source. The inset provides an expanded view of PCFs and TLD-100 response. (Note: in some cases the error bars are smaller than the data points).

4.2.4.2 Irradiation to Co-60 gamma source

Figure 4.9 shows the dose response of the collapsed PCFs and phosphor TLDs subjected to a range from 1 to 5 Gy of ^{60}Co, mean energy 1.25 MeV. The TL response per unit absorbed dose of TLD-200, PCFc-Ge-B, PCFc-Ge and TLD-100 were 1849.5 μC/g.Gy, 471.65 μC/g.Gy, 154.12 μC/g.Gy and 82.07 μC/g.Gy respectively. Specifically, the TL yield of te PCFc-Ge-B and PCFc-Ge have been found to be respectively ~ 22 ×, ~ 5 × and ~ 2 × that of TLD-100.
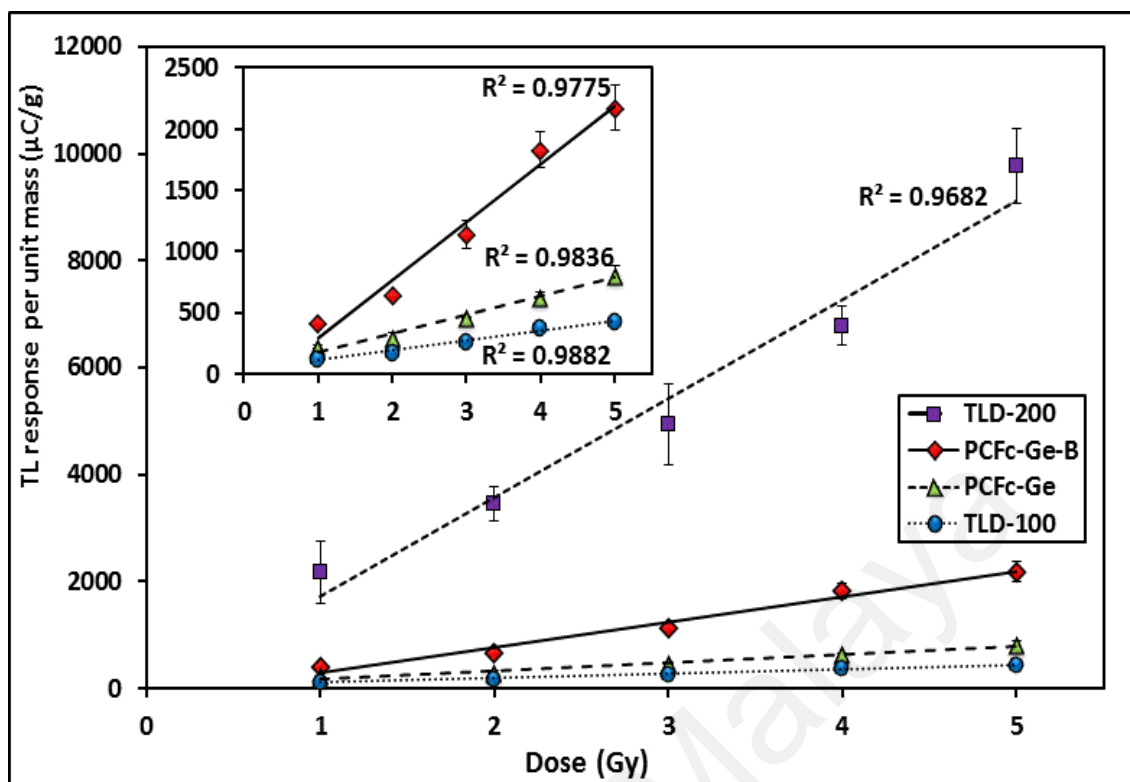
Figure 4.9: TL response of the collapsed PCFs and phosphor TLDs subjected to a range from 1 to 5 Gy of ^{60}Co with mean energy of 1.25 MeV. (Note: in some cases the error bars are smaller than the data points).

4.2.5 TL glow curve

The TL glow curve is plotted in terms of the thermoluminescence intensity as a function of sample temperature during read out. Each trapping level in the material gives rise to its own associated glow peak; so, a glow curve may be formed by several peaks, each related to different trapping levels (Furetta, 2003). Most commercially available TL dosimeters have high glow peak temperature values, indicated of deep electron traps to the extent that the stored signal is highly stable for several months to years (Hashim et al., 2015).

Herein, studies were focused on the PCFs TL glow curve irradiated to different doses. Figure 4.10 shows the PCFc-Ge-B irradiated at 40 keV mean photon of x-ray

with dose ranging from 0.5 mGy to 10 mG. Using the model 3500 TLD reader this was set up at a heating rate of 10 °C/s and maximum readout temperature of 400 °C. The typical glow curves obtained from PCFc-Ge-B provides a representation of all the measured PCF samples. From the figure, it is clear that the peak height intensity of the glow curve and area under the glow curve are both dependent on the amount of dose given to the sample, corresponding well with previous study (Hashim et al., 2015). The area under the curve represents the number of electrons released from traps and thus by association of the radiation energy deposited, while the intensity peak height indicating the maximum number of electrons released for traps. At higher doses, greater numbers of electrons are trapped at various electron trap centres. During the thermal simulation process, these electrons are released from the traps, reflecting the increasing TL response with irradiation dose. The resultant glow curve is composed of a broad, dominant peak with a maximum between 180 to 220 °C, the integrated area indicating the particular sensitivity to the amount of absorbed dose. The general structure of the TL glow curve remains unchanged by repeating the cycles of annealing and irradiation at various doses.
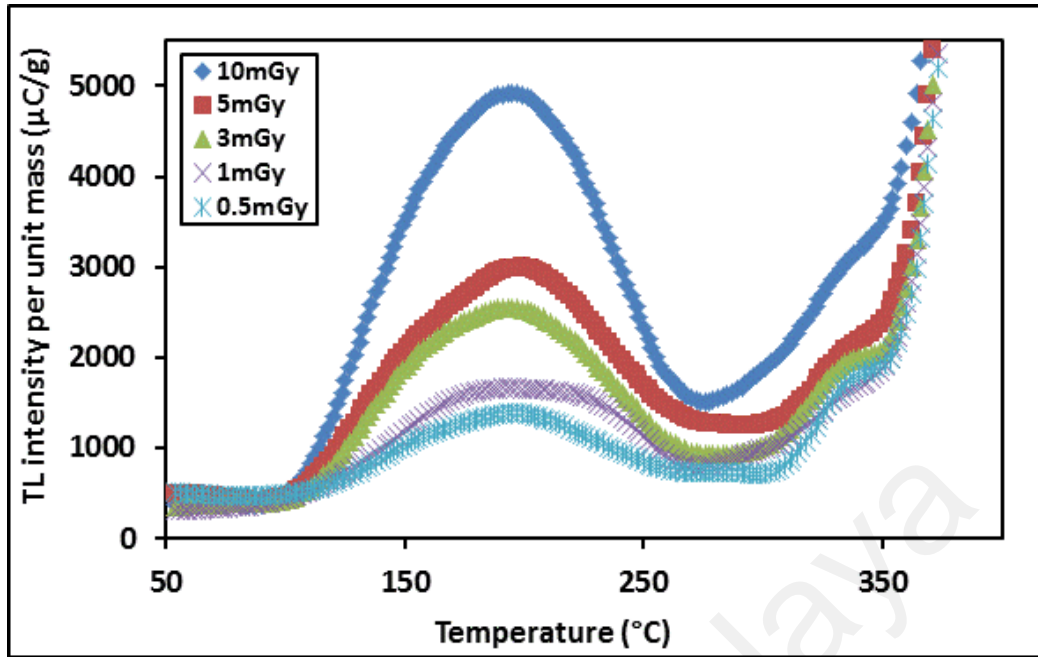
Figure 4.10: TL glow curve of PCFc-Ge-B samples irradiated at 40 keV mean x-ray energy for doses ranging from 0.5 mGy to 10 mGy.

4.2.6 Effective atomic number

As referred to in previous discussions, the strength of photon interaction in a given material is most influenced by its effective atomic number, a single valued representation of the multi-element composition (Table 4.1). A further but less powerful influencing factor is the material density.

Table 4.1: Respective results of collapsed PCFs using EDX.

Element	Weight fractional contribution of each element (W_i)	
	PCFc-Ge	**PCFc-Ge-B**
O	0.6578	0.3025
Si	0.3296	0.5018
Ge	0.0126	0.0134
B	0	0.1823

For a single element, clearly it is represented by its atomic number. However, for a compound or mixture of elements, the effective atomic number, Z_{eff} needs to be introduced. Firstly, by using a Field Emission Scanning Electron Microscope (FESEM) and Energy Dispersive X-ray Spectroscopy (EDX) analysis, the fractional weight of each element of a mixture can be determined. After then, the electron number per gram of each element is calculated as equation 4.1:

$$N_e = \frac{N_A Z}{A_w}(W_i) \tag{4.1}$$

where N_A is the Avogadro number, while Z, A_w and W_i are the atomic number, atomic weight, and fractional weight contribution of each element of the mixture. Then, a which is the fractional contribution of electron number of each element in the mixture can be determined as shown in equation 4.2:

$$a = \frac{N_e}{N_{et}} \tag{4.2}$$

where N_{et} is the total electron number of the mixture (i.e., $N_{e1} + N_{e2} + N_{e3} + ..$). Hence, as shown in Table 4.2, the Z_{eff} of a mixture latter is calculated using the Mayneord equation (Khan 2010), as follows:

$$Z_{eff} = \left(a_1 Z_1^{2.94} + a_2 Z_2^{2.94} + a_3 Z_3^{2.94} + \cdots + a_n Z_n^{2.94}\right)^{\frac{1}{2.94}} \tag{4.3}$$

where $a_1, a_2, a_3 .. a_n$ are the fractional contribution of electron number as calculated in equation 12 and $Z_1, Z_2, Z_3 .. Z_n$ are the atomic number of each element. Here 2.94 is an adopted value, for photon practical purposes typically being 2.94.

Table 4.2: Respective effective atomic number of collapsed PCFs.

Sample	Effective atomic number, Z_{eff}
PCFc-Ge	12.5
PCFc-Ge-B	14.4

In the context of dose measurements in health physics and clinical irradiations, it is favourable for a dosimeter to be soft-tissue equivalent (Z_{eff} = 7.14), ensuring independence of the incident photon energy, TLD-100 being suitably favourable with an effective atomic number, Z_{eff} of 8.2 (Gonzalez et al. 2007). As shown in Table 4.2, the Z_{eff} of both PCFs were not soft-tissue equivalent, with need in calibration for dose deposition in soft tissues to be corrected for (Hashim et al. 2014). Thus said, there were indications from present and other studies that the elevated response of the PCFs make them good candidates for sensitive measurements of low doses, as is also known for TLD-200 as further demonstrated herein, with Z_{eff} of 16.3 (Yazici & Ozturk 2001). The added advantage of the PCFs is that these glassy media are entirely unaffected by moisture, as a result being well-suited for emplacement under field conditions for environmental dose measurements.

4.2.7   Fading

Figure 4.11 demonstrates the post-X-ray irradiation signal loss of collapsed PCFs, TLD-100 and TLD-200 as a function of time. Over a period of 35 days post-irradiation the fading loss for TLD-200 and PCFc-Ge was 21 % while that for PCFc-Ge-B was 15 %; in comparison, the respective loss in TLD-100 was 7 %. The mean loss in TL response for the PCFs has been estimated to be 0.4 % - 0.5 % per day, although as shown the greatest fading occurs in the initial few days, subsequently reducing substantially at later times. Given that most environmental radiation dose rates remain

stable over long periods of time, over durations of years rather than days, the effect of fading can easily be accounted for. One exception would be in the event of micro-fissures in soil as a result of the pre-occurrence of a seismic event. However here, the interest would be in using the dosimeters as an early warning indicator of such an event rather than in definition of dose. The sensitive dosimeters evaluated herein would represent an excellent device type for such application.
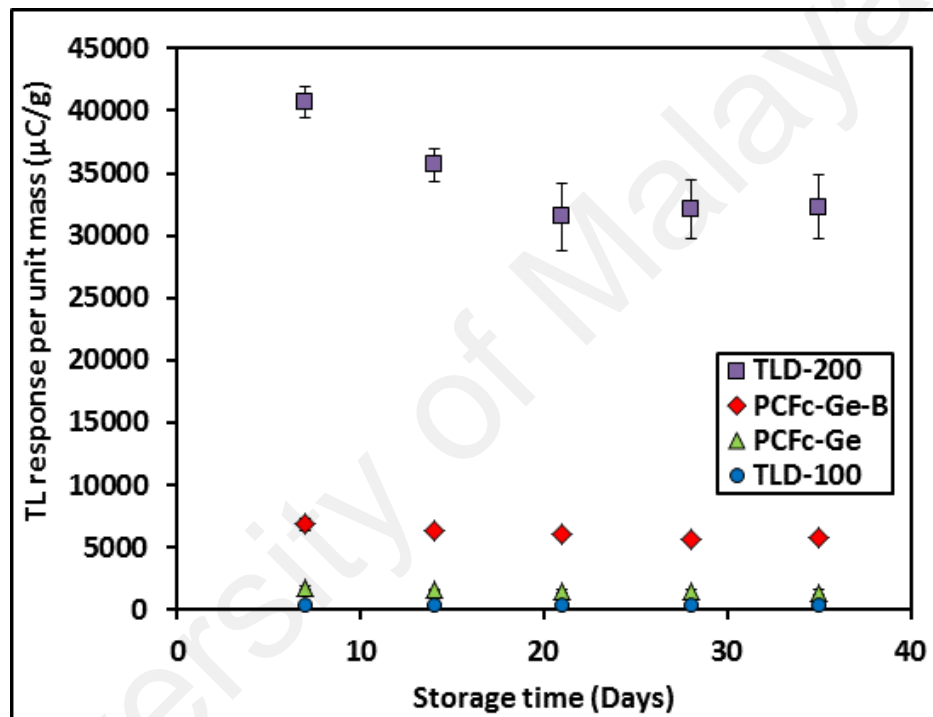
Figure 4.11: The loss in TL yield over a period of 35 days post-irradiation for the collapsed PCFs and phosphor TLDs irradiated to a dose of 1 Gy. (Note: in some cases the error bars are smaller than the data points).

4.3 On site work: Environmental study

For the environmental study, the discussions will be divided into two parts. These are respectively the readout of TLD samples which have been buried at the sampling sites and then gamma spectroscopy of soils collected from the sites, as discussed in Chapter3.

4.3.1 Readout of TLD samples buried at the sites

The samples have been buried at eight selected locations, labelled as L1 to L8 with different duration of sample burial, from two, four, six and eight months. The readout TL response and glow curve of the samples collected from the sites were studied.

4.3.1.1 TL response for different type of samples

Figures 4.12 to 4.15 show the TL response per unit mass for the samples buried for four different durations, from 2 to 8 months. Apparently, on the basis of the figures, PCFc-Ge shows the greatest response compared to the PCFc-Ge-B, TLD-100 and TLD-200. This was the converse of that found in the laboratory study (as discussed in section 4.2.4), where compared to PCFc-Ge-B, PCFc-Ge and TLD-100, TLD-200 showed the greatest response at about ~ 90, ~ 9, and ~7 times (irradiated to x-ray source) and ~22, ~5, and ~2 times (irradiated to ^{60}Co gamma source). The degradation in performance of the phosphor TLDs (especially that of TLD-200) are suggested to be due to the noted moisture which was clearly seen inside the samples bottles collected at site from the soils. The seasonal variation (rainy and dry) occurred at the sampling locations and the water content in the soils has been seen to influence this condition. The properties of TLD-200, a very sensitive dosimeter but one that is highly hygroscopic (Scharmann, 1993) has been shown here.

The readout TL response of PCFc-Ge under real environmental conditions was found to be greater than that of PCFc-Ge-B, again in contrast with the behaviour found in the laboratory study. In this case, boron (B), which is good for neutron capture (Kharisov et al., 2013), has influenced the radiation absorption behaviour and sensitivity of the PCF as a dosimeter. For laboratory study (discussed in section 4.2.3), the samples were directly irradiated using the x-ray (10 to 100 keV) source and ^{60}Co (1.25 MeV) source. However, in the real case the soils released photon energies that more readily fall within the range of 100 keV to 1.25 MeV (see the typical gamma-ray emission from the soils in Table 4.3), which were not overlapping to great extent with the lab-based studies of behaviour of both PCFs.

Based on figures for the two to eight month duration sample burials, sampling location no.7 showed the greatest TL response while sampling locations no. 1 and 3 also showed elevated TL response. The indication is that these three locations present higher concentrations of radioactivity compared to the other locations.
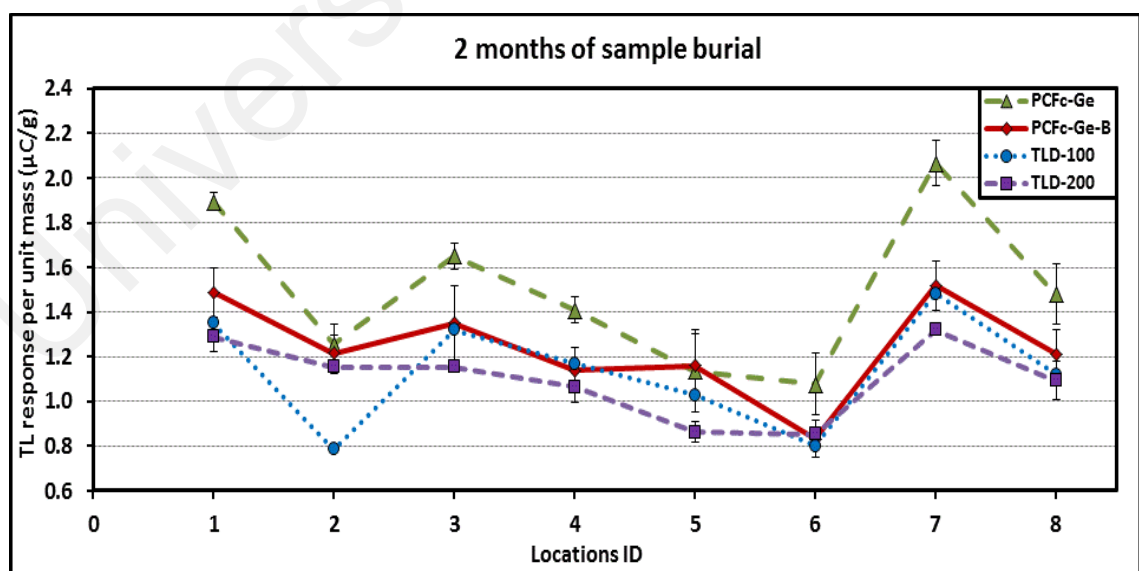
Figure 4.12: Readout TL response per unit mass for two months of sample burial for all TLD samples.
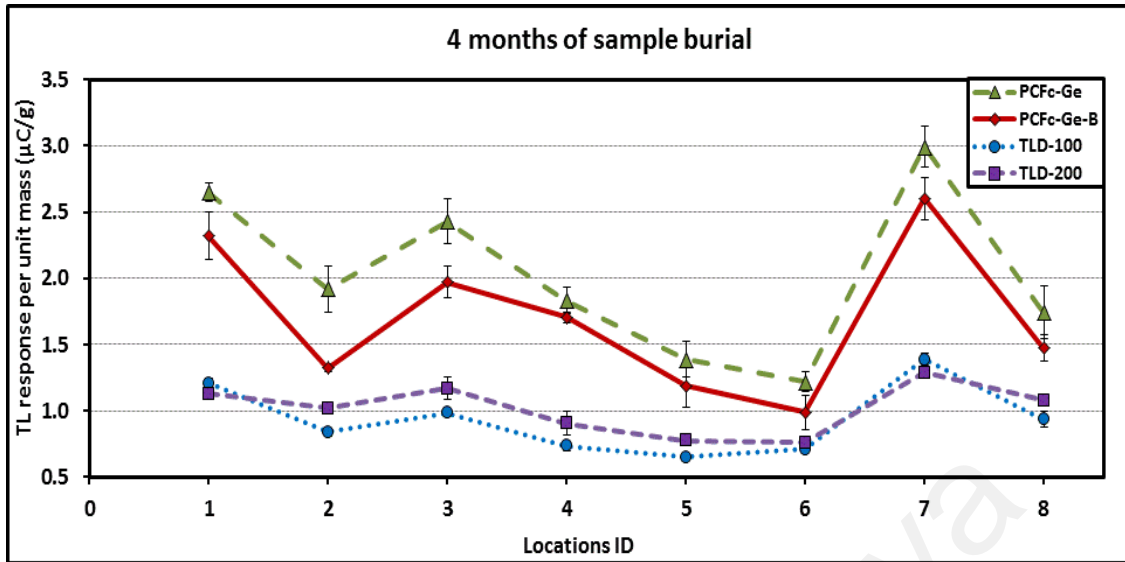
Figure 4.13: Readout TL response per unit mass for four months of sample burial for all TLD samples.
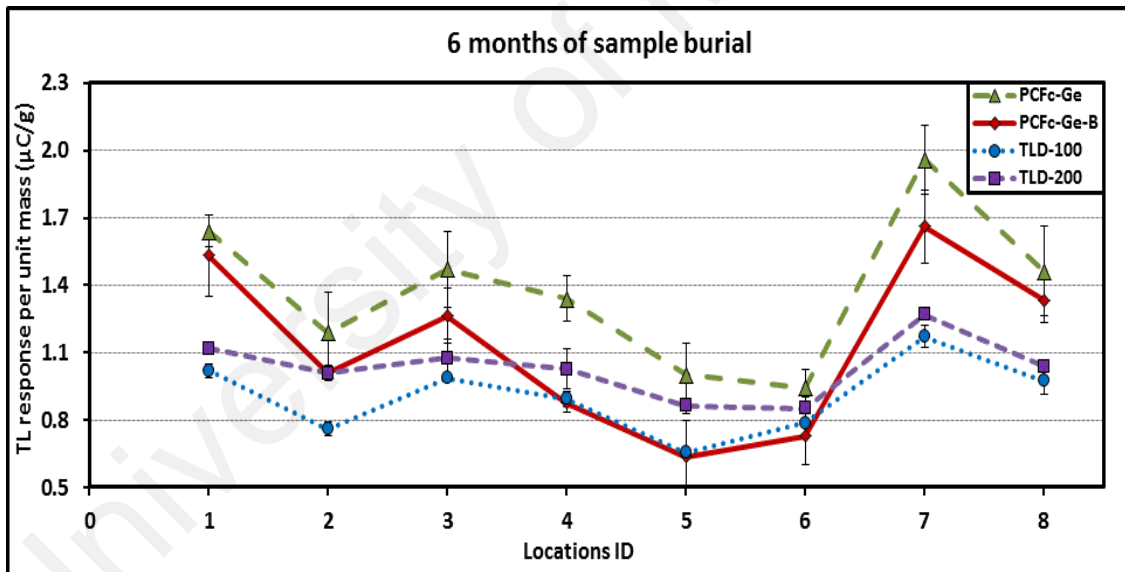
Figure 4.14: Readout TL response per unit mass for six months of sample burial for all TLD samples.
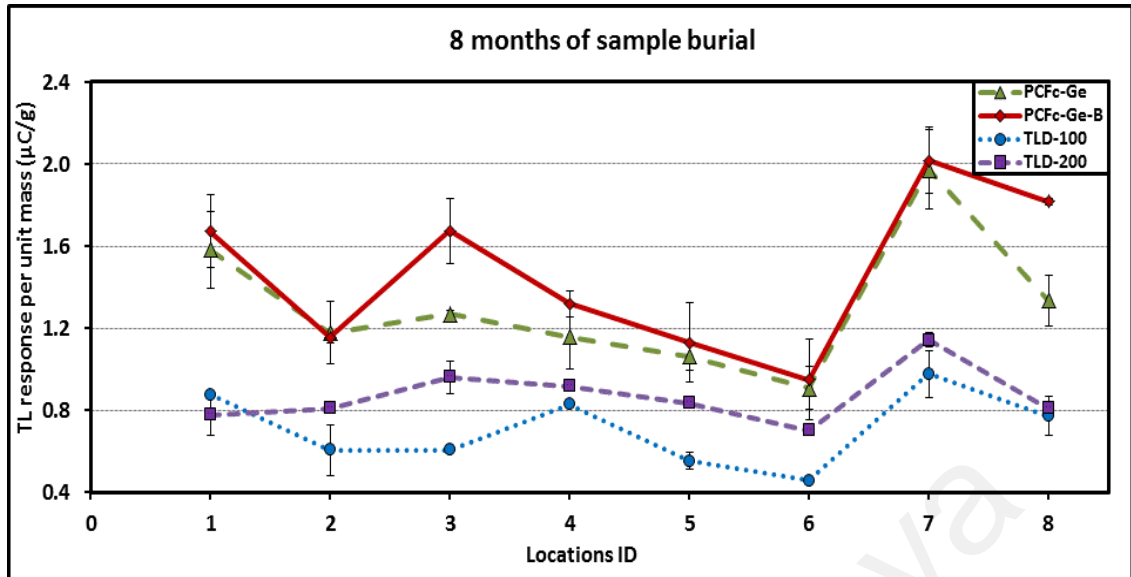
Figure 4.15: Readout TL response per unit mass for eight months of sample burial for all TLD samples.

4.3.1.2 Variation of TL response with samples burial durations

Next, we detail readout TL response against variation in sampling burial durations (from two to eight months) for each type of sample as can be observed in Figures 4.16 to 4.19. The readout TL response of the controlled TLDs being placed in the laboratory for two to eight months are also marked in the figures for clear comparison to that buried TLDs. Overall, the response of both buried Ge and Ge-B doped PCFs were higher compared to that controlled PCFs due to the natural radioactive content in the soil. Meanwhile, for phosphor TLDs, buried TLD-100 demonstrates lower response compared to that controlled TLD-100 subsequent to 2 months of burial. On the other hand, the TLD-200 produces lower response compared to that controlled TLD-200 in the first 2 months of burial. This can be explained by effect of moist in the soil that reduced the efficiency of both buried TLD-100 and TLD-200 compared to that controlled phosphor TLDs. Both PCFs for four months of sample burial was seen to be greater compared to that at two months. However, for the longer duration exposures of six and eight months sample burial, these showed a decreasing

trend of response. Based on weather forecast reported by Ministry of Science and Technology Innovation (MOSTI) (Metrology Malaysia, 2015), the monsoon season in the east coast of peninsular Malaysia, the location where the samples were buried in was during November 2015 until January 2016, explaining the high moisture level in the six to eight months of sample burial. Fading could be one of the factors that influenced the results. Based on discussion in section 4.2.7, the fading for PCFs is 0.4 - 0.5% per day; it can be assumed that for times beyond four months of sample burial, the trapped electrons inside the PCFs was disturbed to an appreciable extent by fading and other factors. For the phosphor-based TLDs, both show decreasing response even from two months of sample burial. This can be related to the hygroscopic problem faced by the phosphor TLD samples (as discussed in section 4.3.1.1).
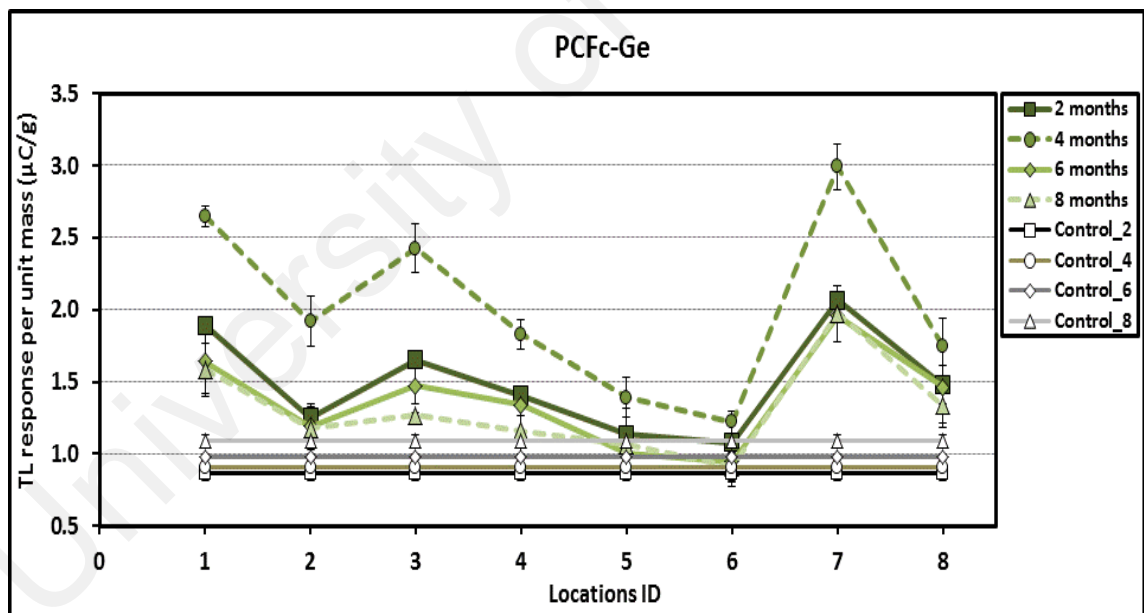
Figure 4.16: Readout TL response per unit mass for PCFc-Ge samples for two to eight months of sample burial and the controlled PCFc-Ge.
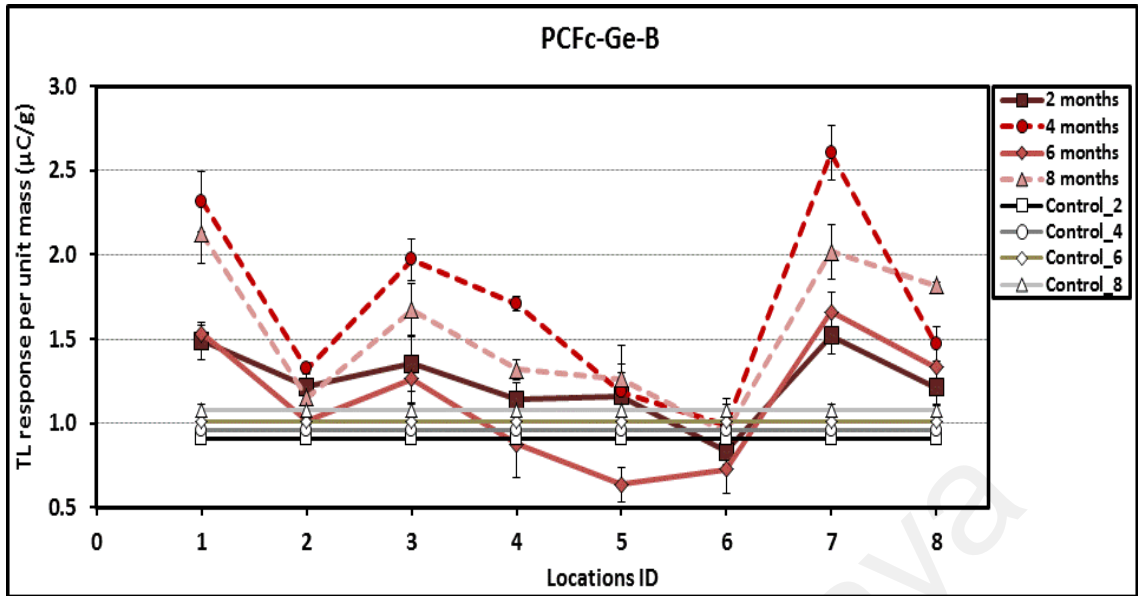
Figure 4.17: Readout TL response per unit mass for PCFc-Ge-B samples for two to eight months of sample burial and the controlled PCFc-Ge-B.
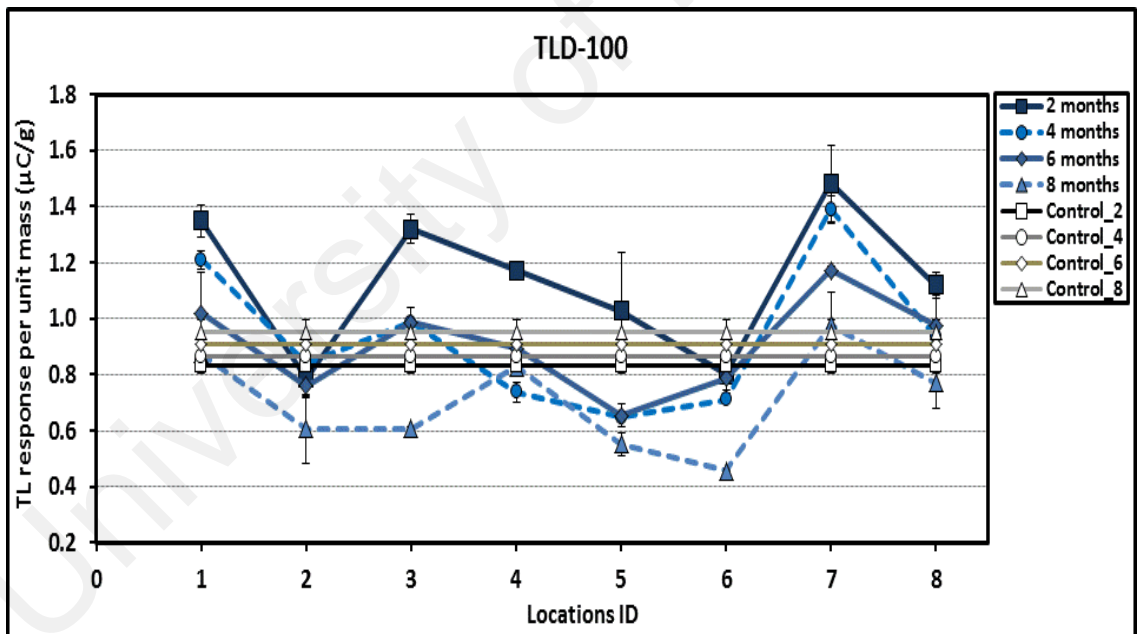
Figure 4.18: Readout TL response per unit mass for TLD-100 samples for two to eight months of sample burial and the controlled TLD-100.
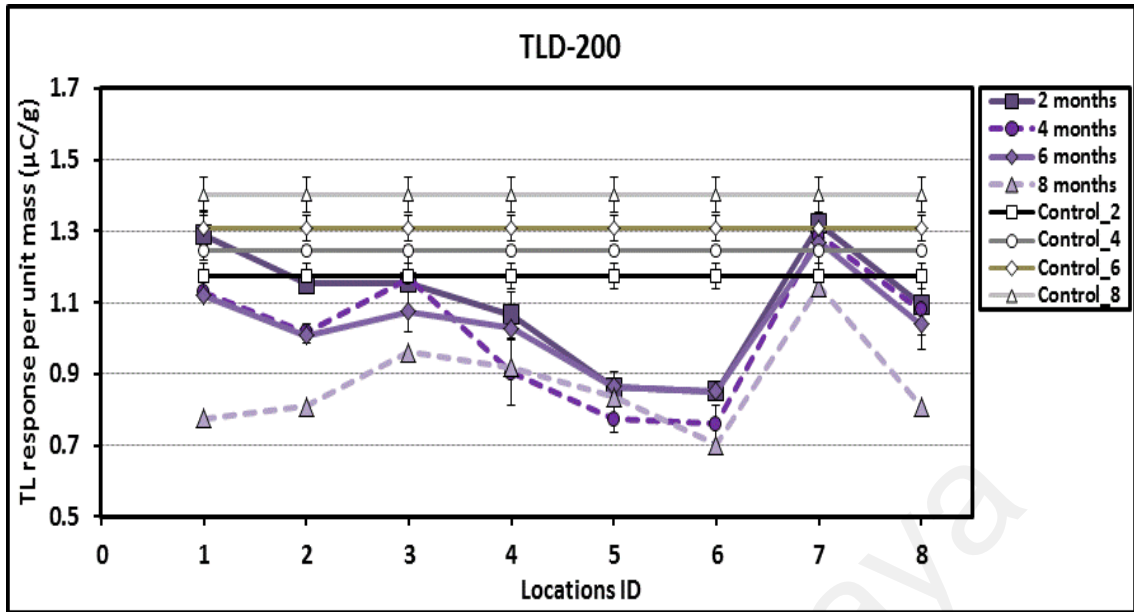
Figure 4.19: Readout TL response per unit mass for TLD-200 samples for two to eight months of sample burial and the controlled TLD-200.

4.3.1.3 TL glow curve

As discussed ealier, results for sampling location L7 show greater TL response when compared to other locations, pointing to greater radioactive concentration at this location. Figures 4.20 and 4.21 show the readout TL glow curves of the PCFc-Ge and PCFc-Ge-B respectively at the L7 sampling location. From the figures, lesser TL intensity can be observed compared to the glow curves discussed in section 4.2.5 due to lesser TL exposure or fewer electrons trapped inside the TLD samples. The area of the glow curves corresponding to the TL response are illustrated in Figures 4.20 and 4.21. The maximum peak positions were almost at the same temperature of 180 to 200 °C, only differing in the magnitude of the peak height.
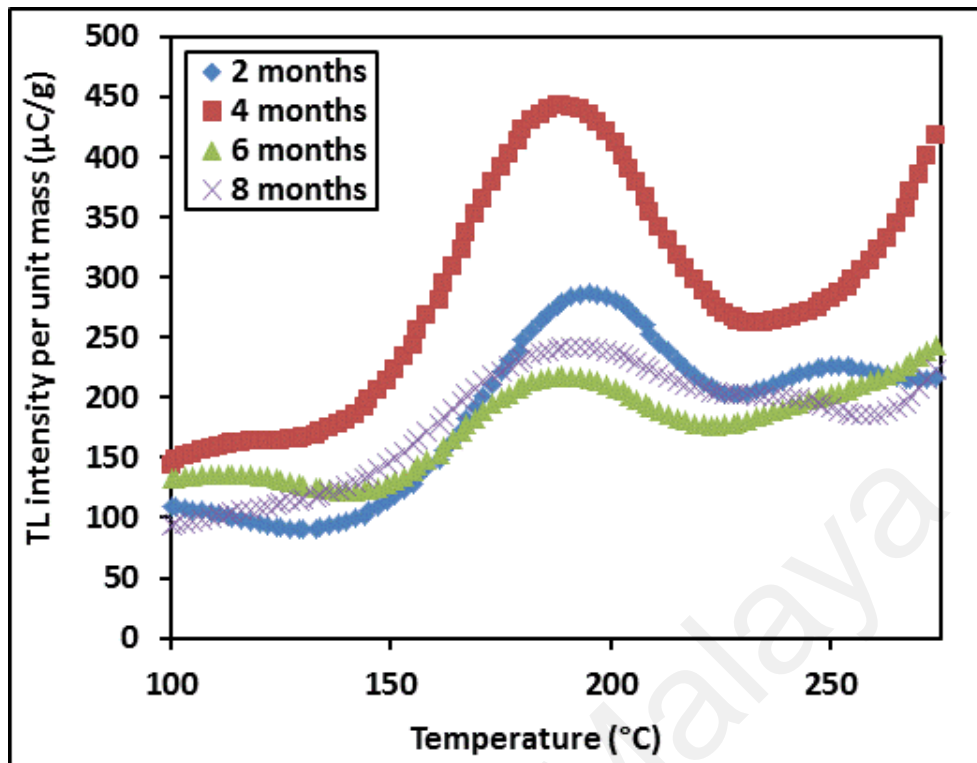
Figure 4.20: TL glow curve for PCFc-Ge at L7 sampling locations, after 2 to 8 months of sample exposure.
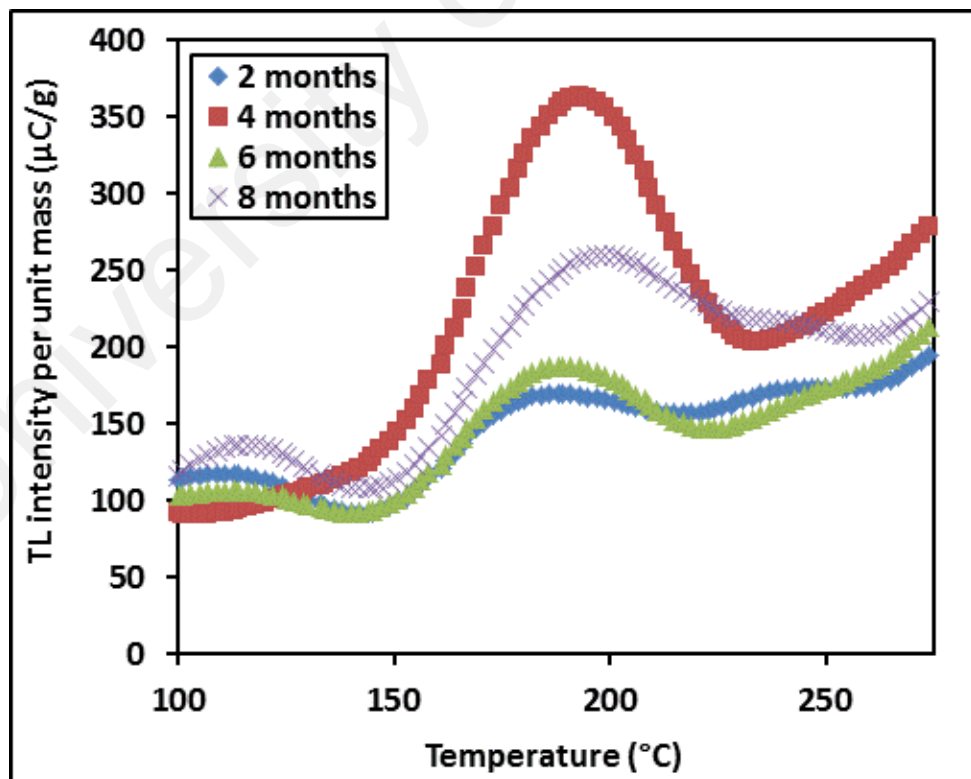
Figure 4.21: TL glow curve for PCFc-Ge-B at L7 sampling locations, after 2 to 8 months of sample exposure.

4.3.2   Soil collections from sites

The assessment of the radioactivity concentration of the ^{226}Ra (^{238}U), ^{228}Ra (^{232}Th) and ^{40}K in all samples were carried out using HPGe gamma-ray spectrometry, with counting for 43,200 s (12 hours). Table 4.3 represents some radionuclides that have very close gamma-lines which could not be resolved properly by using the HPGe detector. For example, the radionuclide ^{212}Pb has only one strong gamma-line of 238.63 keV (43.6 %) with a half-life of 10.64 h. On the other hand, ^{214}Pb has several characteristics gamma-lines of 241.98 keV (7.3.8 %) and 351.92 keV (35.8 %) with a shorter half-life of 26.8 m. In the case of activity counting with a decay time of > 5 h, it could be considered that the activity contribution of ^{214}Pb radionuclide from (238.63 keV) 241.98 keV gamma-line has almost completely decayed (M U Khandaker et al. 2012). However, for gamma spectra having decay times < 5 h, it is possible to separate the contribution of ^{214}Pb from the 238.63 keV gamma-ray line by using a well-known activity distribution formula available in (Mayeen Uddin Khandaker et al. 2012). However, in order to reduce the error in activity determination, only strong and independent characteristic gamma lines (the γ-rays highlighted in bold in Table 4.3 and as shown in Figure 4.22) of the respective radionuclides were used to determine the net activity concentration.
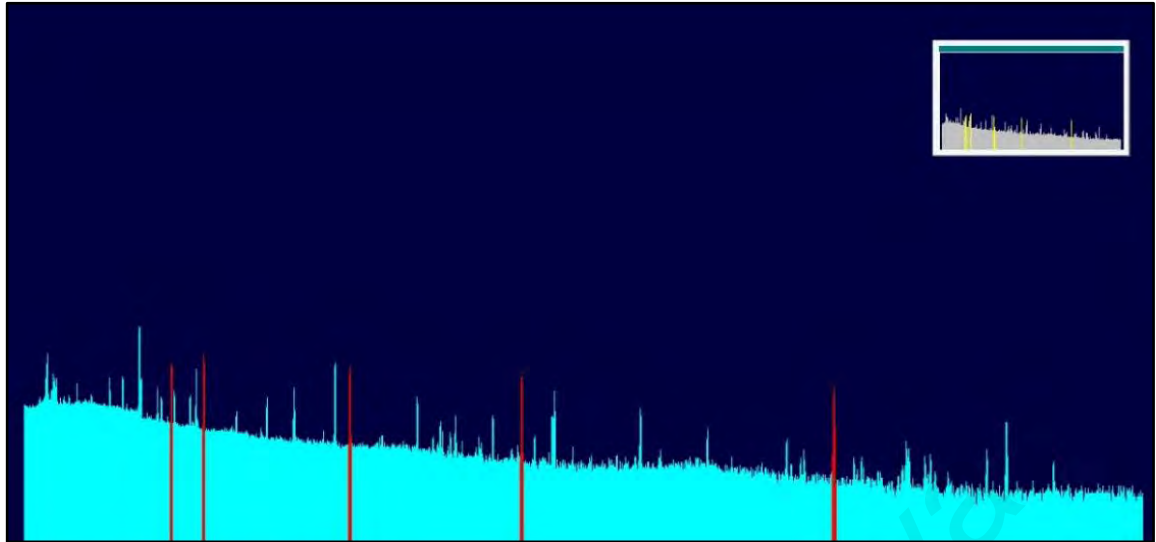
Figure 4.22: HPGe gamma-ray spectrometry for L7 sampling location. The red lines represented the strong gamma lines as highlighted in bold in Table 4.3.

Table 4.3: Decay data for radionuclides of interest, γ-lines in bold were used in activity determination.

Nuclides of interest	Detected nuclides	Half-life	Decay mode (%)	Gamma-ray energy, $E_γ$ (keV)	Gamma-ray intensity, $I_γ$ (%)	Sources / origin
^{238}U	^{214}Bi	19.9 m	α (0.02);	394.05	0.0126	^{238}U(^{226}Ra) series
			β⁻ (99.98)	**609.320**	45.49	
				1764.491	15.30	
	^{214}Pb	26.8 m	β⁻ (100)	241.995	7.251	^{238}U(^{226}Ra) series
				351.93	35.60	
^{232}Th	^{228}Ac	6.15 h	β⁻ (100)	**911.204**	25.8	^{232}Th series
				968.971	15.8	
	^{212}Pb	10.64 h	β⁻ (100)	**238.632**	43.6	^{232}Th(^{228}Ra) series
	^{208}Tl	3.053 m	β⁻ (100)	**583.187**	85.0	^{232}Th(^{228}Ra) series
				2614.511	99.754	
^{40}K	^{40}K	1.248 x 10⁹ y	EC (10.72)	**1460.822**	10.66	Primordial
			β⁻ (89.28)			

Table 4.4 shows the value of activity concentrations of ^{226}Ra, ^{232}Th and ^{40}K in soil samples for the L1 to L8 sampling locations. The observed value variations are suggested to be due to chemical changes of the constituent elements of soils (Miah et al., 2012). The activity concentrations of ^{226}Ra and ^{232}Th (62.17 ± 8.27 and 82.66 ± 12.52 Bq/kg) are found to be greatest at location L7 (the recreation lake) some 20 km from the LAMP site. For ^{40}K, sampling location L2 (opposite the LAMP site), 1 km distance from LAMP, showed the greatest activity concentration at 331.05 ± 43.50 Bq/kg. Although there were variations in the activities concentration of these naturally occurring radionuclides, their values were generally below the safety limits, if we compare to activity concentrations of ^{226}Ra, ^{232}Th and ^{40}K in soil samples of Malaysia (48, 82, and 310 Bq/kg) with the respective world averages of 35, 30 and 400 Bq/kg (UNSCEAR, 2000).

Table 4.4: Activity concentration of ^{226}Ra, ^{232}Th and ^{40}K of soil samples for L1 to L8 sampling locations.

S_ID	Activity concerntration, A (Bq/kg)		
	^{226}Ra	^{232}Th	^{40}K
L1	44.05 ± 6.39	65.88 ± 10.80	28.31 ± 04.05
L2	17.56 ± 2.19	30.26 ± 04.31	331.05 ± 43.50
L3	33.43 ± 4.45	56.74 ± 08.54	276.26 ± 36.42
L4	31.12 ± 4.02	51.59 ± 08.18	290.17 ± 38.24
L5	25.52 ± 3.24	25.94 ± 03.73	21.36 ± 03.02
L6	15.03 ± 1.87	10.35 ± 01.48	18.51 ± 02.61
L7	62.17 ± 8.27	82.66 ± 12.52	246.49 ± 32.79
L8	35.91 ± 4.36	46.87 ± 06.38	201.62 ± 26.45
Min	15.03 ± 1.87	10.35 ± 01.48	18.51 ± 02.61
Max	62.17 ± 8.27	82.66 ± 12.52	331.05 ± 43.50
AM ± SD	33.10 ± 4.35	46.28 ± 06.99	176.72 ± 23.38

In order to assess potential health effects, radiation hazard indicators such as Ra_{eq}, D_R, AEDE, and the hazard index have been calculated for soils collected at the L1 to L8 sampling locations, as presented in Table 4.5. From the table, Ra_{eq} was found to be in the range from 31.24 ± 2.67 to 199.35 ± 19.37 Bq/kg with a mean value of 112.89 ± 12.19 Bq/kg. The gamma absorbed dose rates, D_R in soils at 1 m above the ground were found to be in range from 13.96 ± 1.79 to 88.92 ± 13.08 nGy/h with a mean of 50.61 ± 8.30 nGy/h. This is lower than the Malaysia mean gamma absorbed dose of 92 nGy/h and also the world average of 59 nGy/h (UNSCEAR, 2000) as illustrated in Figure 4.23. Assuming a 20% outdoor occupancy factor, the corresponding annual effective dose showed a mean value of 0.06 ± 0.01 mSv/y, significantly lower than the worldwide average value of 0.07 mSv/y for annual outdoor effective dose as reported by (UNSCEAR, 2000). The mean value of both the external and internal hazard indices are in range from 0.08 ± 0.01 to 0.54 ± 0.01 and 0.13 ± 0.02 to 0.71 ± 0.10 which were less than 1, confirming that the area pose no health hazard to the local populace.

Table 4.5: Radium equivalent, absorbed dose, annual effective dose equivalent and radiation hazard indices for L1 to L8 sampling locations.

S_ID	Radium equivalent, Ra_{eq} (Bq/kg)	Absorbed dose, D_R (nGy.h^{-1})	Annual effective dose equivalent, AEDE (mSv/y)	Hazard index	
				External, H_{ex}	Internal, H_{in}
L1	140.43 ± 14.45	61.32 ± 9.49	0.07 ± 0.01	0.38 ± 0.06	0.50 ± 0.08
L2	86.32 ± 13.30	40.19 ± 9.61	0.05 ± 0.01	0.23 ± 0.03	0.28 ± 0.04
L3	135.84 ± 15.03	61.23 ± 10.41	0.07 ± 0.01	0.37 ± 0.05	0.46 ± 0.06
L4	127.24 ± 14.98	57.64 ± 10.43	0.07 ± 0.01	0.34 ± 0.05	0.43 ± 0.06
L5	64.25 ± 5.57	28.35 ± 3.69	0.03 ± 0.00	0.17 ± 0.02	0.24 ± 0.03
L6	31.24 ± 2.67	13.96 ± 1.79	0.02 ± 0.00	0.08 ± 0.01	0.13 ± 0.02
L7	199.35 ± 19.37	88.92 ± 13.08	0.11 ± 0.02	0.54 ± 0.08	0.71 ± 0.10
L8	118.45 ± 11.44	53.30 ± 7.91	0.06 ± 0.01	0.32 ± 0.04	0.42 ± 0.05
Min	31.24 ± 2.67	13.96 ± 1.79	0.02 ± 0.00	0.08 ± 0.01	0.13 ± 0.02
Max	199.35 ± 19.37	88.92 ± 13.08	0.11 ± 0.02	0.54 ± 0.08	0.71 ± 0.10
Average	112.89 ± 12.10	50.61 ± 8.30	0.06 ± 0.01	0.30 ± 0.04	0.39 ± 0.06
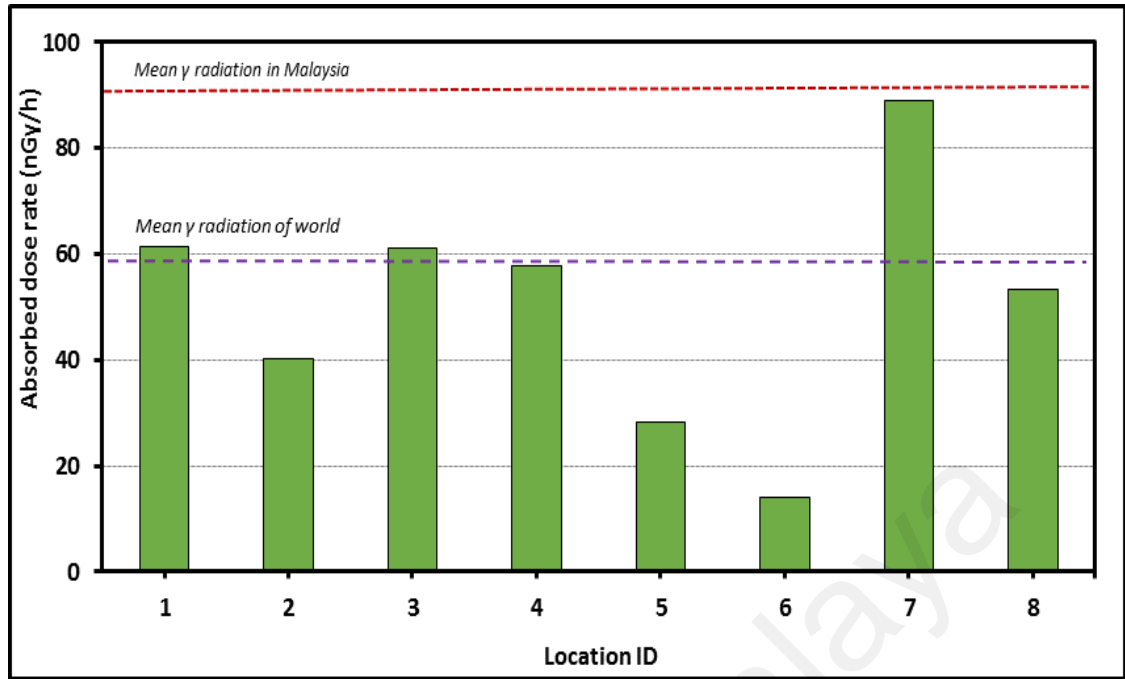
Figure 4.23: Soils gamma absorbed dose rate for each of the locations. Also plotted are: the mean gamma radiation in Malaysia (92 nGy/h) and world (59 nGy/h).

Table 4.6: Comparison of Ra_{eq}, D_R, AEDE of the present study with other parts of the Malaysia and world.

Location	Ra_{eq} (mSv/y)	D_R (nGy.h^{-1})	AEDE (mSv/y)	Reference
Gebeng, Pahang	112.89	50.61	0.06	Present study
Johor Bharu District	237	135	0.17	(Aziz et al. 2014)
Rembau, Negeri Sembilan	-	383	0.78	(Norbani et al. 2014)
Selama District, Perak	-	273	0.96	(Ramli et al. 2009)
Melaka	-	183	0.21	(Ramli et al. 2005)
Malaysia	-	92	-	(UNSCEAR 2000)
World	-	59	0.07	(UNSCEAR 2000)

4.4   Comparison of the gamma absorbed dose from the buried TLD samples and collected soils

Details of the calculation and conversion of both TLD samples and collected soils were discussed in section 3.4. The results are presented in Table 4.6, with comparison of the gamma radiation absorbed dose of the TLD samples and that of the adjacent soils from gamma spectroscopy. They are also then illustrated by Figures 4.22 (a) to (h). The soils radiation absorbed doses were in the range from 0.122 to 0.779 mGy/y. The highest dose can be observed at L7 followed by L1 and L3, while the lowest dose was at L6.

For TLD samples, overall the radiation absorbed dose trends were almost similar for all the locations. The radiation absorbed doses trend towards decrease for extended burial times. Also clearly to be seen from the figures, for the two and four months of sample burial, the absorbed doses mostly were higher than that generally for the soils. But, this case only happened for both PCF TLD samples, not for the phosphor TLD samples. As discussed, it is apparent that the phosphor TLD samples were more greatly affected by moisture. For longer duration exposures, six and eight months, the doses for all the TLD samples were lower. Fading may be one of the factors that influence the results including for PCF TLD samples. Dose absorbed by PCFc-Ge was the highest, followed by PCFc-Ge-B, TLD-100, and TLD-200. Both gamma absorbed dose from TLD samples and soils were the highest at the L7 sampling location while the lowest was that at L6, agreeing with the activity concentrations shown in Figure 4.23.

Table 4.7: Comparison of radiation absorbed dose from TLD samples and soils

S_ID	Burial (month)	TLD samples (mGy/y)				Soils (mGy.y^{-1})
		PCFc-Ge	PCFc-Ge-B	TLD-100	TLD-200	
L1	2	1.275 ± 0.026	0.593 ± 0.044	0.489 ± 0.021	0.045 ± 0.002	0.537 ± 0.083
	4	0.534 ± 0.014	0.308 ± 0.024	0.146 ± 0.004	0.020 ± 0.001	
	6	0.368 ± 0.050	0.204 ± 0.006	0.123 ± 0.017	0.013 ± 0.001	
	8	0.267 ± 0.031	0.166 ± 0.018	0.079 ± 0.001	0.007 ± 0.001	
	Average	0.611 ± 0.031	0.318 ± 0.023	0.209 ± 0.010	0.021 ± 0.001	
L2	2	0.845 ± 0.061	0.484 ± 0.033	0.285 ± 0.025	0.040 ± 0.001	0.352 ± 0.084
	4	0.387 ± 0.035	0.176 ± 0.004	0.101 ± 0.004	0.018 ± 0.001	
	6	0.267 ± 0.016	0.134 ± 0.005	0.092 ± 0.004	0.012 ± 0.001	
	8	0.214 ± 0.025	0.167 ± 0.003	0.055 ± 0.011	0.007 ± 0.001	
	Average	0.424 ± 0.034	0.227 ± 0.011	0.133 ± 0.011	0.019 ± 0.001	
L3	2	1.112 ± 0.039	0.539 ± 0.040	0.478 ± 0.004	0.040 ± 0.002	0.536 ± 0.091
	4	0.489 ± 0.020	0.262 ± 0.005	0.119 ± 0.004	0.020 ± 0.002	
	6	0.330 ± 0.017	0.168 ± 0.026	0.119 ± 0.012	0.013 ± 0.001	
	8	0.214 ± 0.027	0.167 ± 0.006	0.055 ± 0.001	0.008 ± 0.001	
	Average	0.536 ± 0.026	0.284 ± 0.020	0.193 ± 0.009	0.021 ± 0.001	
L4	2	0.948 ± 0.039	0.454 ± 0.040	0.424 ± 0.004	0.037 ± 0.001	0.505 ± 0.091
	4	0.369 ± 0.020	0.227 ± 0.005	0.089 ± 0.004	0.016 ± 0.001	
	6	0.301 ± 0.017	0.116 ± 0.026	0.108 ± 0.012	0.012 ± 0.001	
	8	0.195 ± 0.027	0.131 ± 0.006	0.075 ± 0.001	0.008 ± 0.001	
	Average	0.453 ± 0.026	0.232 ± 0.020	0.174 ± 0.005	0.018 ± 0.001	
L5	2	0.766 ± 0.051	0.463 ± 0.056	0.372 ± 0.076	0.030 ± 0.001	0.248 ± 0.032
	4	0.280 ± 0.028	0.158 ± 0.022	0.078 ± 0.001	0.013 ± 0.001	
	6	0.225 ± 0.036	0.084 ± 0.014	0.079 ± 0.005	0.010 ± 0.001	
	8	0.179 ± 0.011	0.113 ± 0.019	0.050 ± 0.004	0.007 ± 0.001	
	Average	0.362 ± 0.032	0.204 ± 0.028	0.145 ± 0.021	0.015 ± 0.001	
L6	2	0.726 ± 0.094	0.332 ± 0.034	0.290 ± 0.020	0.030 ± 0.001	0.122 ± 0.016
	4	0.246 ± 0.016	0.131 ± 0.017	0.086 ± 0.001	0.013 ± 0.001	
	6	0.212 ± 0.038	0.097 ± 0.020	0.095 ± 0.007	0.010 ± 0.001	
	8	0.153 ± 0.018	0.095 ± 0.019	0.041 ± 0.001	0.006 ± 0.001	
	Average	0.334 ± 0.041	0.164 ± 0.023	0.128 ± 0.007	0.015 ± 0.001	
L7	2	1.391 ± 0.069	0.606 ± 0.044	0.537 ± 0.050	0.046 ± 0.001	0.779 ± 0.115
	4	0.603 ± 0.031	0.346 ± 0.022	0.168 ± 0.006	0.022 ± 0.001	
	6	0.440 ± 0.006	0.221 ± 0.015	0.141 ± 0.002	0.015 ± 0.001	
	8	0.332 ± 0.033	0.201 ± 0.016	0.088 ± 0.010	0.101 ± 0.001	
	Average	0.691 ± 0.035	0.343 ± 0.024	0.234 ± 0.017	0.023 ± 0.001	

L8	2	0.997 ± 0.090	0.483 ± 0.044	0.406 ± 0.017	0.038 ± 0.003	0.467 ± 0.069
	4	0.351 ± 0.040	0.195 ± 0.013	0.113 ± 0.002	0.019 ± 0.001	
	6	0.329 ± 0.063	0.177 ± 0.017	0.118 ± 0.013	0.012 ± 0.001	
	8	0.225 ± 0.021	0.181 ± 0.002	0.070 ± 0.008	0.007 ± 0.001	
	Average	0.475 ± 0.054	0.259 ± 0.019	0.177 ± 0.010	0.019 ± 0.002	
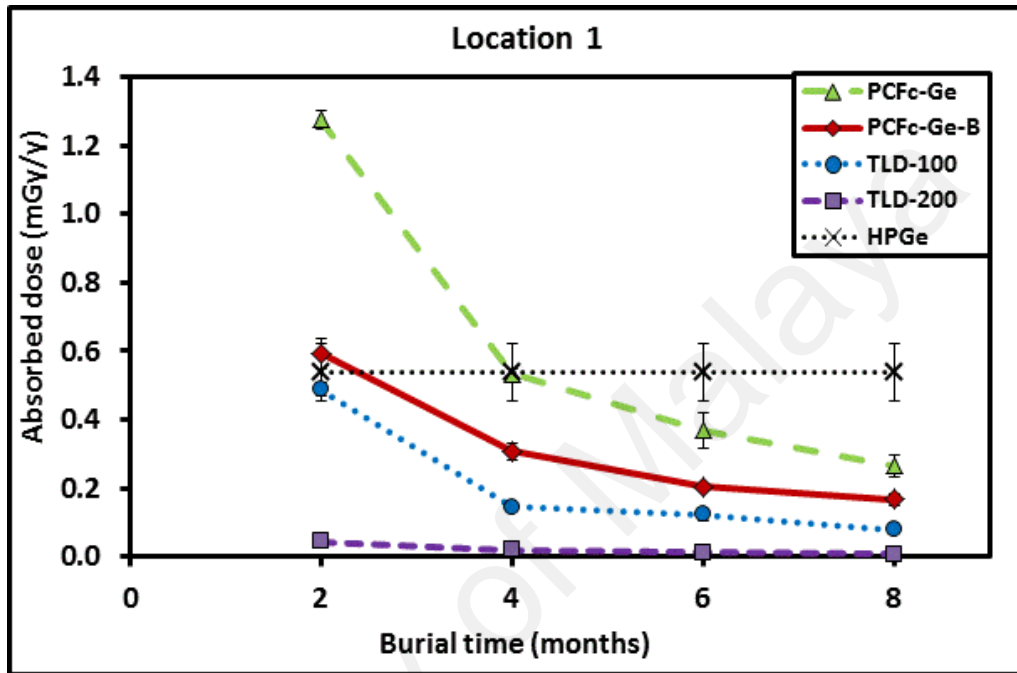
(a)
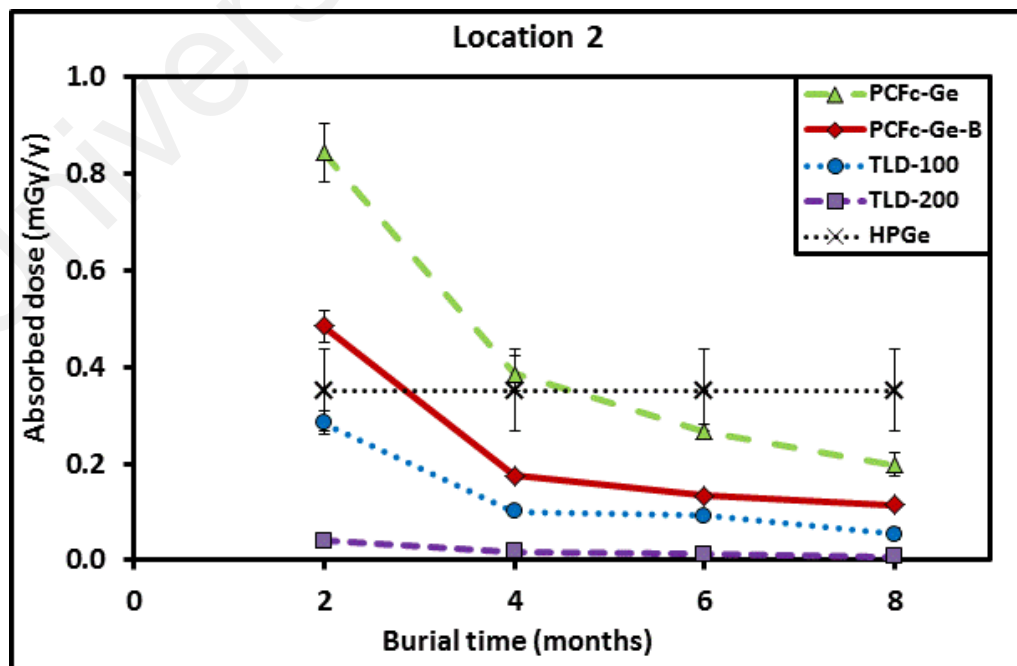
(b)
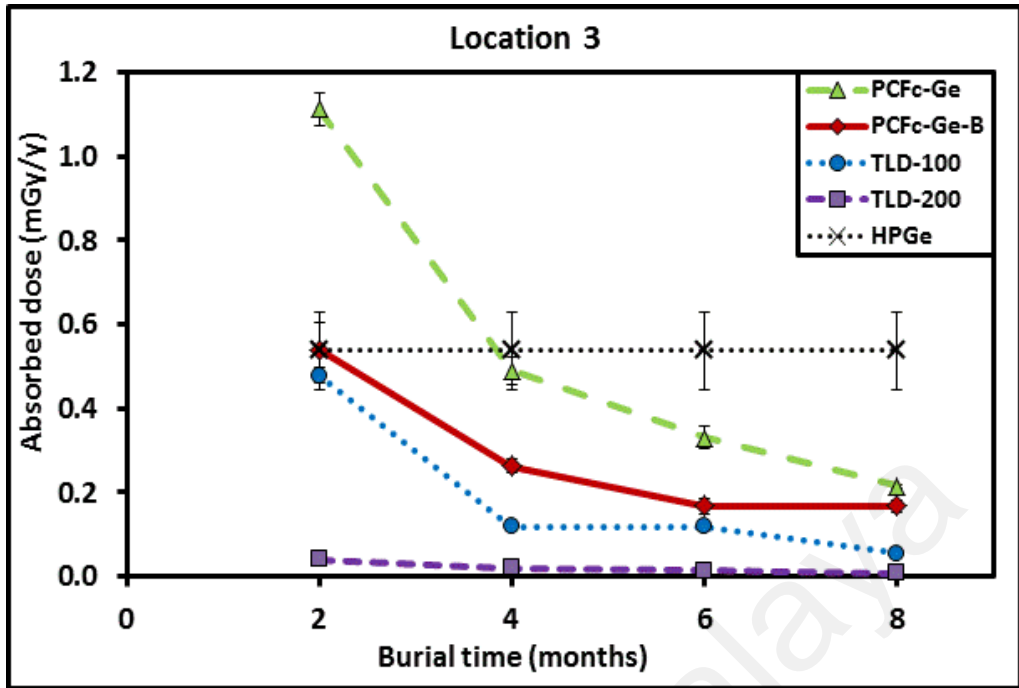
(c)
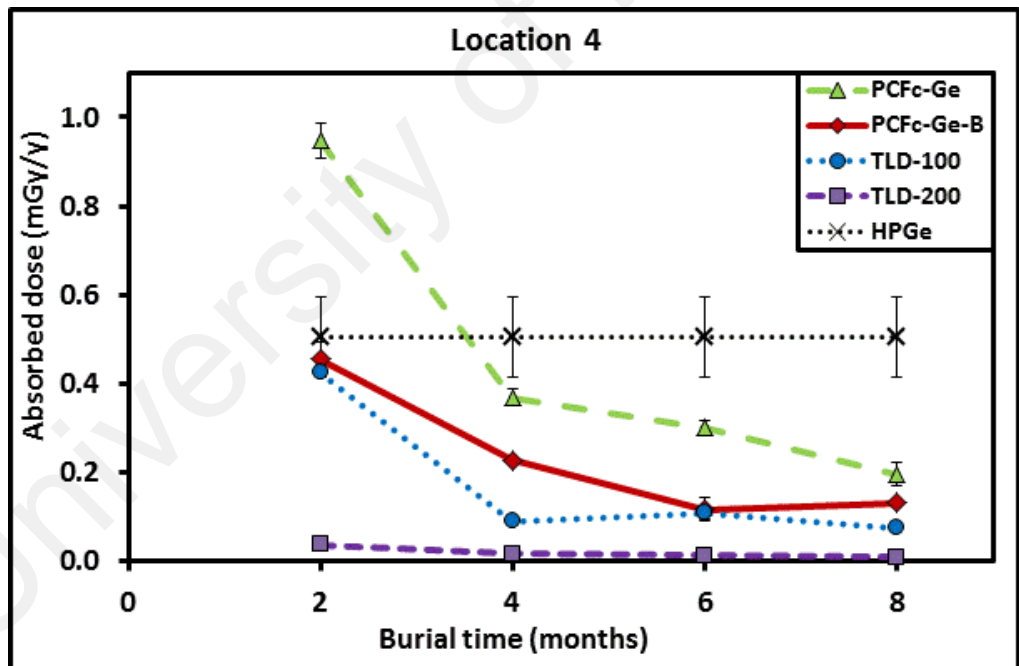
(d)
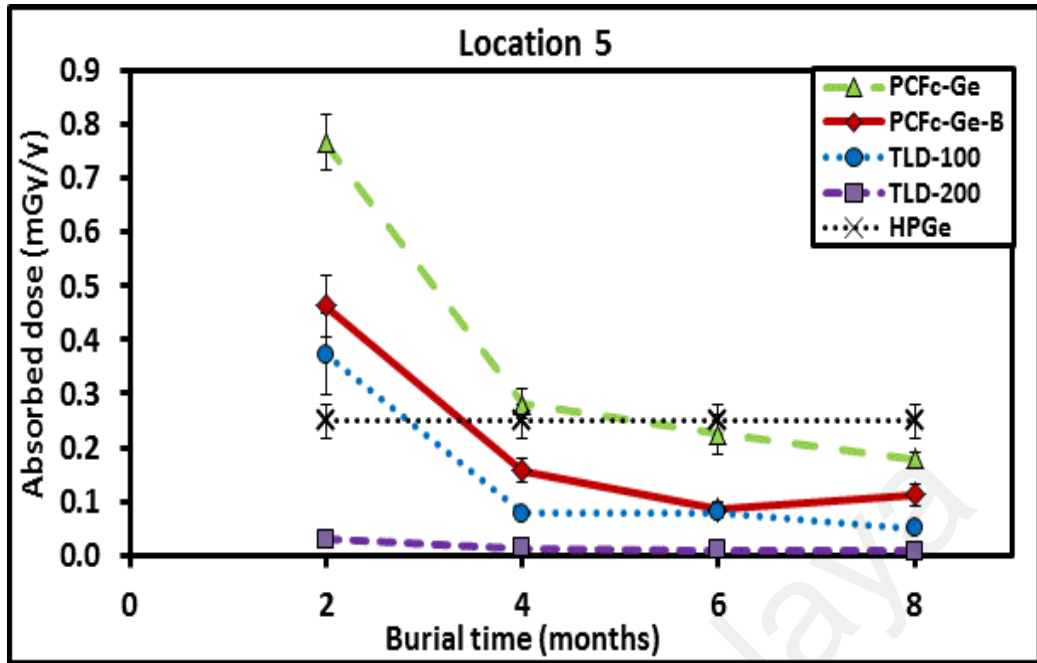
(e)
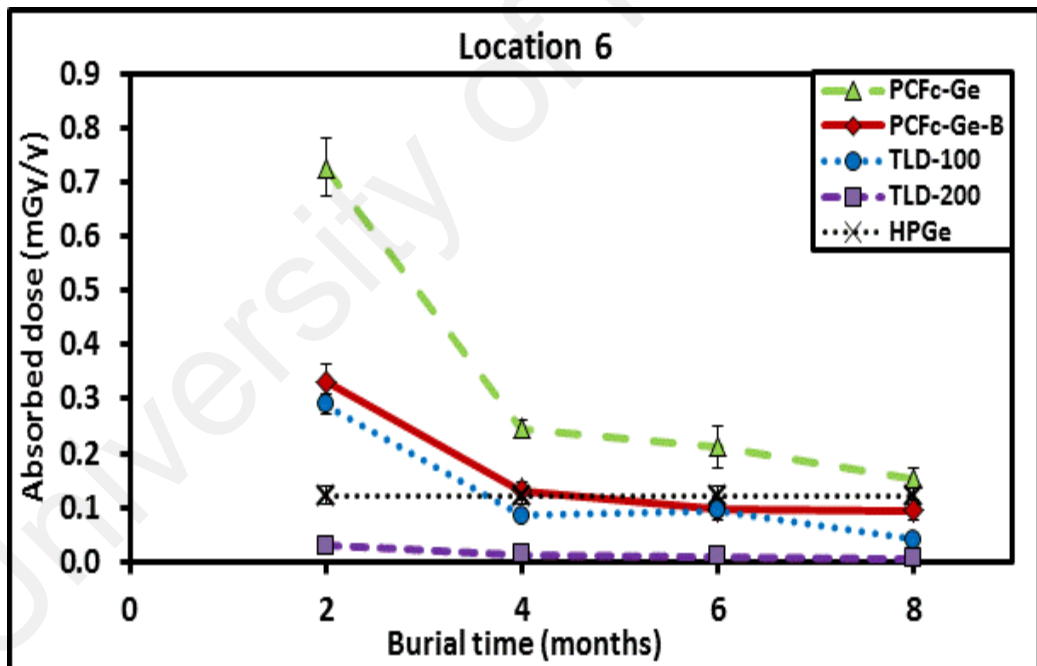
(f)
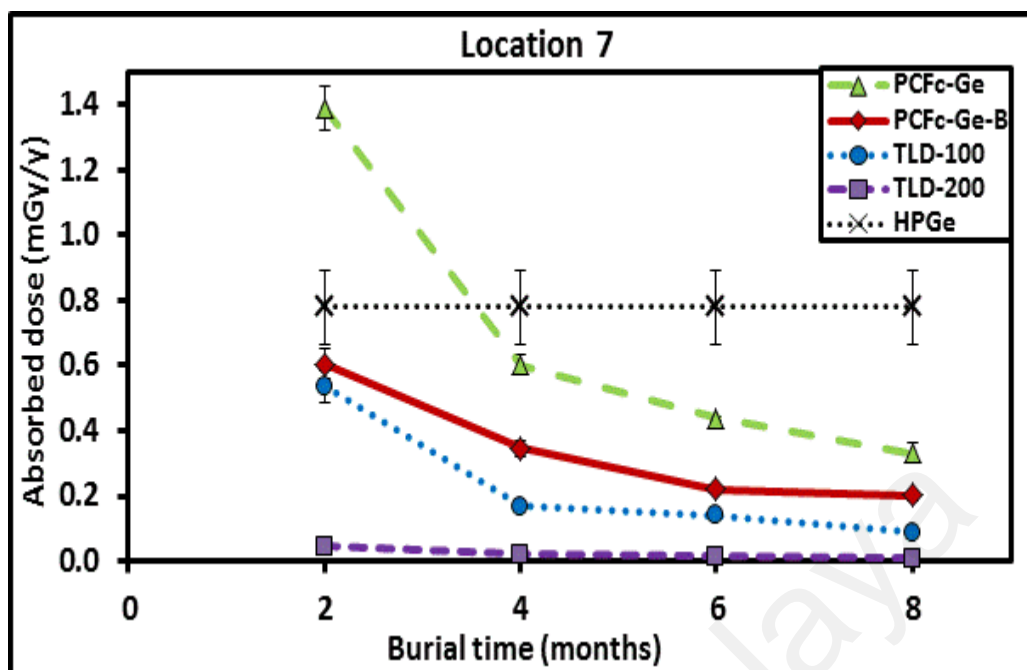
(g)
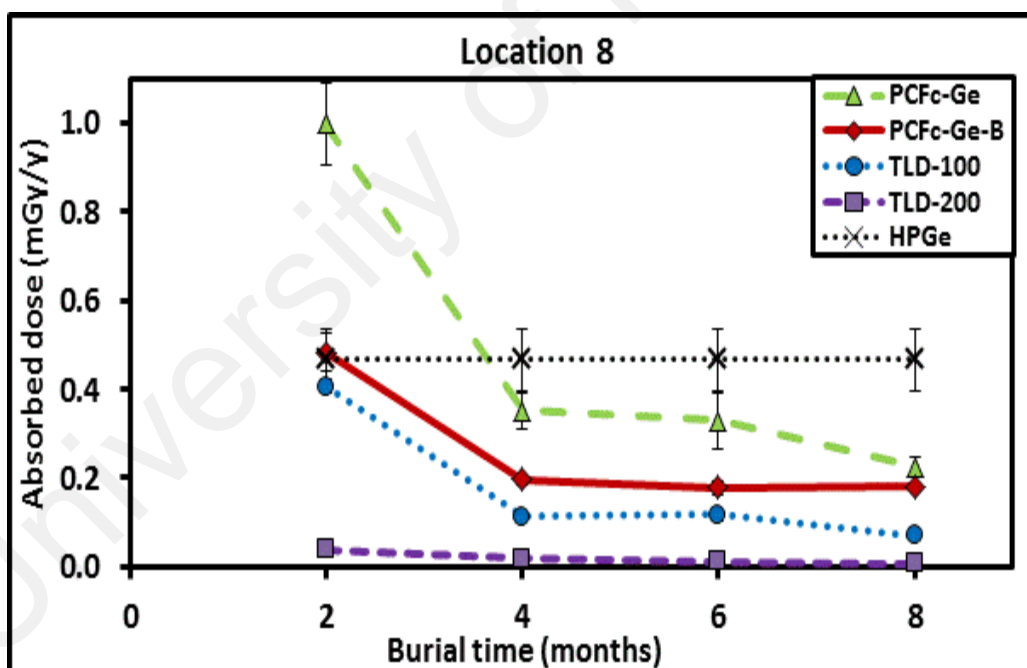
(h)

Figure 4.24: (a) to **(h)**. Illustration of the comparison of gamma radiation absorbed dose of TLD samples buried from 2 to 8 months and the gamma spec adjacent soils analysis results for each location (L1 to L8).

CHAPTER 5 : CONCLUSIONS AND SUGGESTIONS FOR FUTURE WORK

5.1 Summary

The naturally occurring radioactive materials (NORMs) are everywhere around us. Following the remarkable technological advancement, the NORMs level can be enhanced and redistributed, and pose threat to the public health. Monitoring of the environmental radioactivity in the present study area, i.e., Gebeng Industrial Estate (GIE), in Pahang which is off-site of the Lynas Advanced Material Plant (LAMP), is very important as it may enhance the typical NORMs level. Selected study locations are within 1, 5, 10 and 20 km from LAMP. Instead of using the conventional phosphor TLDs (TLD-200 and TLD-100), we investigated the potential of the newly developed collapsed Photonic Crystal Fiber (PCFc) with different dopants of Ge and Ge-B as TL dosimeter (TLD) for environmental radioactivity monitoring. Before being applied them in environmental, the various influencing characteristics of all of the TLD samples were studied. Further, comparison has been made between the radiation absorbed dose ascertained by the TLD samples and absorbed dose of the adjacent soils from the same place as ascertained by gamma-ray spectroscopy.

5.2 Conclusions

Reviewing the results presented in this work, a number of conclusions can be made:

For laboratory study;

1. From the dose response curves obtained using photon energy sources, TLD-200 showed superior sensitivity, followed by PCFc-Ge-B, PCFc-Ge, and TLD-100. TLD-200, PCFc-Ge-B and PCFc-Ge have been found to be respectively ~ 90 ×, ~ 9 × and ~ 7 × that of TLD-100 as irradiated to 0.5 mGy to 10 mGy of 40 keV

mean energy of X-rays. They were ~ 22 ×, ~ 5 × and ~ 2 × that of TLD-100 when irradiated to 1 to 5 Gy of ^{60}Co gamma-rays, the mean energy of which is 1.25 MeV.

2. For the energy dependence study, TLD samples were irradiated to 1 Gy of x-ray mean photon energies from 10 keV to 100 keV and ^{60}Co mean gamma energy of 1250 keV. The results for TL response were greatest at an effective energy of 60 keV for TLD-200, 40 keV for PCFc-Ge-B and TLD-100 and at 30 keV for PCFc-Ge, noting that it was particularly at the lower photon energies ranging from 10 keV to 50 keV that the dominant effect of the photoelectric effect was seen to be most pronounced. Overall, the greatest TL response of the samples was observed for photon energies between 30 keV to 60 keV.

3. TLD-100 has an effective atomic number, Z_{eff} of 8.2 which is close to being tissue equivalent ($Z_{eff} = 7.14$). The stacked capillary structure and the deformation of collapsed PCF help to create a preponderance of strain-related defects. The Z_{eff} of PCFc-Ge and PCFc-Ge-B were 12.5 and 14.4 respectively. Since both PCFs were not soft-tissue equivalent, these need detailed calibration for dose deposition in soft tissues. However, the elevated responses of the PCFs make them good candidates for sensitive measurements of low environmental doses as does TLD-200 with Z_{eff} of 16.3.

4. Over a period of 35 days post-irradiation the fading loss for TLD-200 and PCFc-Ge was 21 % while that for PCFc-Ge-B was 15 %; in comparison, the respective loss in TLD-100 was 7 %. The mean loss in TL response for the PCFs has been estimated to be 0.4 % - 0.5 % per day.

For environmental study;

1. For durations of two to eight months of sample burial, for most of the cases at sampling locations L1 to L8, the PCFc-Ge shows better behaviour (TL response) followed by PCFc-Ge-B, TLD-100, and TLD-200. This was a different pattern to that obtained from the laboratory studies. The degradation in performances of both phosphor TLDs (TLD-100 and TLD-200) have been suggested to be due to the moisture clearly to be seen inside the sample bottles collected from the soils.

2. For most of the cases, the TL response of the TLD samples (both PCFs and phosphor TLD) results in increasing response for two to four months of sample burial, however their response decreased for the six to eight months duration exposures. It was identified that instead of a dominating moisture effect, fading then becomes a factor for these glass fibres. In summary, extended sample burial duration may affect the results of the study.

3. For sampling locations L1 to L8, the average activity concentrations of ^{226}Ra, ^{232}Th and ^{40}K in the adjacent soils were found to be 33.10 ± 04.35, 46.28 ± 06.99 and 176.72 ± 23.38 respectively. The radium equivalent, Ra_{eq} was found to be in the range 31.24 ± 2.67 to 199.35 ± 19.37 Bq/kg, with a mean value of 112.89 ± 12.19 Bq/kg. The gamma absorbed dose rates, D_R in soils were found to be in range 13.96 ± 1.79 to 88.92 ± 13.08 with a mean value of 50.61 ± 8.30, which was lower than the Malaysia mean gamma absorbed dose of 92 nGy/h and world average value of 59 nGy/h. The annual effective dose equivalent, AEDE showed a mean value of 0.06 ± 0.01 mSv/y, significantly lower than the worldwide average value of 0.07 mSv/y. The mean value of both external and internal hazard index were in range of 0.08 ± 0.01 to 0.54 ± 0.08 and 0.13 ± 0.02

to 0.71 ± 0.10 which were less than 1, and confirmed that it is safe to carry out human activities in that area.

4. By converted the value in years, the soils gamma radiation absorbed doses were found to be in the range from 0.122 ± 0.016 to 0.779 ± 0.115 mGy.y-1. For TLD samples, overall, for two and four months of sample burial, the absorbed doses mostly were higher than gamma spec results for the soils. But, this case only happened for both PCF TLD samples, not for the phosphor TLD samples. As discussed, even for relatively short burial durations, the phosphor TLD samples were already affected by the moisture. However, in the case of a longer duration, six and eight months, the doses for all the TLD samples were lower than expected. Fading may be one of the factors that influence the results including for PCF TLD samples. Dose absorbed by PCFc-Ge was the greatest, followed by PCFc-Ge-B, TLD-100, and TLD-200. There was very good agreement in the environmental radiation dose rates trend measured by the TLD samples and gamma spec for adjacent soils, with L7 showing the highest value followed by L1 and L3, while the lowest dose was at L6.

Overall, the newly developed PCFs have the potential to be used as TL dosimeters for environmental radiation monitoring with glassy dosimeters possessing more defects being advantageous in terms of enhanced sensitivity. Among the studied TL dosimeters, PCFc-Ge showed the best behavior. However, for a study aimed in particular at a real application for the samples in respect of environmental monitoring, more detailed study over longer durations could offer greater reassurance of the utility of the PCF dosimeters.

5.3 Suggestions for future work

Based on the studies, the new developed PCFs have the potential to be used as the TL dosimetry for environmental radiation monitoring. Instead of providing the PCFs sample in the very small size (~ 100 μm), we propose trying use of larger size PCFs ~ several mm diameter size. This woud point to greater sensitivity and greater ease in handling for environmental monitoring.

REFERENCES

Abdul Rahman, A. T., Bradley, D. A., Doran, S. J., Thierry, B., Elke Bräuer-Krisch, A. B. (2010). The thermoluminescence response of Ge-doped silica fibres for synchrotron microbeam radiation therapy dosimetry. *Nuclear Instruments and Methods in Physics Research Section A: Accelerators, Spectrometers, Detectors and Associated Equipment*, *619*(1-3), 167–170.

Abbasisiar, F., Hosseini, T., Fathivand, A., & Heravi, G. (2004). Determination of uranium isotopes (^{234}U, ^{238}U) and natural uranium (U-nat) in water samples by alpha spectrometry. *Iranian Journal of Radiation Research*, *2*(1), 35–40.

Abdul Rahman, A. T., Abu Bakar, N. K., Chandra Paul, M., & Bradley, D. A. (2014). Ultraviolet radiation (UVR) dosimetry system and the use of Ge-doped silica optical fibres. *Radiation Physics and Chemistry*, *104*, 129–133.

Ahmad Termizi, R., Bradley, D. A., Suhairul, H. (2009). The thermoluminescence response of doped SiO_2 optical fibres subjected to alpha-particle irradiation. *Applied Radiation and Isotopes*, *67*(3), 428–432.

Alam, L. & Mohamed, C. A. R. (2011). Natural radionuclide of Po^{210} in the edible seafood affected by coal-fired power plant industry in Kapar coastal area of Malaysia. *Environmental health : A Global Access Science Source*, *10*(1), 43.

Amin, Y., Mahat, R. H., Nor, R. M., Khandaker, M. U., Takleef, G. H., & Bradley, D. A. (2013). The presence of natural radioactivity and ^{137}Cs in the South China Sea bordening Peninsular Malaysia. *Radiation Protection Dosimetry*, *156*(4), 1–6.

Argonne National Laboratory. (2005). Natural Decay Series: Uranium, Radium, and Thorium. *Human Health Fact Sheet*, 4.

Attix, F.H. (2008). Introduction to radiological physics and radiation dosimetry.

Aziz, M., Ahmad, S. & Ramli, T. (2014). Natural environmental radioactivity and the corresponding health risk in Johor Bahru District, Johor, Malaysia.

Begum, M., Mizanur Rahman, A. K. M., Abdul Rashid, H. A., Yusoff, Z., Begum, M., Mat-Sharif, K. A., Amin, Y. M., & Bradley, D. A. (2015). Thermoluminescence characteristics of Ge-doped optical fibers with different dimensions for radiation dosimetry. *Applied Radiation and Isotopes, 100*, 79-83.

Bos, A. J. J., Piters, T. M., De Vries, W., & Hoogenboom, J. E. (1990). Comparative study of trapping parameters of LiF (TLD-100) from different production batches. *Radiation Protection Dosimetry, 33*(1-4), 7–10.

Bradley, D. A., Mahdiraji, G. A., Ghomeishi, M., Dermosesian, E., Adikan, F. R. M., Rashid, H. A. A., & Maah, M. J. (2015). Enhancing the radiation dose detection sensitivity of optical fibres. *Applied Radiation and Isotopes, 100,* 43–49.

Bradley, D. A., Hugtenburg, R. P., Nisbeta, A., Ahmad Taufek, A. R., Fatma, I., Noramaliza, M. N. (2012). Review of doped silica glass optical fibre: Their TL properties and potential applications in radiation therapy dosimetry. *Applied Radiation and Isotopes, 71,* 2–11.

Daniels, F., Boyd, C.A. & Saunders, D.F. (1952). Thermoluminescence as a research tool.

Dermosesian, E., Mahdiraji, G. A., Mahamd Adikan, F. R., & Bradley, D. A. (2015). Improving thermoluminescence response through the fabrication of novel microstructured fibers. *Radiation Physics and Chemistry, 116*, 135–137.

Furetta, C. (2003). Handbook of thermoluminescence, World Scientific.

Gofman, J.W. (1981). Radiation and human health.

González, P. R., Furetta, C. & Azorín, J., (2007). Comparison of the TL responses of two different preparations of LiF:Mg,Cu,P irradiated by photons of various energies. *Applied Radiation and Isotopes, 65,* 341–344.

Hallenbeck, W.H. (1994). Radiation protection, CRC Press.

Hashim, S., Ibrahim, S. A., Che Omar, S. S., Alajerami, Y. S. M., Saripan, M. I., Noor, N. M., Alzimami, K. (2014). Photon irradiation response of photonic crystal fibres

and flat fibres at radiation therapy doses. *Applied Radiation and Isotopes, 90*, 258–260.

Hashim, S., Al-Ahbabi, S., Bradley, D. A, Webb, M., Jeynes, C., Ramli, A. T., & Wagiran, H. (2009). The thermoluminescence response of doped SiO$_2$ optical fibres subjected to photon and electron irradiations. *Applied radiation and isotopes : including data, instrumentation and methods for use in agriculture, industry and medicine, 67*(3), 423–427.

Hashim, S., Omar, S. S. C., Ibrahim, S. A., Hassan, W. M. S. W., Ung, N. M., Mahdiraji, G. A., Alzimami, K. (2015). Thermoluminescence response of flat optical fiber subjected to 9 MeV electron irradiations. *Radiation Physics and Chemistry, 106*, 46–49.

Izewska, J. & Rajan, G. (2005). *Radiation Oncology Physics:* A Handbook for Teachers and Students. Radiation Dosimeter.

Jha, D.K. (2004). Radioactivity And Radioactive Decay, Discovery Publishing House.

Khan, F.M. (2010). The physics of radiation therapy, Fourth Ed., 531.

Khandaker, M. U., Jojo, P. J., Kassim, H. A., & Amin, Y. M. (2012). Radiometric Analysis Of Construction Materials using HPGe Gamma-Ray Spectrometry. *Radiation pr*otection dosimetry, *152*(1), 33–37.

Khandaker, M.U., Kim, K. & Kim, G. (2012). Production cross sections of short-lived silver radionuclides from nat Pd (p, xn) nuclear processes. *Nuclear Instruments and Methods in Physics Research Section B: Beam Interactions with Materials and Atoms, 274*, 148–153.

Kharisov, B.I., Kharissova, O.V. & Méndez, U.O. (2013). Radiation synthesis of materials and compounds, CRC Press.

Kolo, M. T., Aziz, S. A. B. A., Khandaker, M. U., Asaduzzaman, K., & Amin, Y. M. (2015). Evaluation of radiological risks due to natural radioactivity around Lynas Advanced Material Plant environment, Kuantan, Pahang, Malaysia. *Environmental Science and Pollution Research, 22*(17), 13127–13136.

Lee, E. M., Menezes, G. & Finch, E. C. (2004). Natural radioactivity in building materials in the Republic of Ireland. *Health physics, 86*(4), 378–383.

Mahdiraji, G. A., Adikan, F. R. M. & Bradley, D. A. (2015). Collapsed optical fiber: A novel method for improving thermoluminescence response of optical fiber. *Journal of Lumine*scence, *161*, 442–447.

Mahesh, K., Weng, P., Furetta, C., & others. (1989). Thermoluminescence in Solids and its Applications, *Nuclear Technology Pub*.

McKeever, S. W. S., Moscovitch, M. & Townsend, P. D. (1995). Thermoluminescence dosimetry materials: properties and uses.

Metrology Malaysia. (2015). Buletin Cuaca Malaysia. *Ministry of Science and Technology Innovation.*

Miah, A., Miah, M. M. H., Kamal, M., Chowdhury, M. I., & Rahmatullah, M. (2012). Natural Radioactivity and Associated Dose Rates in Soil Samples of Malnichera Tea Garden in Sylhet District of Bangladesh. *Journal of Nuclear and Particle Physics*, *2*(6), 147–152.

Norbani, N. E., Abdullah Salim, N. A., Saat, A., Hamzah, Z., Ramli, A. T., Wan Idris, W. M. R., Abdul Rahman, A. T. (2014). Terrestrial gamma radiation dose rates (TGRD) from surface soil in Negeri Sembilan, Malaysia. *Radiation Physics and Chemistry*, *104*, 112–117.

Ramli, A. T., Nursama, H. A. & Wagiran, H. (2009). Assessment of Radiation Dose Rates in the High Terrestrial Gamma Radiation Area of Selama District, Perak, Malaysia. *Applied Physics Research, 1*(2), 45–52.

Ramli, A. T., Sahrone, S. & Wagiran, H. (2005). Terrestrial gamma radiation dose study to determine the baseline for environmental radiological health practices in Melaka state, Malaysia. *Journal of Radiological Protection, 25(*4), 435.

Ramli, N. N. H., Salleh, H., Mahdiraji, G. A., Zulkifli, M. I., Hashim, S., Bradley, D. A., & Noor, M. N. (2015). Characterization of amorphous thermoluminescence dosimeters for patient dose measurement in X-ray diagnostic procedures. *Radiation Physics and Chemistry*, *116*, 130–134.

Hafezi, S., Amidi, J., Attarilar, A. (2005). Concentration of natural radionuclides in soil and assessment of external exposure to the public in Tehran. Iran. *J. Radiat. Res., 3*(2), 85–88.

Savva, A. (2010). Personnel TLD monitors, their calibration and response. University of Surrey.

Scharmann, A. (1993). Techniques and management of personnel thermoluminescence dosimetry services, *Springer Science & Business Media.*

Shale, M. (2011). Understanding Naturally Occurring Radioactive Material in the Marcellus Shale. June, *4*, 1–8.

Siti Shafiqah, A. S , Amin, Y. M., Md Nor, R., Tamchek, N., & Bradley, D. A. (2015). Enhanced TL response due to radiation induced defects in Ge-doped silica preforms. *Radiation Physics and Chemistry, 111*, 87–90.

Tabatabaei, S., Shukohfar, A., Aghababazadeh, R., & Mirhabibi, A. (2006). Experimental study of the synthesis and characterisation of silica nanoparticles via the sol-gel method. *Journal of Physics: Conference Series, 26*, 371–374.

Tiwari, R., Bala Taunk, P., Tamrakar, R. K., Swamy, N. K., & Dubey, V. (2014). Synthesis, characterization and thermoluminescence behavior of (Cd, Zn)S mixed phosphor doped with silver. *Chalcogenide Letters, 11*(3), 141–158.

UNSCEAR, 2000. Annex B. Exposures from natural radiation sources., *1*, 74.

Van Dam, J. & Marinello, G. (2006). Methods for in vivo dosimetry in external radiotherapy 2nd ed., Brussels: ESTRO.

Villa-Sanchéz, G., Mendoza-Anaya, D., Gutiérrez-Wing, C., Pérez-Hernández, R., González-Martínez, P. R., & Ángeles-Chavez, C. (2007). Ag nanoparticle effects on the thermoluminescent properties of monoclinic ZrO_2 exposed to ultraviolet and gamma radiation. Nanotechnology, *18*(26), 265703.

Wilson, W. F. (1993). A guide to naturally occurring radioactive material (NORM), PennWell Books.

Yaakob, N. H., Wagiran, H., Hossain, M. I., Ramli, A. T., Bradley, D. A., Hashim, S., & Ali, H. (2011). Thermoluminescence Response of Ge- and Al-Doped Optical Fibers Subjected to Low-Dose Electron Irradiation. *Journal of Nuclear Science and Technology, 48*(7), 1115–1117.

Yazici, A. N. & Öztürk, Z., (2001). Analysis of the isolated glow peak 6 in CaF_2:Dy (TLD-200) following post-irradiation annealing at 145°C. *Nuclear Instruments and Methods in Physics Research, Section B: Beam Interactions with Materials and Atoms*, *174*, 499–506.

Youssef, D., Abdulla, A., Amin, Y. M., Bradley, D. A. (2001). The thermoluminescence response of Ge-doped optical fibre subjected to photon irradiation. *Radiation Physics and Chemistry*, *61*(3-6), 409–410.

Zielinski, R. A, Otton, J. K. & U. S. Geological Survey (USGS), (1999). Naturally Occurring Radioactive Materials (NORM) in Produced Water and Oil-Field Equipment — An Issue for the Energy Industry. 142–99.

LIST OF PUBLICATIONS AND CONFERENCE

Publications

1. **Z. Siti Rozaila**, Amjad Alyahyawi, M. U. Khandaker, Y. M. Amin, D. A. Bradley, M. J. Maah. 2016. Ge and B doped collapsed photonic crystal optical fibre, a potential TLD material for low dose measurements. *Radiat. Phys. Chem.* 126, 9–13.

2. D. A. Bradley, S. M. Jafari, A. S. Siti Shafiqah, N. Tamcheck, A. Shutt, **Z. Siti Rozaila**, S. F. Abdul Sani, S. N. Sabtu, A. Alanazi, G. Amouzad Mahdiraji, H. A. Abdul Rashid, and M. J. Maah. 2016. Latest Developments in Silica-Based Thermoluminescence Spectrometry and Dosimetry. *Appl. Radiat. Isot.* 117, 128-134.

3. D. A. Bradley, A. S. Siti Shafiqah, **Z. Siti Rozaila,** S. N. Sabtu, S. F. Abdul Sani, A. H. Alanazi, S. M. Jafari, G. Amouzad Mahdiraji, F. R. Mahamd Adikan, M. J. Maah, A. N. Nisbet, N. Tamchek, H. A. Abdul Rashid, M. Alkhorayef, and K. Alzimami. 2016. Developments in production of silica-based thermoluminescence dosimeters. *Radiat. Phys. Chem.* (*In Press, Corrected Proof).*

4. F. C. A. Da Silva, D. A. Bradley, P. H. Regan, and **Z. Siti Rozaila**. 2016. Measurement of the total activity concentrations of Libyan oil scale. *Radiat. Phys. Chem.* (*In Press, Corrected Proof).*

Conference

1. Presented paper at 2nd International Sciences, Technology and Engineering Conferences (ISTEC 2016), Penang, Malaysia 20 - 23 April 2016 on Thermoluminesence Response of Doped Collapsed Photonic Crystal Fibres Subjected to Photon Irradiation.

Details of the calculations and conversion as discussed in section 3.4, used to obtain the radiation absorbed dose of buried TLDs (as presented in section 4.4; Table 4.7). Herein, from on-site work study; only the case of two months of sample burial is shown. Table A.1 shows the readout TL response of the buried samples.

Table A.1: Readout TL response of two months of sample burial.

S_ID	Readout TL response (µGy/g)			
	PCFc-Ge	**PCFc-Ge-B**	**TLD-100**	**TLD-200**
L1	1.893 ± 0.039	1.488 ± 0.110	1.349 ± 0.057	1.289 ± 0.068
L2	1.255 ± 0.091	1.215 ± 0.084	0.787 ± 0.069	1.153 ± 0.027
L3	1.651 ± 0.059	1.352 ± 0.166	1.320 ± 0.051	1.155 ± 0.023
L4	1.408 ± 0.058	1.139 ± 0.101	1.171 ± 0.012	1.065 ± 0.066
L5	1.137 ± 0.183	1.161 ± 0.141	1.027 ± 0.209	0.862 ± 0.046
L6	1.078 ± 0.139	0.833 ± 0.085	0.801 ± 0.055	0.852 ± 0.025
L7	2.065 ± 0.102	1.520 ± 0.110	1.482 ± 0.138	1.320 ± 0.023
L8	1.480 ± 0.134	1.212 ± 0.110	1.120 ± 0.046	1.094 ± 0.087

From the laboratory study, the gradient or calibration factor from dose response graph as discussed in section 4.2.4.1 (TLD samples irradiated to 0.5 mGy to 10 mGy of 40 keV of mean x-ray source);

Table A.2: Gradient or calibration factor from dose response graph.

TLD samples	Gradient, M (µC/g.mGy)
PCFc-Ge	1.493
PCFc-Ge-B	2.000
TLD-100	0.221
TLD-200	20.81

By referring to the energy response curve (discussed in section 4.2.3), the ratio of $TL_{x\text{-ray}}$ to $TL_{\gamma\text{-ray}}$;

Table A.3: Ratio of the ratio of $TL_{x\text{-ray}}$ to $TL_{\gamma\text{-ray}}$ based on TLDs energy response curve.

TLD samples	Ratio $TL_{x\text{-ray}}$ to $TL_{\gamma\text{-ray}}$
PCFc-Ge	5.966
PCFc-Ge-B	7.523
TLD-100	1.144
TLD-200	8.279

Based on A1, A2, and A3, then scaled to a one year period, the absorbed radiation dose are calculated by using equation A.1 and presented in Table A4;

$$Dose\ (mGy) = \frac{TL\ response\ (\mu C/g)}{Gradient, M\ (\mu C/g.mGy)} \times \frac{6}{ratio\ TL_{x-ray}\ to\ TL_{\gamma-ray}} \qquad (A.1)$$

Table A.4: Absorbed dose of TLD samples for two months of sample burial.

S_ID	Absorbed dose of TLD samples (mGy)			
	PCFc-Ge	**PCFc-Ge-B**	**TLD-100**	**TLD-200**
L1	1.275 ± 0.026	0.593 ± 0.044	0.489 ± 0.021	0.045 ± 0.002
L2	0.845 ± 0.061	0.484 ± 0.033	0.285 ± 0.025	0.040 ± 0.001
L3	1.112 ± 0.040	0.539 ± 0.066	0.478 ± 0.018	0.040 ± 0.001
L4	0.948 ± 0.039	0.454 ± 0.040	0.424 ± 0.004	0.037 ± 0.002
L5	0.766 ± 0.123	0.463 ± 0.056	0.372 ± 0.076	0.030 ± 0.002
L6	0.726 ± 0.094	0.332 ± 0.034	0.290 ± 0.020	0.030 ± 0.001
L7	1.391 ± 0.069	0.606 ± 0.044	0.537 ± 0.050	0.046 ± 0.001
L8	0.997 ± 0.090	0.483 ± 0.044	0.406 ± 0.017	0.038 ± 0.003